UNIVERSITA' DEGLI STUDI DI ROMA 'La Sapienza'
Facoltà di Scienze Matematiche, Fisiche e Naturali
Dipartimento di Fisica

Dottorato di Ricerca in Astronomia — Ciclo XXV
A. A. 2012

Multiple Populations in Globular Clusters

Roberta Carini

Relatore: Dott. Paolo Ventura

Coordinatore: Prof. Roberto Capuzzo Dolcetta

This thesis has been carried out at

INAF - Osservatorio Astrofisico di Roma

Dedicated to my wonderful family

" ..The future belongs to those who believe in the beauty of their dreams.." E. Roosevelt

Contents

Introduzione

Gli Ammmassi Globulari sono sempre stati usati come laboratori per testare le teorie di evoluzione stellare, poiché, con buona approssimazione, essi possono essere considerati popolazioni stellari semplici, formati da stelle di stessa età con chimica omogenea.
Ciò offre un'opportunità unica per comparare le tracce stellari teoriche e le isocrone con i dati fotometrici, perché la qualità del 'fit' ottenuto dipende solo dall'età e dalla metallicità, ma non dalla distanza dell'ammasso. Questo paradigma è stato cambiato nelle ultime decadi dalle analisi spettroscopiche ad alta risoluzione, che misero in luce delle differenze tra stella e stella nelle abbondanze degli elementi 'leggeri', fino all'alluminio (Kraft, 1994; Norris et al., 1981). Le differenze tracciano delle relazioni ben definite tra le abbondanze superficiali di vari elementi, come le ben note anticorrelazioni O-Na e Mg-Al (es. Gratton et al. (2004)).
Lo stesso andamento, almeno a livello qualitativo, è stato rivelato non solo in stelle in fase di Gigante Rossa ma anche in Sequenza Principale e nel ramo delle subgiganti. (Gratton et al., 2001); poiché queste stelle al loro interno sono troppo fredde per permettere una nucleosintesi che vada oltre il canale p-p, la loro scoperta conferma che questi andamenti chimici devono essere caratteristici del gas da cui si formano le stelle, e non sono dovuti a processi avvenuti in-situ. Dato che le sorgenti con la chimica anomala vengono depletati in ossigeno e in magnesio, mentre il CNO rimane costante all'interno delle incertezze osservative (Ivans et al., 1999; Cohen et al., 2005), è comunemente accettato che la materia contaminata è stata esposta alla nucleosintesi di cattura protonica. Il rapporto tra il numero di stelle con abbondanze anomale e standard spesso è vicino all'unità (Carretta et

al., 2009a). Questo comportamento è una peculiarità degli Ammassi Globulari, poiché le stelle di campo con la stessa metallicità non mostrano simili anomalie.
La serie di evidenze spettroscopiche successivamente furono corroborate dai risultati fotometrici, i quali indicavano che gli Ammassi Globulari con le anticorrelazioni più estesi erano caratterizzati da Bracci Orizzontali (HB) con una morfologia molto perculiare, ospitando più gruppi di stelle, separati da lacune, sia in magnitudine che in colore (Bedin et al., 2004; Piotto et el., 2005). D'Antona et al. (2002) e D'Antona & Caloi (2004) per prime spiegarono il fenomeno supponendo che la presenza di una popolazione ricca in elio potesse giustificare queste apparenti anomalie nella distribuzione di stelle di HB. Questa teoria fu confermata dalla scoperta di una suddivisione nella MS in alcuni ammassi, nei quali la parte più blu della MS poteva essere spiegata invocando la presenza di una componente stellare ricca in He (Piotto et al., 2007).
Questi risultati confermarono l'esistenza di popolazioni stellari multiple in Ammassi Globulari, e che i processi di cattura protonica fossero i responsabili per la contaminazione del gas da cui le nuove stelle vengono formate.
Il nuovo paradigma per interpretare queste osservazioni è che esiste una seconda generazione (SG) di stelle, nate dalla materia espulsa da stelle in evoluzione della prima generazione (FG) e nuclearmente processata attraverso il ciclo caldo di CNO, possibilmente mischiato con gas non processato.
Le sorgenti di materiale processato proposte fino ad ora sono le seguenti:

1. **AGB Massive** (Ventura et al., 2001). Durante l'evoluzione nel ramo asintotico delle giganti (AGB), la parte inferiore dell'inviluppo convettivo di stelle con massa iniziale maggiore di $\sim 4\,M_{\odot}$ fa l'esperienza del così detto 'Hot Bottom Burning' (HHB) (es. Blöcker & Schönberner (1991)): il materiale viene processato attraverso il ciclo CNO, con la possibile attivazione dei canali Ne-Na e Mg-Al. Il materiale processato è emesso nel messo interstellare rimanendo all'interno della buca di potenziale dell'Ammasso Globulare, grazie alle piccole velocità dei venti delle AGB, consentendo la formazione delle stelle SG. (D'Ercole et al., 2008).

2. **Stelle Massive Rotanti (FRMS)** (Decressin et al., 2007). Le stelle massive posso emettere a basse velocità gas processato attraverso il CNO, se il materiale dal loro interno è trasportato in superficie attraverso un circolazioni meridiane indotte: i tassi di rotazione richiesti sono vicini alla velocità di 'break-up'. Nel caso che si formi una disco di accrescimento, la velocità di emissione è estremamente bassa, il materiale processato può essere trattenuto dal potenziale dell'ammasso, si può mischiare con materiale primordiale e formare stelle SG.

3. **Binarie Massive** (de Mink et al., 2009). Il gas dal quale si formano le generazioni successive non proviene da singole stelle, ma da sistemi binari massivi. Se le stelle massive interagiscono con le compagne nel proto-GC, esse diffondono nell'ambiente circostante una grande quantità di materia processata per nucleosintesi di cattura protonica. La massa verrebbe persa dal sistema attraverso i punti esterni Lagrangiani in un disco circumbinario e dovrebbe mostrare gli andamenti nella abbondanze chimiche osservati nelle stelle degli GCs.

Sills & Glebbeek (2010) provarono a combinare i tre modelli . Trovarono che le collisioni tra stelle massive possono aiutare la produzione delle abbondaze estreme osservate in alcuni Ammassi Globulari, ma la quantità totale di materiale prodotto è troppo piccola per permettere un rapporto 1:1 tra le stelle SG e FG, che invece viene osservato.
I due problemi più critici per questi scenari sono:

- La quantità di massa disponibile per innescare la formazione della seconda generazione di stelle, per una ragionevole funzione di massa iniziale (IMF), è solo una piccola percentuale della massa totale del proto-ammasso, ma questa deve essere in grado di formare circa $10^5\,M_{\odot}$. Quindi il proto-ammasso deve essere stato molto più massivo rispetto ad oggi, circa un fattore 10 più grande, anche assumendo un'efficienza di formazione stellare alta (Prantzos & Charbonnel , 2006).

- I modelli di inquinamento da parte delle stelle AGB massive e super-AGB forniscono una correlazione diretta tra le abbondanze in sodio e ossigeno. Quindi il modello richiede una diluizione del gas processo attraverso il CNO e materia non processata avente la stessa composizione chimica delle stelle FG (Bekki et al., 2007; D'Antona & Ventura, 2007; D'Ercole et al., 2008, 2010). La diluizione è anche necessaria nel modello FRMS (Prantzos & Charbonnel , 2006; Decressin et al., 2007; Lind et al., 2009), e deve essere invocata per spiegare tutti gli ammassi.

Il primo e il secondo scenario, sebbene forniscano un accordo qualitativo ragionevole con le evidenze osservative, soffrono di alcuni difetti, associati alla chimica del gas emesso. Il modello delle binarie massive all'inizio fornisce una grande percentuale di materiale processato, quindi avrebbere bisogno di una massa totale iniziale più piccola per il proto-GC, alleviando il problema del budget di massa.
Mentre molti sforzi sono stati dedicati per la compilazione di 'yields' per i primi due scenari, il modello delle binarie massive non è mai stato esaminato in più dettaglio, così che è impossibile contraddirlo o provarlo fino a quando non viene elaborato un modello

completo di popolazione stellare.
Gli studi presentati finora delineano sotto quali ipotesi ognuno dei meccanismi citati possono potenzialmente produrre gas la cui chimica è in accordo con gli andamenti osservativi. Un' investigazione preliminare fatta da D'Ercole et al. (2008), fissa uno schema teorico per descrivere il processo di formazione delle stelle SG negli ambienti di GCs. Questo metodo può essere applicato ad ogni tipo di sorgente inquinante, purché sia disponibile la chimica del gas emesso nel mezzo interstellare.
In questo lavoro usiamo tale schematizzazione per comparare i risultati ottenuti quando il gas inquinante è emesso dalla binarie massive, con quelli basati sui venti delle stelle AGB. Per queste ultime , usiamo anche le abbondanze chimiche delle SAGB, che sono state compilate appositamente.
Nel Capitolo I presentiamo la problematica dell'esistenza delle popolazioni multiple in Ammassi Globulari, delineando le osservazione che supportano questa ipotesi.
Nel Capitolo II sono discusse le principali proprietà fisiche e chimiche dei modelli di AGB e delle SAGB, usati per l'investigazione. Mostriamo perché lo scenario di auto-arricchimaneto da parte delle AGB appare il più attendibile per spiegare la formazione di popolazioni multiple negli Ammassi Globulari. Nel terzo Capitolo elaboriamo un modello che segue l'idea di de Mink et al. (2009) in cui il gas inquinante è il risultato di binarie massive la cui evoluzione è non conservativa, avente luogo i primi milioni di anni della vita dell'ammasso. Per fare ciò, consideriamo la chimica delle stelle massive fino a $100\,M_{\odot}$ a diverse fasi evolutive. Analizziamo la chimica delle stelle massive e le abbondanze prodotte dei vari elementi chimici. Nel Capitolo IV estendiamo il modello presentato da D'Ercole et al. (2010), focalizzato sullo scenario AGB, includendo i nuovi yields delle SAGB compilati da Ventura & D'Antona (2011); introduciamo l'ipotesi di un 'extra-mixing' nelle stelle giganti ricche di elio, che aiuta a far fronte alle anomalie di ossigeno estreme. Presentiamo questo modello per l'evoluzione chimica degli Ammassi Globulari M4 e NGC 2808, che rappresentano i prototipi delle strutture con anticorrelazioni O-Na blnade ed estreme.
Il capitolo IV è dedicato anche agli andamenti del Litio. Ci focalizziamo su M4, comparando i dati provenienti da Monaco et al. (2011) con i modelli che sono riusciti a riprodurre l'anticorrelazione O-Na dello stesso ammasso, e su NGC 2808. E' presentata una discussione sulla discrepanza tra litio iniziale prodotto durante la nucleosintesi del Big Bang, e le quantità misurate nelle stelle di Pop II. Infine, nel Capitolo V studiamo uno scenario alternativo, dove il gas inquinante viene dai venti delle SAGB e AGB massive, come in D'Ercole et al. (2010), mentre il gas diluente non è il gas 'pristine' accresciuto nell'ammasso, ma mataria proveniente da stelle di prima generazione. Ci focalizziamo

sulla possibiltà che tale materia sia prodotto da incontri distruttivi di binarie soprattutto di FG e SG nelle regioni centrali dell'ammasso, dove le strette interazione sono altamente probabili, dovute alla grande densità delle stelle SG. Le conclusioni sono presentate nell'ultimo Capitolo.

Introduction

Globular Clusters have been extensively used as laboratories to test the stellar evolution theories. The reason is that with good approximation they can be considered as simple stellar populations, made up of coeval and chemically homogeneous stars.
This offers a unique opportunity to compare stellar tracks and isochrones with data from photometric investigations, because the quality of the fit obtained is independent of the distance of the cluster, and depends only on its age and metallicity.
This paradigma has been challenged in the last decades by the analysis of high resolution spectroscopy, that highlights star-to-star differences in the abundances of the 'light' elements, up to Aluminum (Kraft, 1994; Norris et al., 1981). The differences show up as abundance patterns, and trace well defined relations between the surface abundances of the various elements, such as the well known O-Na and Mg-Al anticorrelations (e.g. Gratton et al. (2004)).
The same trend, at least on qualitative grounds, have been detected so far both in evolved giants, and in Main Sequence or Sub Giant Branch stars (Gratton et al., 2001); because these stars are too cool in their interior to allow any nucleosynthesis beyond p-p chain, these findings were a confirm that these chemical patterns characterized the gas from which the stars formed, and were not due to any in-situ process. Because the sources with the anomalous chemistry were depleted in their oxygen and magnesium content, and the total CNO was constant within the observational uncertainty (Ivans et al., 1999; Cohen et al., 2005), it is now commonly accepted that contaminated matter was exposed to proton-capture nucleosynthesis. The relative numbers of stars with anomalous and

standard abundances is often close, or larger than, unity (Carretta et al., 2009a). This behavior is peculiar of GCs, since halo field stars with the same metallicity do not show similar anomalies.
The series of spectroscopic evidences was later corroborated by photometric results, indicating that Globular Clusters with the most extended anticorrelations were characterized by Horizontal Branch (HB) with a very peculiar morphology, harboring more groups of stars, separated by gaps, both in magnitude and in color (Bedin et al., 2004; Piotto et el., 2005). The early speculation by D'Antona et al. (2002) and D'Antona & Caloi (2004), that the presence of a helium-rich population could explain these apparently anomalous distribution of HB stars, was later confirmed by the discovery of MS splitting in some clusters, in which the bluest MS could only be explained by invoking the presence of a He-rich stellar component (Piotto et al., 2007).
These findings further confirmed the existence of multiple stellar populations in Globular Clusters, and that p-capture processes were the responsible for the contamination of the gas, from which the new stars formed. The new paradigma for the interpretation of these observations is that they imply the existence of a second generation (SG) of stars, born from matter expelled by evolving stars of the first generation (FG) and nuclearly processed through the hot CNO cycle, possibly mixed with unprocessed material.
The sources of the processed material proposed so far are the following:

1. **Massive AGBs** (Ventura et al., 2001). During the Asymptotic Giant Branch (AGB) evolution, the bottom of the convective envelope of stars with initial mass exceeding $\sim 4\,M_{\odot}$ experiences the so called 'Hot Bottom Burning' (HBB) (e.g. Blöcker & Schönberner (1991)): the material is processed through the hot CNO cycle, with the possible activation of the Ne-Na and Mg-Al chains. This processed material is ejected into the intracluster medium and retained in the potential well of the cluster, thanks to the small velocities of the AGB winds, and forms SG stars (D'Ercole et al., 2008).

2. **Fastly Rotating Massive Stars (FRMS)** (Decressin et al., 2007). Massive stars can eject at low velocity CNO processed material, if matter from their interior is transported to the surface by rotationally-induced mixing: the required rotation rates are close to break-up velocity. In case that an accretion disk forms, the ejection velocity of the gas is extremely small, the processed material can be retained in the potential well of the cluster, it can mix with pristine matter, and form SG stars.

3. **Massive binary stars** (de Mink et al., 2009). The gas from which further stellar generations form is not supplied by individual stars, but by massive interacting

binary systems. If the massive stars interact with a companion in the proto-GC, they shed into their surroundings large amounts of material processed by proton-capture nucleosynthesis. Mass would be lost from the system via the outer Lagrangian points into a circumbinary disk and a wider double toroidal nebula, and should show abundance patterns that resemble those observed in GC stars.

Sills & Glebbeek (2010) tried to combine the three models. They found that runway collision between massive stars can help producing the extreme abundances which are in some clusters, but the total amount of material produced is too small to allow a 1:1 ratio between SG and FG stars, that is observed.
The two most critical problems of these scenarios are:

- The mass budget available to trigger the second generation star formation, for reasonable initial mass functions, is only a few % of the total protocluster mass, but it must be able to form typical SG masses of about $10^5\ M_\odot$. Thus, the protocluster must have been much more massive than today, a factor $\sim$10 larger, even assuming a high star formation efficiency (Prantzos & Charbonnel , 2006).

- The massive AGB and super-AGB pollution model provides a direct correlation between oxygen and sodium yields (as a function of the initial stellar mass). Thus the model requires dilution of the hot-CNO processed ejecta with non-processed matter having the composition of the FG (Bekki et al., 2007; D'Antona & Ventura, 2007; D'Ercole et al., 2008, 2010). Dilution is also needed when dealing with FRMS ejecta (Prantzos & Charbonnel , 2006; Decressin et al., 2007; Lind et al., 2009) and must be invoked to explain all clusters.

The first and second scenarios, although providing a reasonable qualitative agreement with the observational evidence, suffer from a few shortcomings, associated to the chemistry of the ejecta. The massive binary model in principle provides a larger percentage of processed matter, and so it would require a smaller total initial mass for the proto-GC, alleviating the mass budget problem. While many efforts have been dedicated to the computation of yields in the scenarios (1) and (2), the interacting binary scenario has never been examined in more detail, so that it is impossible to contradict or prove it unless a complete stellar population model is worked out.
The studies presented so far outlined under which hypothesis any of the afore mentioned mechanism could potentially produce gas whose chemistry is in agreement with the observed trends, among the abundances of the light elements. A first, preliminary investigation by D'Ercole et al. (2008) set the theoretical framework to describe the process of

formation of SG stars in the GC environment. This method can be applied to any kind of polluters, provided that the chemistry of the gas ejected into the medium is available.
In this work we use the schematization by D'Ercole et al. (2008) to compare the results obtained when the polluting gas is ejected by massive binaries, with those based on the winds by AGBs. For these latter, we use the yields by SAGBs, that were computed on purpose.
In Chapter I we present the issue of the existence of multiple stellar populations in Globular Clusters, outlining the observations that support this hypothesis.
In Chapter II the main physical and chemical properties of the AGB and SAGB models used in this investigation are discussed. We show why the self-enrichment scenario by AGBs appears the most reliable to account for the formation of multiple populations in Globular Clusters. In the Third Chapter we elaborate a model following the idea by de Mink et al. (2009) that the polluting gas is a result of massive binary non conservative evolution, taking place during the first million years of cluster life. For this, we consider the chemistry of massive stars up to 100 $M_{\odot}$, at several evolutionary stages. We analyze the chemistry of the massive stars and the yields produced. In Chapter IV we extend the models presented in D'Ercole et al. (2010), focused on the AGB scenario, to include the new yields for SAGB models computed by Ventura & D'Antona (2011); we introduce a hypothesis of in situ 'extra-mixing', in the high helium red giants, that help to deal with the extreme oxygen anomalies. We present this model for the chemical evolution of the Globular Clusters M4 and NGC 2808, that represent the prototypes of structures with a mild and an extended O-Na anti-correlation.
Chapter IV is also dedicated to the lithium patterns coming from the chemical evolution models. We focus on M4, comparing data from Monaco et al. (2011) with models aimed at reproducing the O-Na anticorrelation of the same cluster, and on NGC 2808. A detailed discussion on the initial lithium produced during the Big Bang nucleosynthesis, and the discrepancy with the quantities measured in pop II stars, is presented. Finally, in Chapter V we study an alternative scenario, where the polluted gas comes from the super-AGB and massive AGB winds, as in D'Ercole et al. (2010), whereas the diluting gas is not pristine gas re-accreating on the cluster, but matter coming from first generation stars. We focus on the possibility that this material is produced via destructive binary encounters among FG and SG stars in the central regions of the cluster, where close interactions are extremely probable, due to the large density of SG stars. A summary of our conclusions is presented in the last Chapter.

CHAPTER 1

Multiple Populations in Globular Clusters

1.1 Introduction

Globular Clusters (GCs) are gravitationally bound systems, made up of 10^5-10^6 stars, whose spatial distribution is approximately spherically symmetric.
These structures rotate around the galactic core on orbits of high eccentricity and high inclination to the galactic plane. They are thought to have coalesced out of the primordial gas cloud of our Galaxy that only later collapsed, dissipating its energy and settling into the disk. Therefore, an accurate determination of the age of the oldest clusters can provide a lower limits on the age of the Milky Way, and thus of the Universe. The estimated ages range from 10 to 15 Gyr.
About a third of globular clusters are concentrated around the galactic center (see Fig. 1.1). Typical revolution period is around 10^8 years. The Milky Way contains approximately 150 GCs, with mass estimates ranging from $\sim 10^3\ M_\odot$ (e.g. M4) to $2.2 \times 10^6\ M_\odot$ (Omega Cen). They are very tightly bound by gravity, which gives them their spherical shapes and relatively high stellar densities toward their centers.
For each GC it is possible to define some typical scales, useful to infer the main structural

properties:

- **half-mass radius** $\mathbf{r}_{hm}$: it is the distance from the cluster center containing half of the total mass.
- **virial radius** $r_{vir} \equiv \frac{GM^2}{2|U|}$: where M is the total cluster mass, U is the total potential energy and G is the gravitational constant; it is the radius at which the velocity dispersion is maximum.
- **core radius** r_c: It is the distance from the center at which the surface brightness drops by a factor of two from the central value; theorists use two different definitions:
  1. when the central density ρ_0 and the velocity dispersion $\langle v^2 \rangle_0$ are easily defined, $r_c = \sqrt{\frac{3\langle v^2 \rangle_0}{4\pi G \rho_0}}$. It corresponds roughly to the radius at which the three-dimensional stellar density drops by a factor 2, and the surface density by a factor 3;
  2. When ρ_0 and $\langle v^2 \rangle_0$ are difficult to determine (N-body simulations) the core radius is the ρ_i-weighted rms stellar distance from the density center: $r_c = \sqrt{\frac{\sum_i \rho_i r_i^2}{\sum_i \rho_i}}$, where ρ_i is the local density for each star.
- **tidal radius** $\mathbf{r}_t$: It is the distance from the center of a cluster where the gravitational acceleration due to the cluster equals the tidal acceleration of the parent Galaxy.

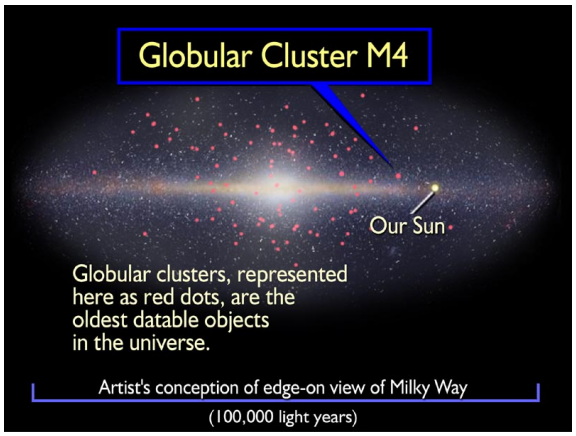

Figure 1.1: Distribution of GCs in the Galactic Plane

The value of r_c and r_{vir} determine the density profile, which is generally assumed to be spherically symmetric. This is the case for the empirical King profiles and dynamical

King models (King, 1962).
Each Globular Cluster, as self-gravitating system, is characterized by the two following time scales:

- **dynamical time scale** t_{dyn}: It is the time required for a star to cross the system

$$t_{dyn} = \left(\frac{GM}{r_{vir}^3}\right)^{-1/2} \sim 2 \times 10^4 yr \left(\frac{M}{10^6\, M_\odot}\right)^{-1/2} \left(\frac{r_{vir}}{1 pc}\right)^{3/2} \tag{1.1}$$

- **relaxation time** t_{rl}: It is the time scale on which two body-encounters transfer energy between individual stars and cause the system to reach thermal equilibrium:

$$t_{rl} = \frac{\langle v^2 \rangle^{3/2}}{15.4 G^2 m \rho \ln \Lambda} \tag{1.2}$$

  where m is the local mean stellar mass, ρ is the local density; the value of the parameter Λ is 0.4N for the ideal case where all stars have the same mass and are distributed homogeneously with an isotropic velocity distribution. Typically, $t_{rl} >>$ t_{dyn}, $t_{rl} \approx \frac{N}{7} \ln \Lambda t_{dyn}$, where N is the number density of the stars.

Historically, Globular Clusters studies have been of crucial importance for the development of the stellar evolution theories. They have been traditionally considered simple stellar populations, made up of coeval and chemically homogeneous stars of different mass, distributed according to an initial mass function (IMF).
Moreover, the Globular Cluster Luminosity Function is used as a secondary distance indicator (e.g. Hanes (1977a,b)); it is thus fundamental to know with high precision their magnitude and distance. There are many methods to calculate the distance to Globular Clusters, including HB, Surface brightness fluctuations (Tonry & Schneider, 1988), brightness of Red Giant branch tip, white dwarf, red clump fitting.
The detailed comparison between the theoretical isochrones and the distribution of GC stars in the observed color-magnitude diagrams allowed a robust calibration of physical phenomena still unknown from first principles, such as convection, velocity of gravitation settling of the various species, details of the atmospheric structure.
The combination of the spectroscopic and photometric data collected in the last decades have partly disregarded the paradigma that GCs are composed by coeval stars, homogeneous in their chemical composition. On the spectroscopic side, already in the 80's we find contributions in the literature suggesting that the surface chemistry of GCs might be much more heterogeneous than commonly believed (Kraft, 1994; Norris et al., 1981). The differences found involved all the species up to aluminium, whereas no difference

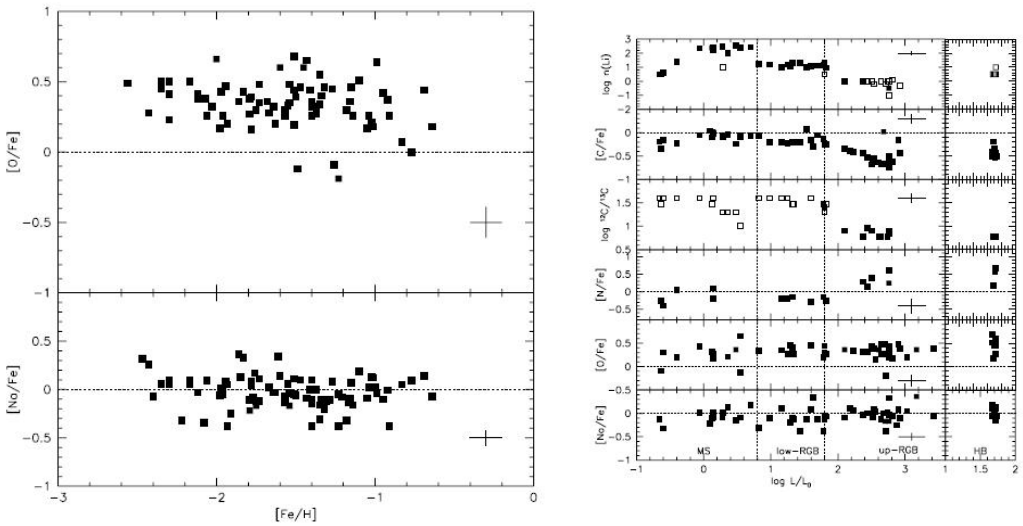

Figure 1.2: Left panel: [O/Fe] and [Na/Fe] abundance ratio of field stars of various metallicity. No a clear trend with the metallicity is present. Right panel: Abundances of lithium, carbon, nitrogen, oxygen, sodium abundances of a sample of field stars by Gratton et al (2000). Use of the luminosity on the abscissa allows to identify the evolutionary stage during the RGB evolution. The vertical, dashed lines, separate different evolutionary phases.

was detected among heavier elements.

This behavior is peculiar of GCs, because halo field stars with same metallicity do not show similar anomalies, the surface abundances of Li, C, N, O, Na being well explained by standard evolutionary models (see Fig. 1.2) (Gratton et al., 2004).

Because the early observations were limited to giants, the most popular interpretation for these chemical anomalies was that they were due to some non canonical extra-mixing taking place after the RG bump, when the smearing of the H-He discontinuity allows a deeper penetration of the surface convective mantle, down to layers previously touched by nuclear activity (Denissenkov & Weiss, 1996).

This hypothesis was disregarded, at least in the capability of providing a full explanation of these observations, when the same chemical patterns were also discovered in stars in less advanced evolutionary stages, such as Main Sequence or Sub Giant Branch stars (Gratton et al, 2000).

On the photometric side, recent investigations have found in some clusters multiple main sequences (Bedin et al., 2004; Piotto et el., 2005), that can be interpreted only on the basis of an excess of Helium, up to Y=0.40. The clusters in which both the chemical anomalies and the multiple main sequences have been detected also show a very peculiar distribution of Horizontal Branch (HB) stars, characterized by extended blue tails, gaps

and anomalous luminosity slope of the flat part.
These observational evidences opened the door to a different interpretation of the evolutionary history of GCs, according to which (at least) a further stellar generation formed, overlapped to the original population. Because no iron spread is observed, this stars must have formed after the epoch of SN II explosion
The gas from which the new stars formed must have been nuclearly processed by high temperature proton-capture nucleosynthesis, and possibly mixed with unprocessed material. A considerable fraction of stars currently in globular clusters belong to the second generations: according to the observations, the percentage of the stars ranges from 30% to 70%.
We shall see that, whatever is the population responsible for the pollution of the interstellar medium, the gas produced is far from being enough to produce a 1:1 ratio between the original population and the newly born stars: we reach the conclusion that GCs were much more massive in early epochs, and most of stars belonging to the original generation were lost.
The multiple populations phenomenon is not peculiar of the Galactic GCs; in fact, Mackey & Brody Nielsen (2007) , thanks to high- precision photometry from ACS/HST images, identified two populations with an age difference of about 300 Myr, in the 2 Gyr old globular cluster NGC 1846 in the Large Magellanic Cloud. Afterwards, Milone et al. (2008), studying Globular Clusters in the Large and Small Magellanic Clouds, found that eleven clusters showed an anomalous spread in color and magnitude around the Main Sequence Turn Off (MSTO) , and confirmed the multiple populations in NGC 1846, NGC 1806, NGC 1751 and NGC 1783.

1.2 Photometric evidence

The first direct observational evidence of the presence of multiple stellar population in GCs was published by Bedin et al. (2004), who found that, for a few magnitudes below the turn-off, the MS of ω Cen splits in two parts, as shown in the left panel of Fig 1.4. Following observations highlighted a much more complex scenario, picking out the presence of multiple sub-giant branch in the same cluster, characterized by different metallicities and ages (Sollima et al., 2005; Villanova et al., 2007). This reinforces the opinion that ω Cen is an anomalous object, probably the remnant of a dwarf galaxy.
Subsequently, multiple MS have been observed also in other GCs, such as NGC2808 (D'Antona et al., 2005), that presents three MS (see the right panel of 1.4). From Piotto et al. (2007), because high resolution spectroscopic investigations could not detect any

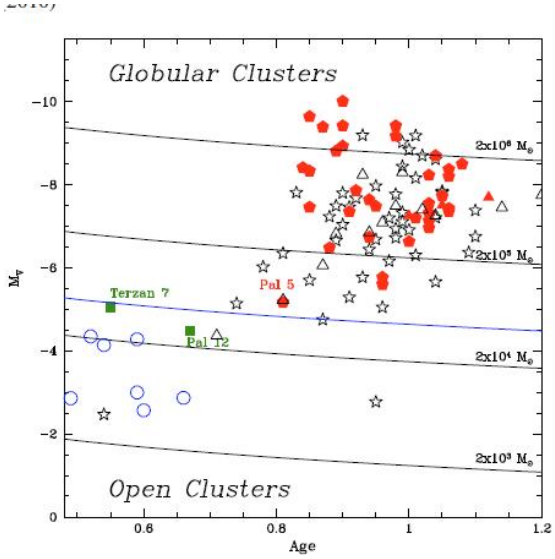

Figure 1.3: Relative age parameters vs. absolute magnitude Mv for globular clusters and old open clusters. Red filled pentagons and triangles are CG with Na-O anticorrelation observed in the Milky way or in the Large Magellanic Cloud, respectively; green squares indicate clusters with no evidence of Na-O anticorrelation, both of them belonging to the Sagittarius dSph; open star and triangles are clusters for which not enough data are available; open circles represent open clusters. The blue line is the proposed separation between globular and open clusters (Carretta et al., 2010).

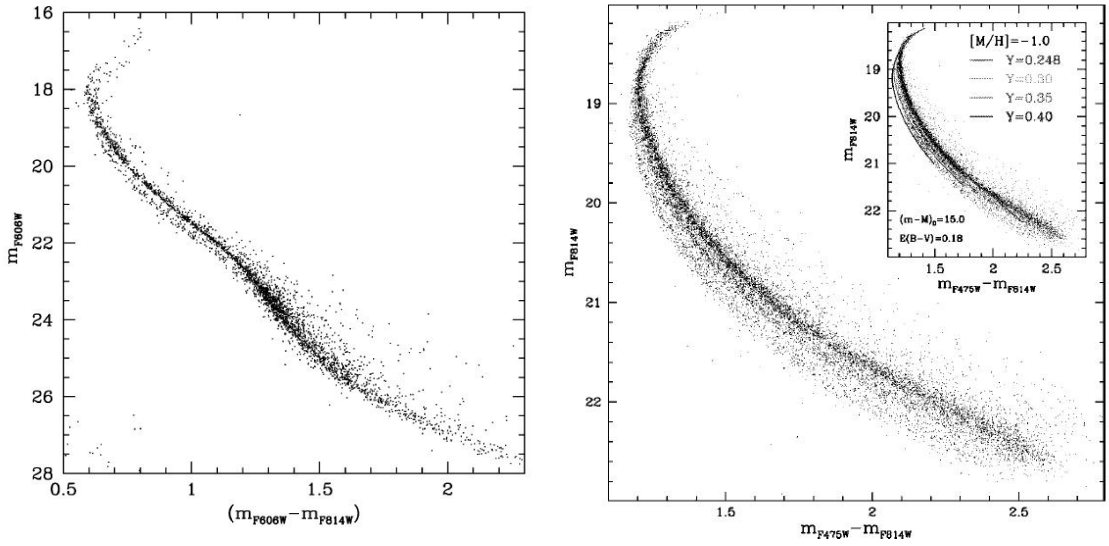

Figure 1.4: Left panel: CMD of Omega Centauri. It is shown MS splitting (Bedin et al., 2004). Right panel: the Multiple MS in NGC 2808 (Piotto et al., 2007).

spread in iron, the explanations for this surprising evidence was that NGC 2808 harbors three distinct populations, with the same metallicity, by differing in their helium content (see Fig. 1.4 right panel). This was in excellent agreement with an earlier speculation by D'Antona & Caloi (2004), that first hypothesized the existence of three populations differing in their helium to account for the anomalous morphology of the HB of the some cluster.
According to the analysis by Piotto et al. (2007) about 13% of the stars belong to the blue MS, 15% to the mild MS, and 63% to the red MS. The remaining 9% are binaries.
The blue MS is populated by stars with an enhanced helium Y $\sim$ 0.40, whereas the red MS, corresponding to the original population in the cluster, is characterized by the Big Bang helium abundance, Y=0.25. The intermediate MS can be reproduced by assuming Y=0.30. This interpretation stems to a well known result from stellar evolution theories, that stars with a higher helium content, due to their larger molecular weight, evolve faster and at higher luminosities, and their MS is bluer than the corresponding MS of stars with a lower helium (see e.g Kippenhahn (1991) Cap. 22).
Further hints of the presence of distinct populations come from the SGB splitting of NGC 1851 (Milone et al., 2008), the broadered MS of NGC 6752 (Milone et al., 2010), 47 Tuc (di Criscienzo et al., 2010; Milone et al., 2012a), NGC 6397 (Milone et al., 2012). The recent analyses by (Piotto et al., 2012) found hints of SGB splitting in eight GCs examined.

1.2.1 Horizontal Branch

The Horizontal Branch of Globular Clusters is populated by stars in the core He-burning phase. This evolutionary stage follows the He-flash, after the degeneracy in the central regions is removed. Stars populating the HB are characterized by sharing the same core mass. The mass of the overlying layers determines the position of these stars in the CM diagram. Stars whose mass barely exceeds the core mass are supported uniquely by the core burning, and populate the blue region of the HB; on the other hand, more massive stars are also supported by a CNO burning shell, and occupy the red portion of the HB.
The distribution of stars in the HB is strongly linked to the age of GCs.
In younger clusters, the evolving mass (i.e. the mass currently in the TO region, which is approximately the same evolving in the RGB tip and in the HB) is larger, which also determines higher masses populating the HB. Older clusters are populated by smaller mass objects. The reason for this is a straight consequence of the faster evolution times of more massive stars. On the basis of the above discussion, it comes out that the HB of younger

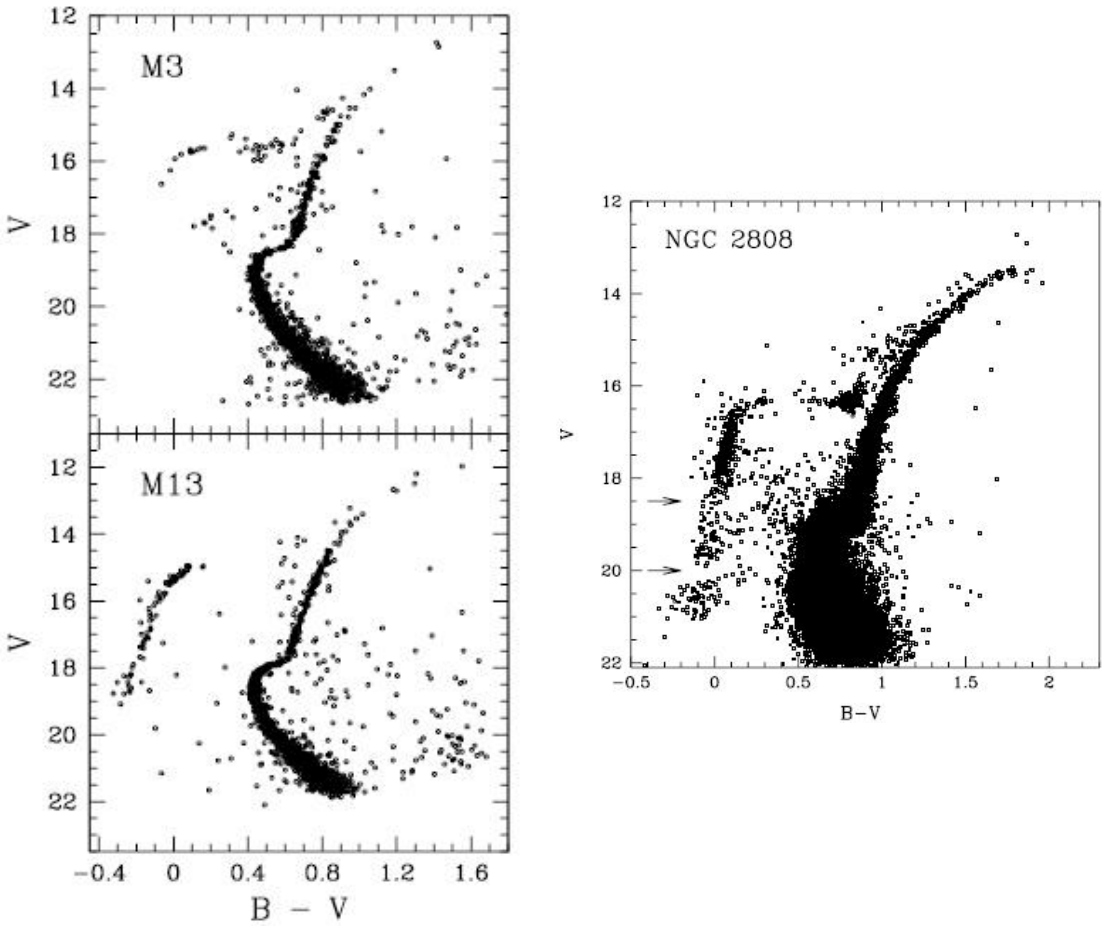

Figure 1.5: Left panel: CMD of the GCs M3 and M13. Right panel : HB morphology of NGC 2808

cluster is red, whereas bluer HBs will characterize older objects.[1] Because age and chemistry are strictly interfaced the composition of stars in GCs is also expected to be relevant in the determining the HB morphology. In particular, because He-rich stars evolve faster, the mass evolving on the HB for a fixed age would be smaller: consequently, the presence of a population enriched in helium would inevitably shift to the blue the distribution of stars in the HB. Note that this would have scarce impact on the MS morphology (see D'Antona et al. (2002)) Historically, the difference in the HB morphology of Globular Clusters similar in age and metallicity (see the CDMs of M3 and M15 in Fig. 1.5) has been referred to as the 'second parameter' problem, to indicate that a further factor, other than age, was relevant in determining the HB morphology. The idea that helium could be the second parameter came when some GCs were observed, whose HB show a rather

[1]This consideration clearly holds assuming the same mass loss along the RGB.

complex structure, in which the distribution of stars in the CMD presents gaps, separating the various components. The classical example is NGC 2808, whose HB presents gaps and clumps, that can be interpreted on the basis of the helium differences (D'Antona & Caloi, 2004)It is possible to distinguish at least three different gaps (see Fig 1.5, right panel), one in the RR Lyre instability strip, the other two on the blue extension and delimit three distinct segments. Use of a helium variation was also invoked to explain the HB morphology of NGC 6441 (Caloi & D'Antona, 2008), and NGC 2419 (di Criscienzo et al., 2011).

1.3 Spectroscopy evidence

High resolution spectra of stars within nearly all GCs studied to date reveal internal spreads in light element abundances such as Na, O, Mg and Al, beyond what can be explained by measurement errors. This feature has not been found so far in any open cluster. The magnitude of the internal spread varies from cluster to cluster, thus suggesting a possible trend with cluster mass and orbital properties (see e.g. Gratton et al. (2004)).
Originally, the first detections of unusual abundances came from the brighter, more accessible RGB. The first was Osborn (1971), that discovered two N-enhanced stars in M 10 and M 5. By now, RGB's of many GCs have been studied, also by means of high-resolution spectroscopy, to discover intrinsic abundance variations in the light elements. See Carretta et al. (2009a,b) for the more recent results. The collection of spectroscopic data are reported in Fig. 1.6.

Spreads in iron abundances have been found only in the most massive GCs, such as ω Cen, M54, M22, Terzan 5 (Ferraro et al., 2009; D'Antona et al., 2010), and it was proposed that these structures are not true GCs, rather relics rests of dwarf galaxies.
Until only the brightest GC red giants stars were accessible for detailed spectroscopic observations, it was plausible that the chemical anomalies are generated in situ, by some non conventional mixing mechanism, occurring during the RGB phase.
At the beginning of the 80's variations were found in light elements in MS stars. Hesser & Bell (1980) found different CN band strengths in seven MS stars of 47 Tuc, similar to those found for giants. This discovery was fundamental for the theory of the origin of the second generation stars: low mass stars do not have a convective envelope able to transport the nuclearly precessed material to the atmosphere, thus the mixing can no longer be invoked to explain the peculiar abundances; moreover, during the MS and SGB phase these objects are not hot enough for the required set of nuclear reactions to occur within

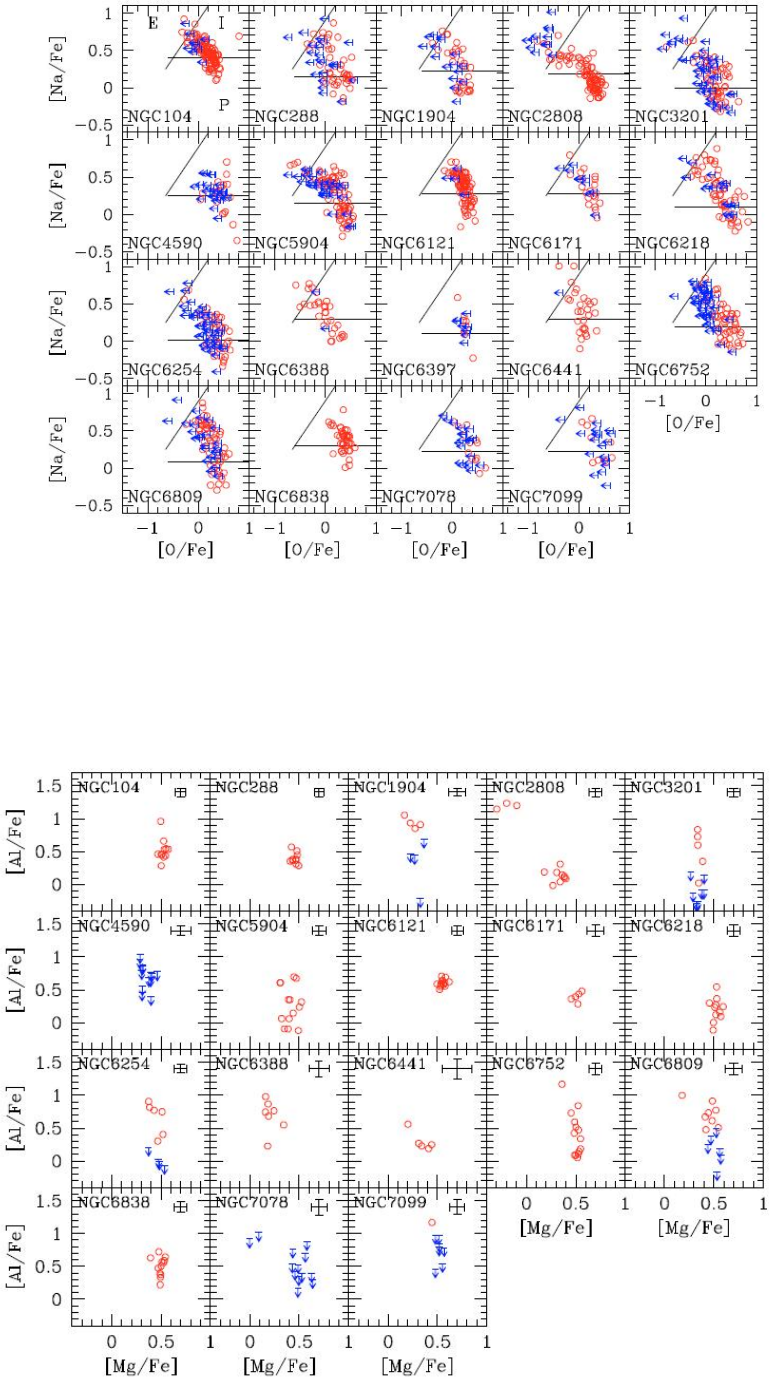

Figure 1.6: Spectroscopic data by Carretta et al. (2009a,b) for several GCs. For every GC are shown Na-O and Mg-Al anticorrelations in the top and bottom panel, respectively.

their interior.
Following observations confirmed variations in the light elements for MS stars (Gratton et al., 2001). The recent results by Bragaglia et al. (2010a) though limited to two stars, are a further indications of the intrinsic pollution of the gas from which He-rich stars, populating the blue MS of GCs, formed. The Sub Giant Branch (SGB) stars contributed, together with the even less evolved MS ones, to the definitive acceptance of a primordial origin for the light elements 'anomalies' (Gratton et al., 2001; Carretta, 2003; Ramírez & Cohen, 2002, 2003; Pacino et al., 2010), since no efficient mixing is possible before the first dredge up episode and the RGC bump.

1.4 Possible Polluters

The discovery of the chemical anomalies in involved or scarcely evolved stars addressed the scientific community to search for some self-enrichment mechanism, able to favor formation of stellar populations in Globular Clusters, overlapped to the original, first generation. This is clearly interfaced with the look for possible polluters, i.e stars belonging to the FG that ejected gas contaminated by process of internal nucleosynthesis.
Whatever are the responsible for such pollution, they must have evolved rapidly, because no clear age difference has been detected so far between stars belonging to different generations. Based on the combination of photometric and spectroscopic results available, it is also possible to infer the kind of nucleosynthesis the polluting gas was exposed to: because the new generations are enriched in Helium, depleted in the oxygen and magnesium content, and show high abundance of sodium and aluminum, we are left with the only possibility that p-capture nucleosynthesis was active, as also confirmed by the approximately constant C+N+O (Ivans et al., 1999)

1. **Massive rotating stars**: Massive stars that rotates with velocity close to break-up. In the internal regions the temperatures are sufficiently high to activate advanced nucleosynthesis. The material is transported to the surface by meridional currents induced by rotation (Prantzos & Charbonnel , 2006; Decressin et al., 2007);

2. **Massive binary systems**: Massive stars in binary systems lose gas via the outer Lagrangian point into a circumbinary disk (de Mink et al., 2009);

3. **Super-AGB and AGB**: Stars composed by a degenerate core and two nuclearly active shells, where helium and hydrogen burning occur. These regions are below

a massive, extended envelope, characterized by strong convective currents, stars with mass M > 4 $M_{\odot}$ experience a penetrating second dredge-up, and a series of p-capture reactions at the bottom of their outer convective zone, and are thus predicted to expel helium-rich matter (Ventura et al., 2001).

1.4.1 Fast Rotating massive Stars

That He-rich stars in ω Cen could be formed from winds of fast rotating massive stars was early proposed by Maeder & Meynet (2006). Prantzos & Charbonnel (2006) completed this model, suggesting that these winds provide the metal-enriched material for the next stellar generations, whose formation was triggered by supernova explosion.
The contaminated gas is produced in the H-burning cores of massive stars. Rotational mixing brings this CNO-processed material to the surface, from where it can then be ejected via a slow wind, when the stars rotate at the critical limit. It has been already shown by many authors (Sackmann & Anand, 1970; Langer, 1998; Maeder & Meynet, 2002) that massive stars can reach the critical velocity[2] during the main sequence under three conditions:

- the initial rotating velocity is sufficiently high;
- they do not lose too much angular momentum via stellar winds;
- an efficient mechanism transports angular momentum from the core to the envelope.

Once the critical limit is reached, the surface velocity remains near this value during the rest of the main sequence, and the material ejected by winds forms an equatorial disk.
Decressin et al. (2007) studied in qualitative way this model, considering stars with initial mass between 20 and 120 $M_{\odot}$. When the critical velocity is reached, the mass loss from equator is released into a Keplerian disk, but when the stars moves away from this limit, the radiatively-driven fast winds take over. The rotational mixing is the key to produce the modifications of the surface abundances, because it allows to transport outwards the products of central burning, through various instabilities induced by rotation. The most important among these are the meridional currents and the shear turbulence: the first carries the angular momentum, while the second behaves as a diffusive process.

Decressin et al. (2007) found that the chemistry of the mass lost from a 60 $M_{\odot}$ model with respect to the original values is the following (see Fig 1.7):

- Carbon and oxygen are diminished, respectively, by 0.9 and 1 dex;,

[2]It is the equatorial surface velocity when the centrifugal acceleration balances the gravity

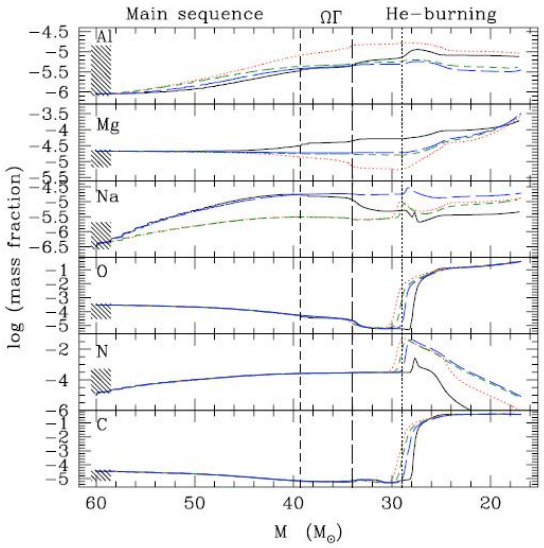

Figure 1.7: Evolution of the surface abundances of a 60 $M_{\odot}$ rotating model computed with various sets of nuclear reactions (Decressin et al., 2007). The vertical lines indicate respectively the end of the second phase(short-dashed), the third phase (long-dashed), and the moment in which the He-burning products appear at the surface.

- Nitrogen and sodium are increased, respectively, by 1.5 dex and 0.8 (or 1.6 dex depending on the assumed nuclear reaction rates);

- Aluminum can be hardly increased, because of the large temperatures required to start ^{24}Mg p-capture. Increase of the relevant cross-section by two orders of magnitude would help allevating this problem.

This scheme allows to reproduced the Na-O and Mg-Al anticorrelations.
The abundances depend on the initial mass of star: more massive stars have higher temperature, thus the rotational mixing is more efficient, and NeNa and MgAl chains are more active in the warmer convective core.
To reproduce the observed data, this model needs the presence of a pristine gas (about 30 %). This model is plausible because according to Maeda & Nomoto (2003), if a supernova explosion occurs, the fast rotation of the core may favour ejection along the rotational axis. In this way the disk is not destroyed. There is an other limitation in this model, that can be possible only if the process of formation is relatively short, it happens between two supernovae events. The new stars form in the disk, or more probably in the interstellar medium. From what has been written, is clear that , even if this model can be plausible, is very unlikely, because we need too much constraints that operate simultaneously.

1.4.2 Massive binary stars

Massive binaries have been proposed as candidate for the internal pollution of Globular Clusters. In fact, theoretical and observational considerations support the idea that most interacting binaries shed large amounts of mass. This material is lost from the system via outer Lagrangian points into a cyrcumstellar disk, and a wider double toroidal nebula.
An example of this is the well studied system RR Scuti, in which the nebula shows signature of CNO processing, is enriched in helium and nitrogen, and depleted in oxygen and carbon (Smith et al., 2002; Grundstrom et al., 2007). Moreover, the winds of these stars have velocities (30-70 Km/s) lower than the present-day escape velocity of massive globular clusters.
The chemistry of the gas lost by this kind of systems was investigated by de Mink et al. (2009). They focused on a system formed by a 20 and 15 $M_{\odot}$ stars, with an orbital period of 12 days, and initial rotation rates synchronized with the orbital revolution. For the initial composition of these stars, it has been assumed an α-enhanced mixture, with a metallicity Z= 5$\times$ 10^{-4}.
After the exhaustion of hydrogen in the center, the primary star begins to expand and transfer mass to the secondary, that initially accretes efficiently mass and angular momentum, thus it spins up.
After accreting 1.5 $M_{\odot}$ it approaches critical rotation, and the majority of the mass of the envelope is ejected from the system. By the time deep layers are ejected, with signatures of nuclear processing. After transferring the whole envelope, the donor contracts, ignites helium, and become a Wolf-Rayet star. At this point the star expands again, and loses further 1 $M_{\odot}$, that will be the most nuclearly contaminated matter. The evolution end when the primary star ignites carbon in the center and fills its Roche lobe; soon after, it will explode as a type Ib/c supernova The average composition of the matter ejected by this

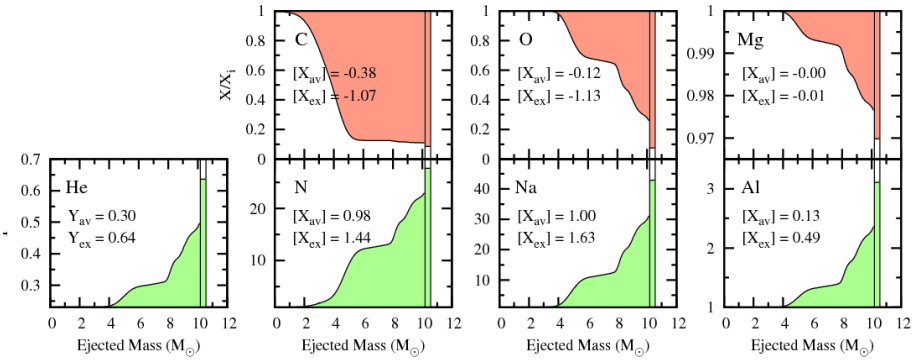

Figure 1.8: Composition of the gas ejected by binary system modeled by (de Mink et al., 2009).

specific system (the total mass expelled is about 10 $M_{\odot}$) is shown in Fig. 1.8: for Carbon Oxygen, Nitrogen, Sodium, and Aluminum we consider the stable isotope, whereas for Mg we show the sum of the three isotopes ^{24}Mg, ^{25}Mg, ^{26}Mg; to understand the extent of the modification compared to the initial chemistry the mass fractions are given relative to the initial mass fraction X_i in a logarithmic scale, [X] = $log_{10}(X/X_i)$. For helium, the absolute mass fraction is shown.

At first, the gas ejected is unprocessed, afterwards we can note the signatures of the CN cycle, thus nitrogen begins to enhanced; in later phases we find helium enrichment and the O-Na anticorrelation is produced. Finally, an average helium of 0.30 is found, an enhancement in sodium by 1.0 dex, whereas oxygen is depleted by -0.12 dex. The sum of carbon, nitrogen and oxygen is constant within a few percents. The temperature in these stars are not high enough to activate efficiently the Mg-Al cycle, that is required to explain the depletion of Mg and the enhancement of Al. In an attempt of solving the mass budget problem (we racall that the observed FG/SG ratio is approximately unity in the GCs so far examined), it is assumed that every star with M > 3 $M_{\odot}$ belongs to an interactive binary system, and that the whole envelope is lost in the ICM. Under these assumptions, the gas available for the SG formation amounts to 26% of the total mass of FG stars, thus rendering less dramatic the mismatch between the required and available gas. The analysis just discussed is however highly qualitative. One of the scopes of the present work is to reconsider the massive binary scenario on more quantitative grounds, by considering the whole range of masses, in all the evolutionary phases. In Chapter 3 we will demonstrate that this model can not produce ejecta in agreement with the observations, because these stars can not reach temperatures sufficiently high to deplete enough oxygen and magnesium.

sur

CHAPTER 2

Asymptotic Giant Branch evolution

2.1 Introduction

The evolution of stars, in particular their final fate, is mainly determined by their initial mass. Stars of different mass follow different evolutionary paths. The various behaviors are separated by some threshold values, of paramount importance in the context of stellar evolution theories.

Of particular interest here are the values of M_{up} and M_{mas}. The former is the limit below which stars do not reach in their interiors temperatures sufficiently large to ignite carbon burning, and will therefore evolve through the AGB phase, on a core made up of carbon and oxygen. M_{mas} represents the limit separating stars that undergo carbon burning in conditions of partial degeneracy, and develop a core of oxygen and neon, from more massive sources, that explode as supernovae[1].

The AGB (1 $M_{\odot}$< M < M_{up}) or SAGB (M_{up} < M < M_{mas}) evolution follows the end of the core helium burning phase.

Following the consumption of internal helium, these stars evolve on a core made up of

[1] M_{up} and M_{mas}decrease with Z and with overshooting. In fact with less metals, the opacity drops and the temperature and surface luminosity increase, the star develops a bigger core which is more inclined to ignite C., Taking account the overshooting, increasing the size of the core and makes the star behave as if it was more massive. M_{up} ranges about 7-9 $M_{\odot}$

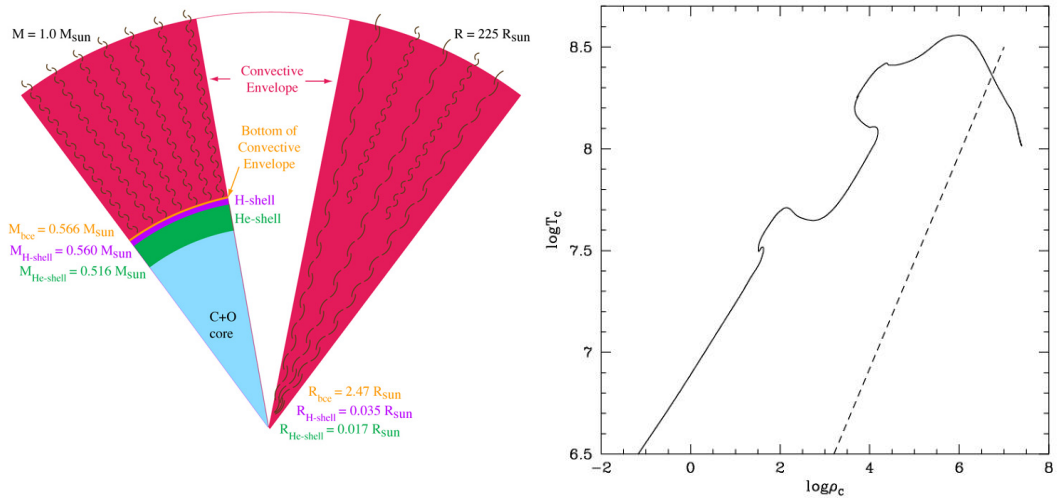

Figure 2.1: Left panel: internal structure of a 1 $M_\odot$ model during the AGB phase. We can distinguish the CO core, two H and He shells, and the external envelope. Both the representations in mass (left) and radius are shown (in this latter, the high central densities make the core and the shell to be indistinguishable). Right panel: the evolution of the central thermodynamic conditions during the evolution of a 6 $M_\odot$model. The two major phases of core H and He-burning can be seen in the temporary decrease in the central densities. The center of this model is seen to become degenerate after the core He-burning phase.

carbon the oxygen. As helium burning moves to a shell close to the center, the core contracts, releasing gravitational energy, and eventually becomes degenerate. The right panel of 2.1 shows the evolution of the central thermodynamic conditions (in terms of density and temperature) of a 1 $M_\odot$ model, during the whole evolutionary history. We may clearly see the two phases of hydrogen and helium burning in the core, and the final cooling, when the track enters the region of degeneracy, ideally limited by the dashed line.

A schematization of the internal structure of these stars is shown in the left panel of 2.1, where the CO core, two layers where helium and hydrogen burn, and an expanded, convective envelope, are indicated.

While the time-scale of the AGB evolution is given by the rate with which the CNO burning shell moves outwards, the overall duration of this phase is determined by the rate at which the envelope is ejected via stellar winds. Typical evolution times range from $\sim 10^6$yr for low-mass stars ($\sim 2\ M_\odot$), down to $\sim 10^4$ yr for M $\sim M_{up}$. After the envelope is ejected, the central core will evolve as a CO (AGB) or ONe (SAGB) White Dwarf. The expanding shell of gas surrounding the WD progenitor in commonly referred to as Planetary Nebula.

The last decades have seen a graving interest toward the AGB evolution:

M/ $M_\odot$	$\tau_H/10^6$	$\tau_{He}/10^6$	$M_{core}/M_\odot$	log(L/ $L_\odot$)$_{max}$	T^{bce}_{max}(MK)
Z=0.001					
2.0	736	221	0.50	4.40	15
3.0	280	55	0.73	4.50	60
4.0	147	25	0.85	4.55	93
5.0	91	15	0.94	4.75	100
6.0	63	9	1.01	4.95	112
7.0	47	5.5	1.20	5.08	120
8.0	37	4.7	1.36	5.30	148

Table 2.1: Evolutionary properties of stars of different mass. The luminosity and the temperature is related to AGB phase.

- AGB stars could be important stellar sources of dust in the high-redshift Universe (Valiante et.al, 2009);
- AGB stars have been suggested as the mainly responsible for the self-enrichment of globular clusters, to explain the existence of multiple populations.

2.2 Physics of AGB

The AGB phase is generally divided into two phases: the early AGB (E-AGB) and the thermally pulsating AGB (TP-AGB).
The early AGB is by far the longest part of the AGB evolution, and begins after central helium burning stops. The star is then supported by two active burning shells, and double mirror effect operates: the core contracts, the He-rich layers above expand, and the outer envelope contracts.
The hydrogen shell cools down in response to the expansion of the layers below thus CNO burning is extinguished. In this phase the whole envelope expands in response to core contraction, and the stellar luminosity is provided almost entirely by the He-burning shell. The release of gravitational energy in the contracting envelope eventually favor re-ignition of CNO burning. At this stage the He-burning shell that lies underneath becomes geometrically thin. Because nuclear burning in such a thin shell is not thermally stable, He-burning is not continuous, rather periodic: the ignition of the 3α shell is commonly referred to as ”thermal pulse”. Two thermal pulses in a row are separated by the inter pulse phase, during which the only nuclear support is provided by the CNO activity in the

hydrogen burning region.
The number of thermal pulses experienced by the star and the duration of this phase is determined by the mass loss rate.

Thermal Pulses

A detailed description of the instability behind the thermal pulse phenomenon can be found in Appendix A.
Each pulse can be divided in 4 phases:

- *off phase*: the He shell is off, the surface luminosity is provided by the H-shell. It goes on for 10^4-10^5 years, depending on the core-mass;

- *on phase*: when the mass of the inter-shell region reaches a critical value, helium burning starts in conditions of thermal instability, giving rise to a thermonuclear runaway; the He-shell burns very strongly, producing a luminosity that reaches $\sim 10^8\, L_\odot$. This enormous amount of energy drives the expansion of the overlying layers. This phase is very quick, lasting only about 10-100 years;

- *power down phase*: 3α-burning begins to die down, and the inter-shell convection is shut-off. The expansion continues, pushing the H-shell to such low temperatures and densities that CNO burning is extinguished;

- *dredge-up phase*: the convective envelope, in response to the cooling of the outer layers, extends inward and, in more advanced phases, can reach zones contaminated by 3α nucleosynthesis.

In the left panel of fig. 2.2 we show the trend of the total luminosity of the star (L), and of the individual contributions from CNO (L_{CNO}) and He-burning ($L_{3\alpha}$) during a pulse for an intermediate mass model, of initial mass M= 5 $M_\odot$; in the right panel we show the trend of the radius of the star during some pulses. We note that the total luminosity keeps constant, because the increase in $L_{3\alpha}$ is counterbalanced by the decrease in L_{CNO}. During the thermal pulse the radius of the star decreases, because the external layers contract to compensate the deficiency in the CNO channel; when CNO-burning is re-ignited the radius increases, as also the total luminosity. In the HR diagram the evolutionary tracks undergo a series of loops, while climbing on the red giant region.
The stellar properties of the AGB stars depend mainly on the mass of the degenerate core; core mass and luminosity are found to obey the classical relation derived by Paczynski

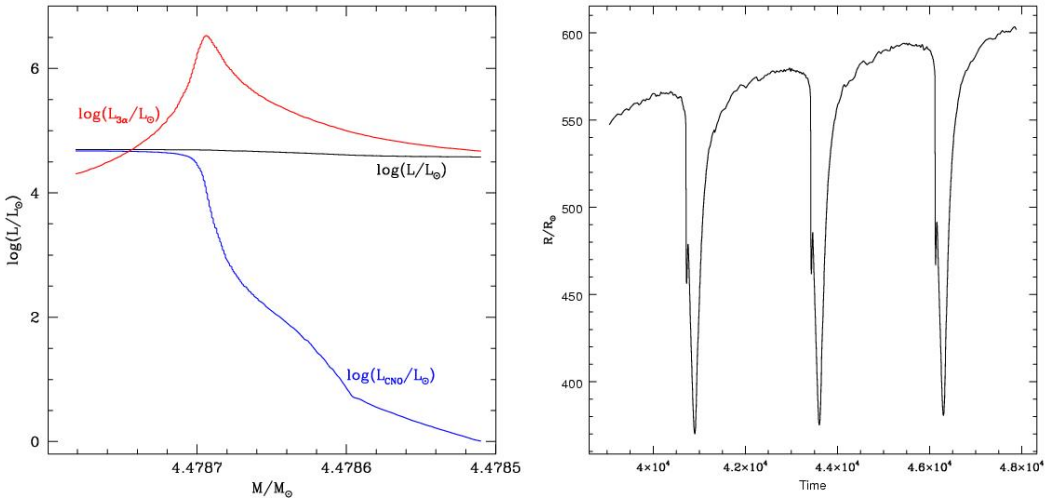

Figure 2.2: Left: Variation of the total luminosity (black) and of the individual contribution from the CNO(blue) and 3α-burning (red) shell, during a thermal pulse of a model with initial mass 5 $M_{\odot}$. The total mass of the star (decreasing with time) has been chosen as abscissa. Right: Variation with time (counted from the beginning of the AGB phase) of the stellar radius, during 4 inter-pulse phases. Occurrence of thermal pulses can be deduced by the sudden drop in the radius.

(1970):

$$\frac{L}{L_{\odot}} \sim 6 \times 10^4 \left(\frac{M_c}{M_{\odot}} - 0.52 \right) \tag{2.1}$$

This relation finds a motivation in the large densities and pressures in the interior of massive, degenerate cores: these extreme conditions reflect into the CNO burning shell laying above, which will evolve at large pressure, thus experiencing nuclear activity at very large temperatures. This is the reason for the increase in the luminosity accompanying the growth of the core mass.

The gradual increase in the overall luminosity during the AGB evolution is halted at a certain stage by the reduction of the mass of the surface envelope, due to mass loss: the luminosity is thus expected to reach a maximum during this evolutionary phase, and to decline after a substantial loss of the envelope has occurred. Fig. 2.3 shows the evolution of the luminosity of stars with different mass during the AGB phase. In the left panel we show the evolution with time for two models of initial mass 3 $M_{\odot}$ and 6 $M_{\odot}$. Times in the abscissa are counted from the instant when central helium is consumed.

The evolution time decreases with mass: this is because the CNO shell of more massive models is more efficient, thus proceeds outwards more quickly, provoking a faster growth of the degenerate core, hence, on the basis of eq.2.1, of the luminosity.

The right panel of Fig. 2.3 shows the variation of the luminosity of models with mass

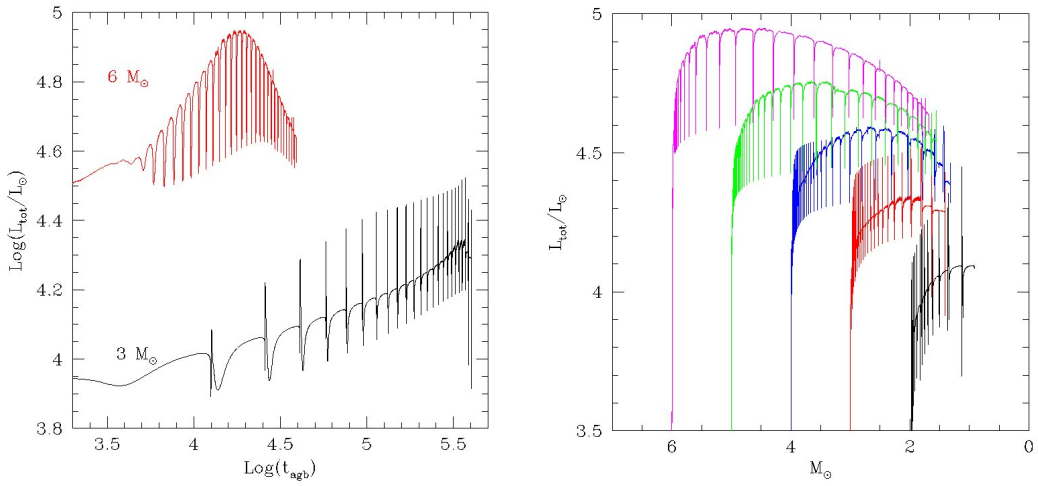

Figure 2.3: Left:Variation with time (counted from the beginning of the AGB evolution) of the luminosity of two models of initial 3 $M_{\odot}$and 6 $M_{\odot}$. Note the difference in the evolution times. Right: Variation of the luminosity of AGB model pf different initial mass as a function of the total mass of the star (decreasing during the evolution.)

in the range 2 $M_{\odot}\leq$ M $\leq$ 6 $M_{\odot}$. In this case we use the total mass of the star (decreasing during the evolution) as indicator of the evolutionary stage. This modality of representing the AGB evolution will turn particularly useful when discussing the variation of the surface chemistry, because pollution is determine by the mass lost at given evolutionary stage, not by its duration. More massive models, in agreement with eq. 2.1, evolve at higher luminosities. The difference in the maximum luminosity reached by models of the initial mass 2 $M_{\odot}$and 6 $M_{\odot}$amounts to almost a factor 10. In all cases we note the initial increase in the luminosity, followed by a phase of decrease, associated to the mass lost by the star.

Chemistry

The first process that alters the surface chemistry of the AGB stars takes place shortly after the end of the helium burning phase. In the early AGB phase, as the core continues to contract, the helium-burning shell narrows and strengthens, forcing the material above it to expand and cool. As the effective temperature continues to decrease, the convective envelope deepens again, extending downwards until crossing the chemical discontinuity between the hydrogen-rich outer layers and the helium-rich region above the helium-burning shell: this phenomenon is called **II dredge up (II DU)** .

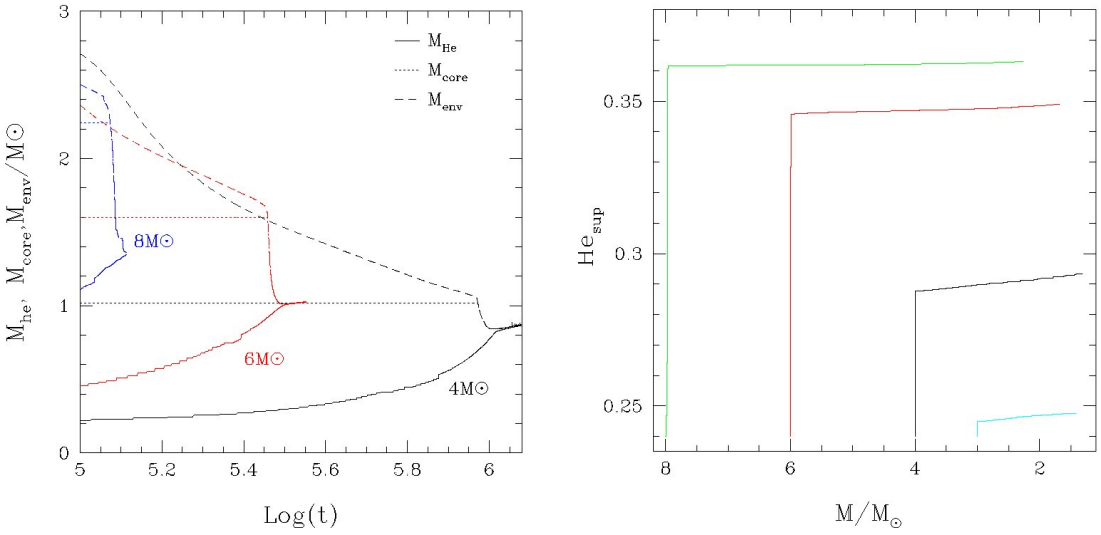

Figure 2.4: left panel:Time variation of masses of core (point line) envelope(dashed line) and of helium (solid line) for a 4 $M_{\odot}$ (black) 6 $M_{\odot}$(red) and 8 $M_{\odot}$(blue). Right panel:Abundances of surface Helium with different initial mass

The mixing that results increases the surface abundances of He, ^{13}C and ^{14}N in the envelope, whereas H, ^{16}O and ^{12}C decrease.

Fig. 2.4 (left panel) shows the occurrence of the II DU for models of mass 4 $M_{\odot}$, 6 $M_{\odot}$ and 8 $M_{\odot}$. The lines in the figure indicate the base of the convective envelope (dashed), the H/He interface (dotted) and the border of the C-rich zone (solid). The difference in mass between the H/He interface and the CO core gives the mass of He-rich buffer.

The location in mass of the H/He interface does not change, because the CNO burning shell is temporary extinguished. The II DU begins when the base of the convective zone reaches the H/He discontinuity, and penetrates further inwards, until it approaches the helium burning shell (that can be approximately identified with the solid lines in the figure), that forces convection to reced. Mixing of helium-rich matter below the H/He interface with the hydrogen-rich envelope favors the increase in the surface helium, which can be clearly seen in the right panel of 2.4, showing the variation of the surface helium during the whole AGB phase of the same models shown in the left panel.

From the trend of surface helium with mass we deduce that most of the helium enrichment is achieved during the IIDU, with little additional contribution from the following phase. The helium increase at the surface is larger for models of higher mass, whose envelope penetrates more inwards.

In the 4 $M_{\odot}$ model (black) the surface helium reaches almost 0.30, whereas for a M=8 $M_{\odot}$

(green) the helium rises up to 0.36. Conversely, for a M= 3 $M_{\odot}$ (cyan) the helium remains unchanged (Ventura, 2010).
During the AGB phase, other two mechanism can alter the surface chemistry:

1. **Third Dredge Up (TDU)**: In the phases following the He-ignition, the CNO burning shell is temporary extinguished (see 2.2). The convective shell that forms spreads the products of 3α burning, mainly carbon, to more external layers, just below the H/He discontinuity. In these conditions, the inwards penetration of the surface convective zone may eventually cross the H/He interface, determining an increase in the surface carbon. This phenomenon, called Third Dredge Up may eventually lead to the formation of a carbon star.
   The physics of the TDU phenomenon is far from being completely understood (see Mowlavi (1999) for an exhaustive discussion on this topic); the results are unfortunately extremely sensitive to the treatment of the convective borders for what concerns the base of the envelope, and the extension of the convective shell driven by the thermal pulse.

2. **Hot Bottom Burning (HBB)**: in more massive AGBs (M > 4 $M_{\odot}$), the base of the external envelope becomes so hot ($T_{bce} > 30 \times 10^6$ K) that it triggers strong p-capture nucleosynthesis (Renzini & Voli, 1981; Blöcker & Schönberner, 1991). The consequent changes in the original chemistry might easily reach the surface of the star because of the rapidity of the convective motions, so that the ejecta of these stars are contaminated by such advanced nucleosynthesis: carbon and oxygen decrease, whereas surface nitrogen increases; when the temperature exceeds $\sim$ 70 MK, the Ne-Na and Mg-Al chains are also activated, with the increase in the surface sodium and aluminum, and the decrease in the magnesium abundance (Ventura & D'Antona, 2011; Ventura et al., 2002).

The yields of AGBs depend strongly on which of the two above mechanisms dominates. The first favors a rapid increase in the carbon an nitrogen content of the envelope, leaving unchanged the abundances of Na, Al, Mg and O, whereas when the second is active we expect a constant C+N+O, while the abundances of the various elements will reflect the equilibrium values, of p-capture nucleosynthesis corresponding to the temperature at the base of the convective envelope. While the TDU is crucial for a number of astrophysical context, we focus here on the effects of HBB, because the working hypothesis of the present work is that only the most massive AGBs, whose chemistry is mainly determined by HBB, produced the gas from which further star formation occurred in Globular Clusters.

2.2.1 Hot Bottom Burning (HBB)

Massive AGBs do not follow the classic L-M_c relation found by Paczynski, given by 2.1. The temperature and density gradients are so steep in their interiors that the CNO burning shell is partially overlapped with the external envelope, with no radiative buffer separating the two regions.

In this conditions, advanced nucleosynthesis can occur in the internal regions of the envelope; given the rapidity of convective currents, the effects of such nuclear activity will easily reach the stellar surface. This phenomenon, called **Hot Bottom Burning**, is important because it is an efficient way to pollute the interstellar matter with nuclearly processed gas from p-capture reactions (Ventura et al., 2001).

We show in Fig. 2.5 the variation of the surface abundances of the CNO elements for the same models of 3 $M_\odot$ and 6 $M_\odot$ shown in the left panel of Fig 2.3. Times are counted from

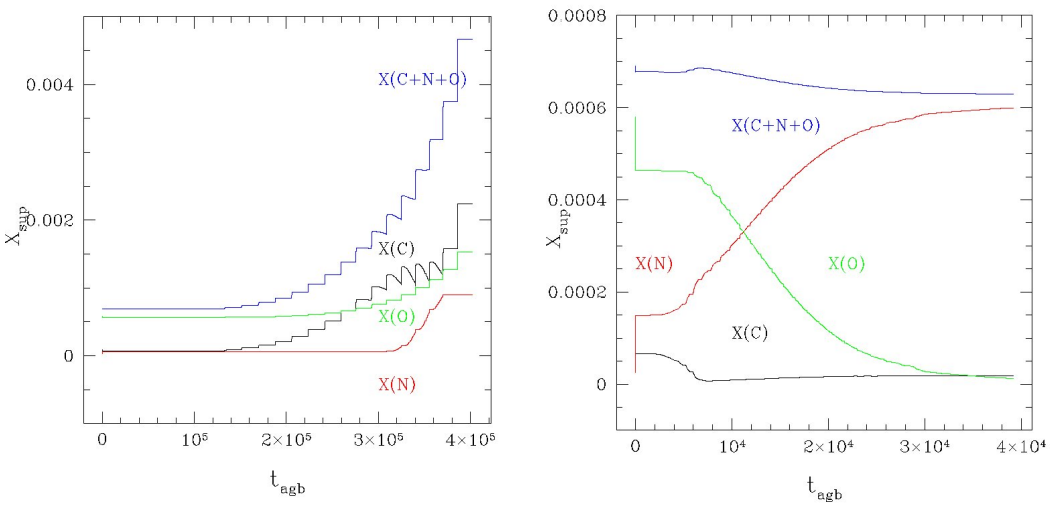

Figure 2.5: Variation of the surface abundances of C, N, O and on the C+N+O total during the whole AGB phase of models of initial mass 3 $M_\odot$ (left) and 6 $M_\odot$ (right)

the beginning of the AGB phase.

The surface chemistry of the 3 $M_\odot$ model is dominated by TDU. The abundances of C, N, O keep constant during the first part of the AGB evolution, until TDU occurs, favoring the increase in the carbon (and also oxygen) content of the envelope.

We also note in the temporary decrease in the carbon abundance during the inter-pulse phase the effects of a soft HBB. The overall C+N+O content, in agreement with the discussion in the previous session, increases.

The chemistry of the 6 $M_\odot$ is entirely determined by HBB. We first note at the beginning

of the AGB phase a decrease in the carbon and the oxygen surface content, and an increase in nitrogen. The overall C+N+O content keeps practically constant during the following phases, the depletion of oxygen and carbon being balanced by the increase in the surface nitrogen.

Before entering into the description of the yields expected by massive AGBs, we address the issue of lithium synthesis. Historically, lithium production was the first argument that stimulated the debate on the HBB, because AGBs were recognized as the only class of stars where lithium could be produced, rather than destroyed.

This opened the way to further investigations, aimed at understanding under which conditions AGBs could account for the super-rich lithium stars observed in the Galaxy and the Magellanic Clouds.

The mechanism of lithium productions was hypothesized by Cameron & Fowler (1971). When the temperature at the bottom of the surface mantle reaches $\sim$ 30MK, α-capture by ^3He nuclei leads to the formation of beryllium ($^3He + \alpha \rightarrow ^7 Be + \gamma$). This latter element is unstable against electron-k capture, and forms lithium; because this process is rather slow ($\tau \sim 60$ days), part of the beryllium is carried to outer layers by convective motions before it decays to lithium. This interplay between nucleosynthesis and convective current makes part of the lithium to be produced in cool, external regions, where it may survive to proton capture.

Fig. 2.6 shows the variation of the surface lithium in models with M > 4 $M_\odot$, experiencing HBB. The quantity shown in the ordinate is Log$\epsilon(Li)$ =12+Log$\frac{n(Li)}{n(H)}$. We see that independently of mass the surface lithium increases by a factor $\sim 10^4$, and later declines; the lithium-rich phase lasts until there are ^3He nuclei available in the envelope, after which no lithium can be reproduced in the external layers.

Because we are interested in the role that massive AGBs might have played in the pollution of the interstellar medium of Globular Clusters, to understand whether they may account for the observed chemical patterns defined by GC stars, we now focus on the variation of the elements defining the classic O-Na and Mg-Al anti-correlations.

The variation of the surface Oxygen and Sodium abundances at the surface of models with different initial mass, are shown in the left panel of Fig. 2.7.

The 6 $M_\odot$ model achieves the strongest destruction of oxygen, the final value being decreased by a factor $\sim$ 30 compared to the initial abundance. Lower mass models experience a softer HBB, thus the oxygen destruction is weaker. In more massive models, in the SAGB domain, the stronger HBB is accompanied by a higher mass loss rate, such that the envelope is lost before an advanced depletion of the surface oxygen occurred: this is the reason why in the 8 $M_\odot$ the gas ejected is more rich in oxygen than the 6 $M_\odot$ model.

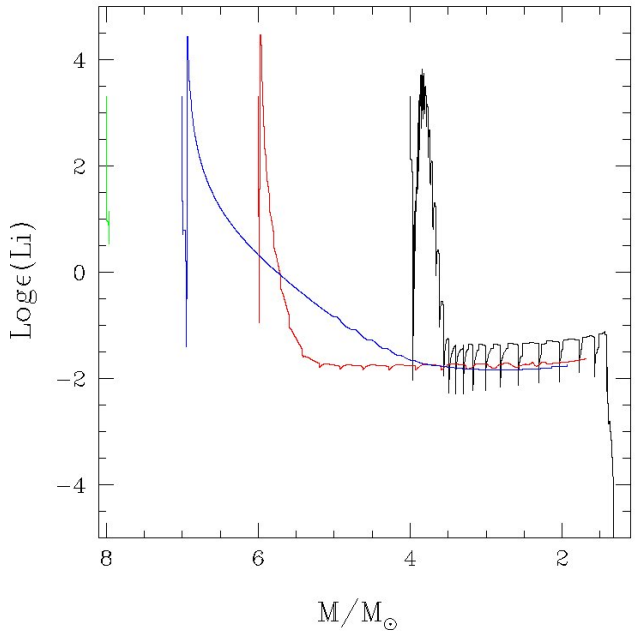

Figure 2.6: Variation of the surface lithium content during the whole AGB phase of models with initial mass 4 $M_{\odot}$, 6 $M_{\odot}$, 7 $M_{\odot}$, 8 $M_{\odot}$. The quantity reported on the y-axis is Log$\epsilon(Li)$= 12+Log$\frac{n(Li)}{n(H)}$

Unlike helium, we find that for the other species the variation is not monotonic with mass, and that the most extreme chemistries, those mostly different from the initial mixture, are achieved in models M $\sim$ 6 $M_{\odot}$, at the edge between AGB and SAGB. The behavior of sodium is more trickly, because it depends on the relative equilibrium between the production and destruction channels:

$$^{22}Ne + p \rightarrow ^{23} Na + \gamma \tag{2.2}$$

$$^{23}Na + p \rightarrow ^{24} Mg + \gamma \tag{2.3}$$

Until T_{BCE} < 60 K the production channel prevails, while at larger temperatures the situation is reversed; the combined effects of the second dredge up and the early burning of ^{22}Ne is partially compensated by the activation of the destruction channel via proton capture by sodium nuclei. On the average, these models are expected to produce sodium, but the yields are predicted to be anti-correlated with the stellar mass.
The sodium yields determined by HBB activity are presently the least reliable, not only because the surface sodium comes from the balance between two p-capture channel, but also because the cross-sections of the relevant reactions, particularly the $^{22}Ne(p,\gamma)^{23}Na$, are uncertain by factor $\sim 10^3$.

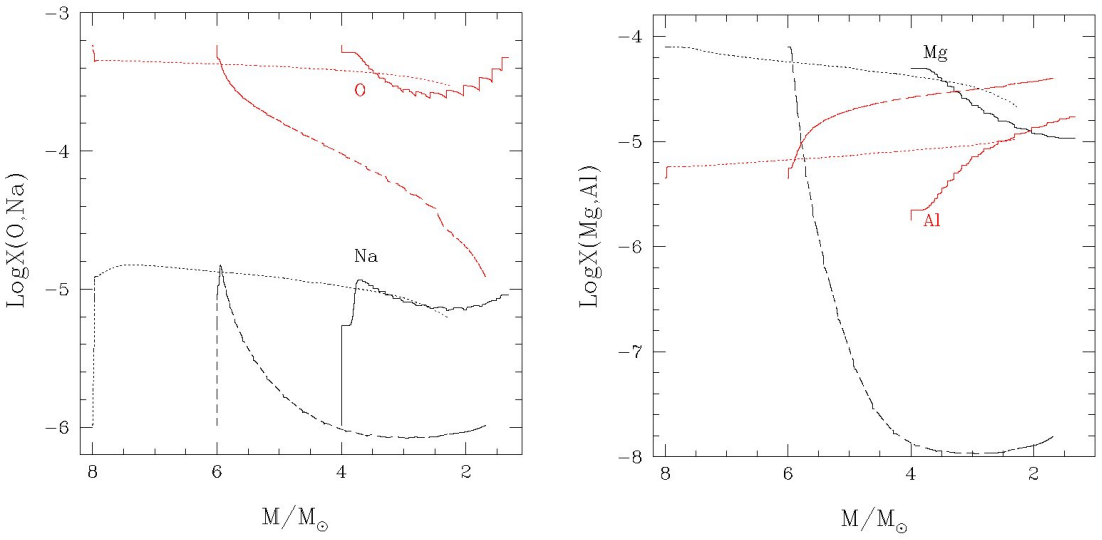

Figure 2.7: Left Panel:Variation during the evolution of AGB of Oxygen (red color) and Sodium (black color) abundances at the surface of models with initial masses 4 $M_{\odot}$(solid line) 6 $M_{\odot}$(dashed line), 8 $M_{\odot}$(dotted line). Right Panel: Variation during the evolution of Magnesium (black color) and Aluminum (red color) abundances at the surface of models with initial masses 4 $M_{\odot}$(solid line), 6 $M_{\odot}$(dashed line) and 8 $M_{\odot}$(dotted line)

The Mg-Al chain is composed by the reactions:

$$^{24}Mg + p \rightarrow \gamma +^{25} Mg \tag{2.4}$$

$$^{25}Mg + p \rightarrow \gamma +^{26} Mg \tag{2.5}$$

$$^{26}Mg + p \rightarrow \gamma + 27Al \tag{2.6}$$

$$^{27}Al + p \rightarrow \gamma +^{28} Si \tag{2.7}$$

^{24}Mg is destroyed when $T_{Be} \sim$ 60-70 MK and ^{27}Al is produced by a p-capture chain that also increases the surface mass functions of the two heavy magnesium isotopes, ^{25}Mg and ^{26}Mg

The right panel of Fig. 2.7 shows the variation in the surface abundances of Magnesium and Aluminum. We show here the total magnesium, given by the sum of the mass fractions of the individual isotopes.

Similar to the oxygen nucleosynthesis, we find that the strongest depletion of magnesium (and consequently the largest Al-production) is produced in models at the edge between AGB and SAGB evolution. The production of Al increases with the mass, to an upper limits [Al/Fe] $\sim$ 1, after the mass loss prevails. The uncertain of the cross sections of the reactions of the Mg-Al channel make the results uncertain by about 0.3 dex.

2.3 Uncertainties on the theoretical ejecta

The theoretical modeling of the AGB phase turns out to be extremely sensitive to the physics adopted, and particularly to some phenomena not known from first principles. The biggest uncertainties concern the treatment of convection (both for what regard the efficiency of convection and the treatment of the borders), the mass loss mechanism, and also the poorly known cross-sections. We analyze these effects and show how they influence the yields of AGBs.

2.3.1 Convection

Convection is an energy transport mechanism active in stellar interiors. It can be schematized by bubbles moving into the star, that after traveling a certain distance dissolve, and release their gravothermal heat excess (Kippenhahn, 1991).
There is no reliable analytic way to predict the flux carried due to convection, because turbulence is a highly nonlinear diffusive phenomenon. This is the reason why in the modern evolution codes convection is treated as a local phenomenon: the temperature gradient is calculated by means of the values that some physical quantities assume in a given layer, independently of the thermal stratification of the surrounding regions. Although this approach neglects non locality, which is known to play a fundamental role, particularly close to the borders, it can be easily implemented into any evolution code, allowing a determination of the temperature stratification in regions unstable to convective motions.
Two models have been proposed so far : the traditional Mixing Length Theory (MLT;Vitense (1953)), and the Full Spectrum of Turbulence (FST) model (Canuto & Mazzitelli, 1991; Canuto et al., 1996).
The MLT treatment is extremely simple. Although convective turbulence is characterized by eddies of all sizes, and is compressible, the MLT considers only one large eddy, and treats turbulence as incompressible (speed of sound $c_s^2 \rightarrow \infty$). The dimension of the convective eddies and the mixing length are expressed by the equation:

$$l = \alpha H_p \tag{2.8}$$

where H_p is the pressure scale height defined as $\frac{1}{H_P} \equiv -\frac{1}{P}\frac{dP}{dr}$; it is the distance over which the gas pressure decreases by a factor e. α is the free parameter calibrated in order to reproduce the evolution of the Sun (the most recent estimates give α =1.7).
The FST description of turbulence is more realistic, for it includes the large spectrum of eddies that characterize a nearly inviscid medium, such as the stellar interiors. The mixing

scale is assumed to be the distance from the nearest convective border.
The differences between the results obtained from the two models are:

1. In regions where most of the energy is transported by convection, the degree of overadiabacity ($\Lambda - \Lambda_{ad}$ where $\Lambda = \frac{dlogT}{dlogP}$) predicted by FST model is smaller.

2. In regions where the efficiency of the convection is low, FST model shows an over-adiabatic peak, higher and narrower than the MLT model.

The difference in the convective modeling is not relevant in the description of the MS phase, because core convection is so efficient that the stratification is nearly adiabatic. The description of the Red Giant Branch (RGB) phase partly depends on the convection model adopted: the reason is that a considerable fraction of the extended envelope is at low convection efficiency, thus the temperature stratification is over-adiabatic. This has only a modest impact on the evolutionary time-scales, because the nuclear active regions are within the radiatively stable region, but may influence the radius of the star.
The modeling of the AGB phase is, within the context of stellar evolution, the most sensitive to the description of convection. This is particularly true for the models with the highest core masses, where the gradients of the thermodynamic variables are steeper. The stratification of the temperature in regions close to the internal boundary of the convective mantle changes according to the convection model adopted, and this, in turn, reflects on the location of the boundary. Use of the FST model leads to a steeper ∇_{rad}, with the consequent, inner location of the convective/radiative interface (Ventura & D'Antona, 2005). Also, because the regions close to border are of high convection efficiency, the temperature profile predicted by FST is flatter, thus extending the region potentially touched by nuclear activity.
In models with large core masses, we thus find in the FST case an 'extra luminosity', because hydrogen and CNO-rich material is exposed to large temperatures.
Because most of the mass is lost from AGBs during the phases of maximum luminosity, and since use of a more efficient convection modeling favors higher temperatures at the bottom of the convective envelope, the theoretical yields calculated with the FST treatment will show-up a clearer signature of HBB.
Independently of the convective model adopted we find:

- The treatment of convection has a scarce affect on the amount of helium produced and expelled by AGB, because most of the helium enrichment takes place during the second dredge-up (see right panel of Fig 2.4) with negligible increase in the following phases.

- The lithium content of the ejecta is also expected not to be extremely sensitive to convection modeling: this latter influences the maximum temperature reached by the bottom of the envelope during the AGB phase, but has no effect on the earlier phases, when lithium is first produced, then destroyed (see Fig. 2.6)

For the other elements, the change in the surface chemistry, and thus the pollution of the interstellar medium, is different according to the convective model used. In MLT models we find a modest depletion of oxygen, a scarce production of sodium, and an increase in the overall C+N+O content. On the contrary, using the FST model for convection, we find a greater destruction of the surface oxygen. Because the stronger HBB in the FST framework, leads to a great increase in the rate at which mass loss occurs (as a consequence of the increase luminosity) the number of thermal pulses experienced is small: the effects of TDU are negligible, thus the overall C+N+O keeps approximately constant.

The overall CNO keeps approximately constant, because of the smaller number of thermal pulses experienced.

2.3.2 Rate of mass loss

Throughout this work, mass loss during the AGB phase was modeled following the treatment outcome of Blöcker (1995). The outcome of the Blöcker analysis is a modification of the Reimer's formula to simulate the rapid increase in mass loss with the luminosity, as suggested by hydrodynamical simulation of M-stars winds (Bowen, 1988):

$$\dot{M} = 4.83 \times 10^{-9} M^{-2.1} L^{2.7} \dot{M}_R \tag{2.9}$$

Here $\dot{M}_R = 10^{-13} \eta_R \frac{LR}{M}$ is the Reimer's mass loss rate, and η_R is a free parameter directly connected with mass loss rate; based on a calibration aimed at reproducing the luminosity function of Li-rich stars in the Magellanic Clouds, we assume as standard value $\eta_R = 0.02$. The treatment of mass loss is extremely important for the AGB evolution, as discussed in 2.2, mass loss eventually halts the increase in luminosity, because it determines a general cooling of the structure, reducing the HBB intensity at the base of the convective envelope. The effects of mass loss become evident when the envelope is considerably reduced (see Fig. 2.3). Use of a higher mass loss rate not only leads to a shorter duration of the AGB phase, and to a smaller number of thermal pulses; even more important, the maximum luminosity reached by the star, and the temperature at the bottom of the convective mantle, are consequently reduced. This has a direct feedback on the extent of the HBB

experienced, which is straightly related to the temperature at which the base of the envelope is exposed.
When we use a great η_R the consequences are:

1. A smaller enrichment in nitrogen, the abundance of carbon in independent is unchanged;

2. A smaller depletion of oxygen, because a substantial part of the envelope is lost when the abundance of oxygen is still large, in the early AGB phases;

3. The overall C+N+O is constant, because a higher mass loss prevents a great number of TDU episodes;

4. The gas ejected is sodium-rich, because a great fraction of mass is lost during the phase when the envelope is enriched in this element, before the destruction channel prevails;

5. The extent of Mg-depletion is reduced.

The only exception is the production of He: its prediction is rather robust, because its increase in the surface is preliminary to the TP phase.

2.3.3 Nuclear cross sections

A variation of the cross sections of nuclear reactions could potentially favor a change in the release of the total energy, that in turn could influence the thermal stratification of the star.
From the chemical point of view, it may alter the equilibrium abundances, thus the average yields of the ejecta. The comparison of models calculated with NACRE and the CF88 (Caughlan & Fowler, 1988) compilation show that the physical behavior of the stars is the same, because the rate of the reactions that contribute mostly overall energy release, namely the proton-capture by carbon and nitrogen nuclei.
In the CF88 case the cross section of $^{17}O(p,\alpha)^{14}N$ is smaller, thus we find a higher production of the heavy isotopes of oxygen, ^{17}O and ^{18}O, and the abundances of ^{12}C, ^{14}N, ^{16}O are smaller.
In the NACRE compilation the cross section of the reaction $^{22}Ne(p,\gamma)^{23}Na$ is higher, thus the production of ^{23}Na is reached more efficiently. Moreover, in CF88, the reaction rate of $^{26}Mg(p,\gamma)^{27}Al$ is higher (of a factor 10), favoring the production of aluminum and the destruction of ^{26}Mg, while the isotopic ratio $\frac{^{25}Mg}{^{24}Mg}$ is similar in both cases.

2.4 Super Asymptotic Giant Branch

The evolution of stars in the range mass between $\sim$ 6.5-8 $M_{\odot}$is characterized by the off-center ignition of Carbon in conditions of partial degeneracy; this is followed by the development of a convective flame, that will transform the CO core into a degenerate neon-oxygen mixture. These stars can either enter in the super-AGB phase, where recurrent thermal instabilities develop in the helium burning shell as in standard thermally pulsing AGB stars, and end as NeO white dwarf or, if the NeO core mass exceeds $\sim$ 1.37 $M_{\odot}$, electron capture can induce core collapse, and a supernovae explosion ensues.
SAGB stars are more luminous and bluer than AGBs, and obviously have a shorter lifetime. The evolution of the internal structure is however very similar in the two cases.
The reason why carbon is ignited off-center, is that during the late stages of He-burning there is a strong loss of energy due to neutrinos in the center of the core, thus the maximum temperature ($\sim 7 \times 10^8$ K) is reached in a more external region. The two most active reactions involved in carbon nucleosynthesis are:

$$^{12}C +^{12} C \rightarrow^{20} Ne + \alpha$$

$$^{12}C +^{12} C \rightarrow^{23} Na + p$$

In the interior of SAGB stars the temperature never exceeds 90 MK, thus the contribution from the ^{12}C + ^{16}O reaction is negligible. The α particles from the above reaction is assumed to be absorbed by ^{16}O via:

$$^{16}O + \alpha \rightarrow^{20} Ne + \gamma$$

This results in the overall reaction :

$$^{12}C +^{12} C +^{16} O \rightarrow 2^{20}Ne + 2\gamma$$

The fundamental parameter that determines the achievement of the Carbon burning is the mass of core, in turn dependent on the mass of star. C-burning requires massive CO cores, so that their contraction provides enough energy, sufficient to reach the temperature able to trigger the reactions.
The evolution of the degenerate CO core is similar to that of the degenerate helium cores in low-mass stars. The structure of the core is independent of the details of the envelope. While the mechanical structure of such a core is determined by its mass M_c, its thermal properties depend on the surrounding shell source and on neutrino losses. Carbon burning can be divide in two parts:

- carbon flash
- flame, that propagates all the way to the center

The flash is the first phase of C-burning, it is very energetic, the nuclear luminosity emitted, L_C, reaching $10^6 \lesssim L_c/\, L_\odot \lesssim 2 \times 10^8$.
The energy released during the flash induces a large expansion of the burning shells. As the carbon luminosity decreases, core contraction resumes, the region of maximum temperature moves inward and increases again, until carbon reignites. But now the degree of degeneracy is lower, because part of the flash energy was absorbed by the core, thus less carbon is made available to power the instability, and the resulting luminosity is weaker. The second event of the C-burning is called flame; the propagation of the nuclear reactions can reach the center of the core, convection disappears, carbon-burning proceeds radiatively in a shell surrounding the core. The lower panel of Fig 2.8 shows the temporal evolution of the extension of the convective zones (indicate with shaded regions) in a 9.5 $M_\odot$ model with metallicity Z=0.001. The flame forms shortly after the extinction of the carbon flash, and is followed by subsequent episodes of carbon burning, that moves progressively outwards. The upper panel of Fig. 2.8 shows the various contributions to the total luminosity, which is seen to remain approximately constant during C-burning. This is associated to the unstable nature of this nuclear activity, so that the energy produced is used to expand the above regions, with little effect on the surface luminosity.
With increasing initial mass, the core temperature is higher and its degeneracy lower, thus the strength of the flash and the duration of the flame decrease. Furthermore, neutrino losses are also weaker, and carbon ignites closer to the center, until it reaches the center, in which case the evolution proceeds up to the formation of the iron core in massive stars. At the end of the carbon burning phase, the core is essentially composed of ^{16}O ($\sim$ 50-70 %) and ^{20}Ne ($\sim$ 15-35 %). Similarly to the classic AGB evolution, the exhaustion of the C-burnings followed by the second dredge-up; however this case convection penetrates more inwards, and brings to the surface large amounts of helium, whose mass fraction increases up to $\sim$ 0.40-0.45. Now the evolution is the same of the classic AGB, and proceeds in an alternate shell burning mode. The main differences are the mass and the composition of the core. Because the SAGBs have more massive cores, the gravitational pull is stronger, and the burning shells are more compressed, thus they are thinner and their temperature is higher. For this reason the structure reacts more quickly; the results is that the thermal pulses are weak and their duration shorter. HBB very efficient: the temperature on the basis of the envelope ranges between 10^8 and 1.4×10^8K. The very strong proton burning increases the surface abundances of ^{14}N, ^{25}Mg and$^{26,27}Al$.

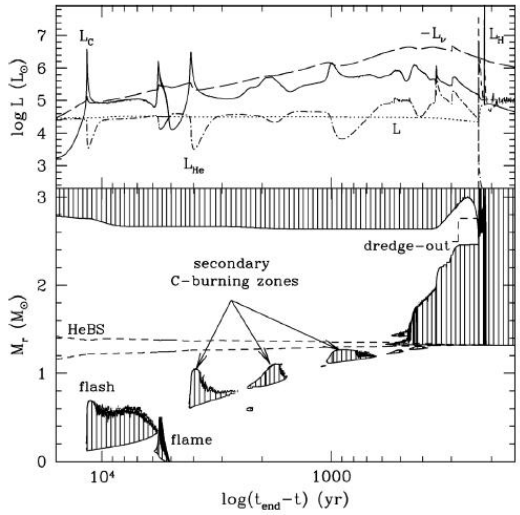

Figure 2.8: Diagram of 9.5 $M_{\odot}$with Z=0.001 star during the C-burning and dredge-out phases. The time is counted backward from the end of the SAGB phase.The hatched areas represent the convective regions. The upper panel shows the evolution of the luminosities associated with C (L_c, solid line), H (L_H dashed line), He (L_{He}, dotted-dashed line) urning, with neutrino emission (L_ν, long-dashed line) and total surface luminosity (L, dotted line).

2.4.1 Role of the AGB and S-AGB in the Multiple populations in Globular Clusters

We have seen that the yields of AGBs depend strongly on which of the two mechanism of nucleosynthesis dominates. When HBB is active, we expect to see the signature of p-capture nucleosynthesis, with a constant C+N+O. When TDU is favored, the C increases, and consequently also the C+N+O content. HBB is dominant in the high mass stars, because the higher core masses favor higher temperatures at the bottom of the convective region, thus leading the HBB conditions. Lower mass stars, not experiencing HBB, live longer, and experience many TDU episodes. The value of the M_{thresh} is uncertain, and depends on the assumed extramixing from the core during the two phases of core burning, and on the convective model adopted. To study this problem, we used a model in which convection is modeled according to the FST prescription, mass loss is treated according to the Blöcker's recipe, and the cross sections are given by NACRE: the M_{thresh} is about 4 $M_{\odot}$. To explain the formation of population with anomalous chemistry we consider that the stars most contaminated are formed directly from winds of the most SAGB, where the intermediate chemistry would be the outcome of the depletion of the gas of massive AGB (M> 4 $M_{\odot}$) with pristine gas survived within the cluster.

CHAPTER 3

The massive Binary Scenario

3.1 Introduction

In Chapter I, discussing the possible polluter that contaminated the interstellar medium in Globular Clusters, we mentioned the possible role played by massive binary systems. This scenario, suggested by de Mink et al. (2009), invokes non conservative mass transfer in binary systems as a viable mechanism to produce gas contaminated by proton-capture nucleosynthesis; qualitatively, a great contamination can be produced when a massive star in a binary system is stripped of the external layers, down to internal regions exposed at large temperatures.
Here we follow a more quantitative approach, and discuss the role played by the various parameters (initial mass function, mass range of the polluters and of the secondary, modality of mass transfer) on the resulting abundances of the helium, oxygen, sodium, magnesium and its isotopes, and aluminum in the intracluster medium where this gas can form the 'second generation' stars.

3.2 The Stellar Evolution Code ATON

To simulate pollution from binary systems, we assume that mass is lost by the primary at a certain evolutionary stage, when mass transfer is assume to begin. To mimic this pollutions demanded computation of a series of evolutionary sequences of stars with different mass, followed until the end of the core He-burning phase.
The stellar evolution code used is ATON, that can follow all the evolutionary phases from the pre-MS, prior to deuterium-ignition, up to Carbon burning (Ventura et al., 1998). The ignition of oxygen and the following pre-supernova phases are not accounted for. The code describes spherically symmetric structures in Hydrostatic equilibrium.
The internal structure is integrated via the Newton-Raphson relaxation method, from the center to the base of the optical atmosphere assumed to be at τ =2/3 (see Chap.11 Kippenhahn (1991)). The independent variable is the mass, whereas the dependent ones are temperature, pressure, radius and luminosity.
The zoning is reassessed after each physical timestep, with particular care to the central and surface regions, in the vicinities of convective boundaries and H or He-burning shells, and close to superadiabaticity zones.
Once a physical structure of the model is determined via the relaxation method, a time step is applied to achieve the chemical evolution.
To this purpose, each time step is divided in 10 'chemical' time steps. Any mechanism leading to a variation of chemical composition, such as nuclear burning, gravitationl settling and convective mixing, is repeatedly applied for the number of chemical time steps; pressure and temperature are projected via extrapolation based on the variation during the previous time step.
In the evolutions presented in this work convection was modeled by means of the Full Spectrum of Turbulence (FST) treatment (billion of eddy scales are considered) with the appropriate convective fluxes distribution (Canuto & Mazzitelli, 1991). Mixing of chemicals within convective zones is treated as diffusive process: for any individual element X_i the code solves the equation (Cloutman & Eoll, 1976):

$$\frac{dX_i}{dt} = \left(\frac{\partial X_i}{\partial t}\right) + \frac{\partial}{\partial m_r}\left[(4\pi r^2\rho^2)^2 D \frac{\partial X_i}{\partial m_r}\right] \tag{3.1}$$

where D is the diffusion coefficient:

$$D = 16\pi r^4 \rho^2 \tau^{-1} \tag{3.2}$$

τ is the turbulent diffusion timescale and it is related to the one-point density-radial velocity correlation.

$$< \rho_i v_i >= -\tau \partial \rho_i / \partial r \tag{3.3}$$

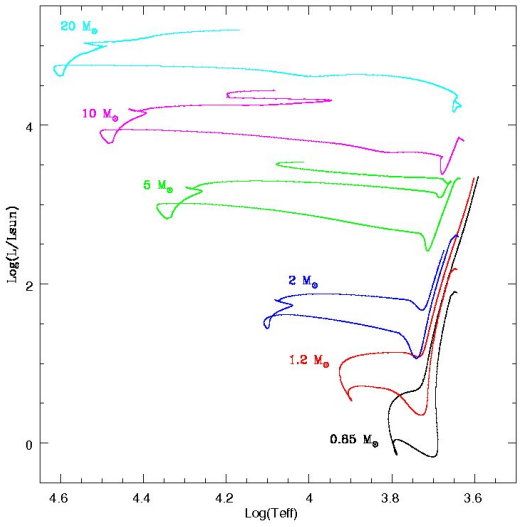

Figure 3.1: Theoretical tracks in the HR diagram of model of different mass during the main sequence and the core Helium burning.

Since knowledge of the second order momentum in this last equation requires previous solution of the Navier-Stokes equations for a compressible stellar fluid, not yet available, we use the local approximation D = $vl_d/3$, where v is the average turbulent velocity and l_d is the convective scale length.
The nuclear network consists of 30 chemical species, and is articulated in 64 nuclear reactions. The cross sections are taken from the NACRE compilation (Angulo et al., 1999), with the following exceptions:

- $^{14}N(p,\gamma)^{15}O$ (Formicola et al., 2004)
- $^{22}Ne(p,\gamma)^{23}Na$ (Hale et al., 2002) (upper limit)
- $^{23}Na(p,\gamma)^{24}Mg$ (Hale et al., 2002)
- $^{23}Na(p,\alpha)^{22}Ne$ (Hale et al., 2002) (lower limit)
- $^{4}He(2\alpha,\gamma)^{12}C$ (Fynbo et al, 2005)
- $^{12}C(\alpha,\gamma)^{16}O$ (Kunz et al., 2002)

Regions unstable to convection are identified via the Schwarzschild Criterion (Kippenhahn, 1991). We take into account convective overshooting for the convective core and for the surrounding convective shell, assuming that the turbulent velocity vanishes exponentially beyond the formal convective border; this is simulated by introducing the

parameter ξ, which defines the scale length over which the velocities decay into the radiatively stable regions.
In this study we adopt ξ=0.02, in agreement with the calibration given in Ventura et al. (1998) based on the MS fit of open clusters. No overshooting is used for the evolutionary phases following the core He-burning phase.
Pair, photon, bremsstrahlung and plasma neutrino have been taken from Itoh et al. (1992). Recombination neutrinos have not been included, since they are of interest only for more advanced (pre-supernova) evolutionary phases, which presently lie out of the domain of this program.
The mass loss is modeled according to Blöcker (1995):

$$\dot{M} = 4.83^{-22}\eta_R M^{-3.1} L^{3.7} R \tag{3.4}$$

where M, L and R are expressed in solar units, η_R is a free parameter. We use η_R=0.02, in agreement with the calibration of the luminosity function of lithium-rich stars in the Magellanic Clouds (Ventura et al., 2000). The models span the mass range 0.4 $M_\odot \leq$ M $\leq$100 $M_\odot$. The chemistry used is typical of GCs of intermediate metallicity, with Z=10^{-3}, Y=0.24. The mixture is α-enhanced, with [α/Fe]=+0.4; the relative distribution of the various species is taken from Grevesse & Sauval (1998).
The evolution start from the pre-main sequence, and, for the model not experiencing the helium flash, are followed until all the central helium is consumed.

3.3 Internal Chemistry of Main Sequence stars

Before discussing the overall context of the massive binaries scenario, and the possibility that it may account for the formation of multiple population in Globular Clusters, we focus on the variation of the internal chemical stratification of stars during their Main Sequence and Giant evolution. This is essential to understand the composition of the gas ejected by the stars, once they are stripped of the more external layers.
In particular, to understand whether the observed chemical patterns defined by GC stars can be reproduced with this method, we focus on the evolution of the abundances of those elements often investigated in the spectroscopic surveys, i.e. oxygen, sodium, magnesium, and aluminum. Because the O-Na and Mg-Al anti-correlations characterize the almost totality of the GCs examined, we look for conditions where it is possible to produce gas enriched in sodium and aluminum, and depleted in the oxygen and magnesium content.
To achieve this it is mandatory that oxygen is destroyed by proton capture via the reaction

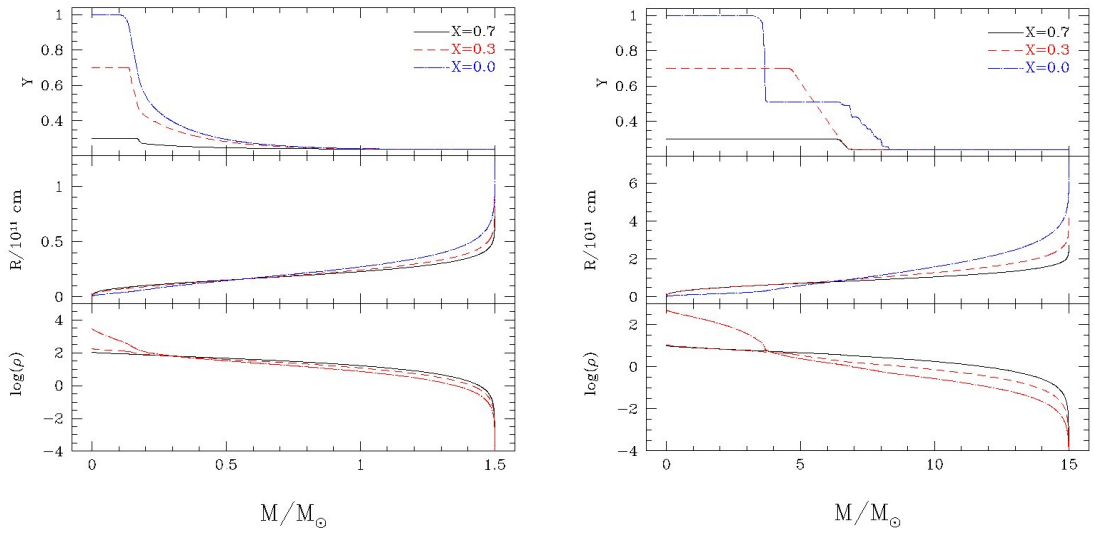

Figure 3.2: Evolution of the internal chemical and physical structures of two models of 1.5 $M_\odot$ (left) and 15 $M_\odot$ (right). The evolution of the helium content (top), radial distance from the center (middle) and density (bottom) are shown. The lines indicate different phases during the MS evolution, when the central hydrogen mass fractions is X=0.7 (black, full line), X=0.3 (red, dashed) and X=0.0 (blue, dotted-dashed).

$^{16}O(p,\gamma)^{17}F$, and that the Ne-Na cycle nucleosynthesis is activated. This latter consists in a series of proton capture reactions, that start from ^{20}Ne, to end with sodium synthesis:

$$\begin{aligned} {}^{20}Ne + p &\rightarrow {}^{21}Ne + \gamma \\ {}^{21}Ne + p &\rightarrow {}^{22}Na + \gamma \rightarrow {}^{22}Ne + e^+ + \nu \\ {}^{22}Ne + p &\rightarrow {}^{23}Na + \gamma \end{aligned} \tag{3.5}$$

Among all the reactions above, proton capture by ^{22}Ne nuclei is by far the most efficient. However, given the modest initial abundance of ^{22}Ne, this is not sufficient to produce sodium in the quantities required to reproduce the observations.

Fig. 3.2 shows the internal structure during various evolutionary phases (identified by the central hydrogen) of two models of 1.5 $M_\odot$ and 15 $M_\odot$; the profiles of the helium mass fraction, radius and density are shown.

The helium profile in the 15 $M_\odot$ model outlines the presence of a convective core (as argued by the flat profile of Y in the central regions), which shrinks as hydrogen is consumed.

The 1.5 $M_\odot$ model also has a convective core, though the change in size is much less evident. In both cases we note (bottom panels) the strong increase in the density of the

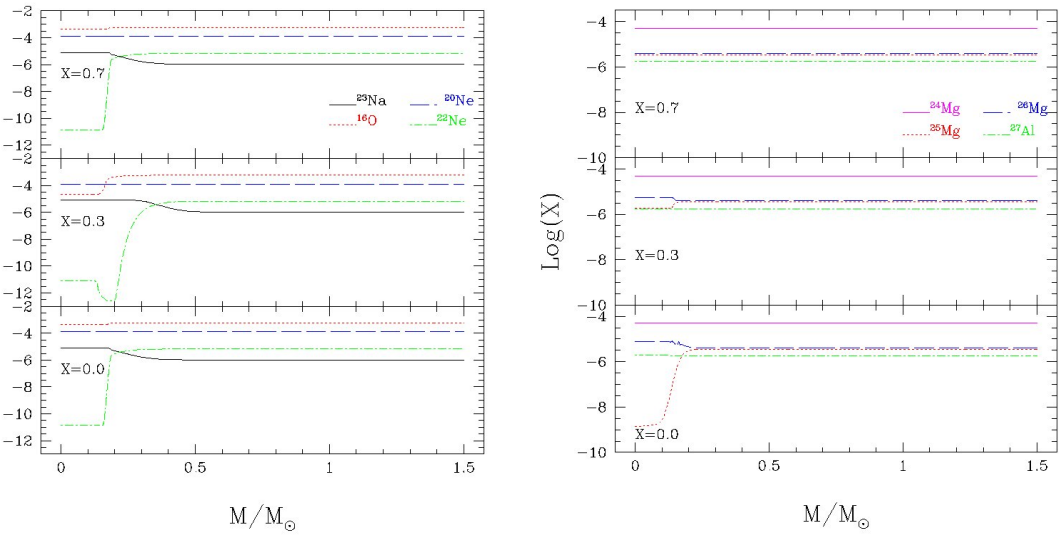

Figure 3.3: Internal chemical stratification of a model of 1.5 $M_\odot$ in terms of the abundances of ^{16}O, ^{20}Ne ^{22}Ne and ^{23}Na (left), and ^{24}Mg, ^{25}Mg, ^{26}Mg and ^{27}Al (right). The three different panels refers to three evolutionary phases during the MS evolution, when the central hydrogen is X=0.7 (top), X=0.3 (middle) and X=0.0 (bottom).

central regions, as hydrogen is exhausted in the core. The density in the 1.5 $M_\odot$ model reaches extremely high values ($\rho_c \sim 10^4\ g/cm^3$), which sets the basis for the degeneracy of the core.
Central density of low-mass stars during H-burning are typically $\sim 100\ g/cm^3$: these values require $\sim$ 25 MK for the activation of the full CNO cycle, and $\sim$ 30 MK for the ignition of the Ne-Na nucleosynthesis. For masses exceeding 10 $M_\odot$ the densities are smaller ($\sim$ 10 g/cm^3), thus temperatures $\sim$ 35-40 MK are required.

To understand the kind of nucleosynthesis developed in stars of different mass during the MS phase, we show the internal chemical stratification of stars of initial mass 1.5 $M_\odot$, 15 $M_\odot$ and 40 $M_\odot$, respectively in Fig. 3.3, 3.4 and 3.5. Left panels refer to oxygen and to the species entering the Ne-Na cycling, whereas right panels show the elements involved in the Mg-Al nucleosynthesis. In the 1.5 $M_\odot$ representative of low-mass stars, nuclear burning is restricted to the most internal $\sim$ 0.2 $M_\odot$.
The profile shown in the left panel of the Fig. 3.3 indicate that ^{20}Ne burning never starts; some sodium is produced by p-capture by ^{22}Ne nuclei.
The Mg-Al nucleosynthesis is hardly activated only in the last phases of the H-burning stage, and limited to some Aluminum production via ^{25}Mg and ^{26}Mg burning.
In the 15 $M_\odot$ and 40 $M_\odot$ models the fraction of the stellar mass touched by p-capture nu-

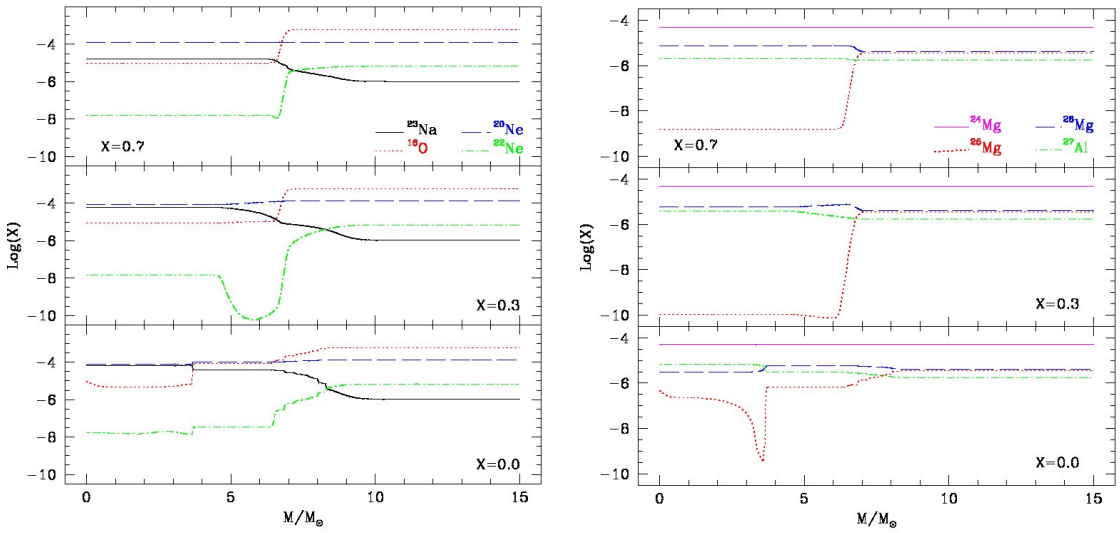

Figure 3.4: Same as in Fig 3.3, but for a 15 $M_{\odot}$model.

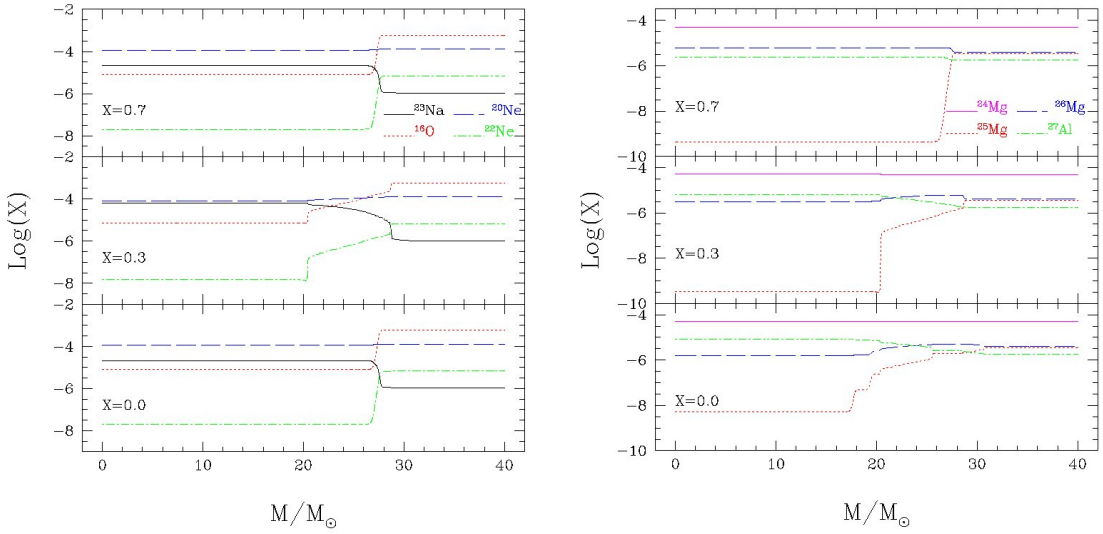

Figure 3.5: Same as in Fig. 3.3 but for a 40 $M_{\odot}$model.

cleosynthesis during the MS phase reaches 50%.

We see from the left panel of Fig.3.4 that in the 15 $M_\odot$ model the oxygen depletion is achieved already in the early MS phase, along with ^{22}Ne burning, whereas in later phases the full ignition of ^{20}Ne burning occurs. The same holds for the 40 $M_\odot$, as can be seen from Fig. 3.5. Unlike oxygen, whose change is rendered hard by mixing of the O-poor interior with uncontaminated material from the external layers, sodium can be produced efficiently, the increase in the average sodium being more sensitive to the extent of the nucleosynthesis reached. For the temperatures relevant here ^{22}Ne reaches rapidly its equilibrium abundance, thus rendering the sodium produced dependent on the rate at which ^{20}Ne is consumed, and scarcely dependent on the choice of the cross section for the $^{22}Ne(p,\gamma)^{23}Na$ reaction.

Turning the Mg-Al nucleosynthesis, needed to produce gas enriched in Aluminum and depleted in magnesium, the relevant reactions are:

$$\begin{aligned} {}^{24}Mg + p &\rightarrow {}^{25}Mg + \gamma \\ {}^{25}Mg + p &\rightarrow {}^{26}Mg + \gamma \\ {}^{26}Mg + p &\rightarrow {}^{27}Al + \gamma \end{aligned} \tag{3.6}$$

Activation of the first reaction in a time-scale comparable to a fraction of the MS life time requires a temperature[1] of the order of 100 MK, which is not consistent with the thermodynamic structure of even the most massive models investigated: in fact, ^{24}Mg is practically unchanged in all the models calculated, as can be seen by the right panels of Fig. 3.4 and 3.5, where the internal stratifications of the magnesium isotopes and ^{27}Al in three phases of the MS evolution of two models of 15 $M_\odot$ and 40 $M_\odot$ are reported. On the contrary, proton capture by the two heavy magnesium isotopes requires $\sim$ 40 MK, a temperature which is easily reached in the central regions of all stars with M $\geq$ 10 $M_\odot$: these elements are seen to burn efficiently in the three right panels of Fig 3.4 and

[1] To find the required temperature I have to consider the equation :

$$\frac{d\ln {}^{24}Mg}{dt} = -X_{in}({}^{24}Mg)X(p)S_{{}^{24}Mg(p,\gamma)^{25}Mg} = -X_{in}({}^{24}Mg)X(p)\frac{10^{\sigma}\rho_c}{N_A} \tag{3.7}$$

where S is the rate of the reaction, e.g the number of nuclear reactions that happens in a second,-$X_{in}(^{24}Mg)$ and X(p) are the abundances in mass fraction [mol/g], σ is the cross section of the reaction in $\frac{cm^3}{smol^2}$, ρ_c is the density in the core of the star. The solution of the differential equation is $X(^{24}Mg) \propto X_{in}(^{24}Mg)e^{\frac{t}{\tau}}$ where $\tau \sim S_{{}^{24}Mg(p,\gamma)^{25}Mg}X(p)$. The MS life time τ_{MS} of a 15 $M_\odot$ is about 13 Myr, if the ^{24}Mg has to be destroyed during a time t $\sim \frac{1}{\tau_{MS}}$ we have X(p) $\sim$ 0.6. Thus, in this case we have $S_{{}^{24}Mg(p,\gamma)^{25}Mg} = 1/4.5$ Myr. From this value I get the cross section. This quantity changes with central temperature, and is tabulated; knowing the cross section we can find the temperature, that is about 90 MK.

3.5. Aluminum is produced in these structures, but the impossibility of starting the ^{24}Mg burning makes the Al-enhancement modest, the largest attainable Al- production being associated to the small initial (and uncertain) abundances of ^{25}Mg and ^{26}Mg.

3.4 Modeling of pollution from binaries

In Chapter I we mentioned the massive binary scenario, according to which these type of stars can be a source of processed material viable to explain the chemical anomalies of the SG stars in GCs In the paper by de Mink et al. (2009) this idea is exemplified by showing that a 20 $M_\odot$ star in a close binary may shed about 10 $M_\odot$ of material into the intracluster medium (ICM), at low velocity thanks to non conservative mass and angular momentum transfer, with a possible role also for rotation and tidal interactions. The envelope of these stars are enriched in He, N, Na, Al and depleted in C and O, similar to the abundance patterns observed in GCs.

According to their simulations, mass transfer occurs in two episodes; while most of the mass is lost during the first step, the second stage of mass transfer provides only $\sim 1\ M_\odot$ of material. Although this gas is more processed, the global result will be dominated by the first episodes, that occurs shortly after the end of the core hydrogen burning, owning to the contact with the Roche Lobe associated to the expansion of the star. The model fails to reproduce the significant depletion in total Mg found in the 'extreme' population of the most massive clusters. In addition, the work by de Mink (2009) does not take into account the chemical yields provided by other binaries shedding mass at different possible evolutionary stages. The authors estimate the mass available for the formation of the SG stars, and show that it is larger than that available from fast rotating massive stars and/or AGBs (Sackmann & Anand, 1970; D'Ercole et al., 2008).

Considering also the contribution from binaries down to 3 $M_\odot$ could further alleviate the mass budget problem.

In this work we describe the possible role of massive binaries with a number of simple assumption that maximize the possible effect on the cluster evolution, in order to understand the chemistry and the quantity of the processed matter available for the SG formation. This must be considered as a preliminary step before addressing a full binary evolution description. A negative result of such an investigation would make further, even more complicate, attempts useless.

I assumed that initial dynamical conditions in the cluster central regions are such that binary encounters and formation of binaries becomes a dominant mechanism of evolution: in this case, we may also think that close binaries are preferentially formed, and mass

transfer does not have to wait for the primary expansion to occur. Although the physical central conditions of globular clusters today do not allow the great number of dynamical encounters we wish to consider, we are allowed to make such hypothesis to test the binary model for the formations of second generation stars. Summarizing, this model is based on the following simple assumptions:

1. Donor stars are assumed to have a maximum mass of 100 $M_{\odot}$, and are allowed to evolve until the end of the core helium burning phase. The mass range for the primary is limited to a minimum mass of 3 $M_{\odot}$. The binary importance is maximized by assuming that all these stars are in binaries, whose mass transfer phase begins random at different times during the cluster life.

2. Starting from time zero, the time of formation of the cluster, the loss of mass to the ICM is maximized by assuming that in these binaries the primary and the secondary star mass functions are independent each other. Consequently, by any reasonable choice of the initial mass function (IMF), the probability of having a low mass star companion to the donor is much larger than the probability of equal or slightly different masses (see point 3).

3. The evolution with mass loss from the primary to the secondary is either fully non-conservative, or that mass transfer to the secondary interests only some percentage of the secondary mass. For the stars in the core hydrogen burning stage when mass transfer begins, we assume that the loss of angular momentum associated to the mass loss from the binary during the mass transfer phase are such that the orbit shrinks -as it would for a conservative mass transfer- until the primary is reduced down to the secondary mass, and that mass transfer stops (or mass loss from the system stops, that is the interesting limitation for my computation) afterwards. The secondary mass considered is either its initial mass (in the fully non conservative case) or its initial mass, plus the transferred percentage. The assumption of independent IMFs for the two components will result in a larger mass fraction lost into the ICM with a chemistry more contaminated.

4. When the mass transfer begins after the exhaustion of the hydrogen in the core and the primary has developed a dense He-core of mass M_c, the mass ejected is assumed to be M_1 - M_c. This choice is consistent with a simplified binary evolution, maximizing the mass that can be lost from the donor, as stripping of layers from the compact core is not allowed.

$M/\ M_\odot$	T_c	ρ_c	Y	$[O/Fe]^{(a)}_{av}$	$[Na/Fe]^{(a)}_{av}$	$[Mg/Fe]^{(a)}_{av}$	$[Al/Fe]^{(a)}_{av}$	$\frac{^{25}Mg}{^{24}Mg}$	$\frac{^{26}Mg}{^{24}Mg}$
initial chemistry			0.24	0.4	0.0	0.4	0.0	0.07	0.08
3.0	34	86.9	0.31	0.31	0.57	0.34	0.010	0.058	0.093
5.0	38	45.3	0.33	0.28	0.91	0.34	0.03	0.054	0.1
10.0	45	20.6	0.38	0.23	1.22	0.34	0.09	0.048	0.1
15.0	49	14.0	0.43	0.18	1.36	0.34	0.18	0.043	0.14
20.0	51	11.3	0.46	0.12	1.40	0.34	0.27	0.038	0.09
30.0	54	8.3	0.54	0.05	1.5	0.34	0.4	0.032	0.069
50.0	57	6.0	0.62	-0.05	1.56	0.35	0.5	0.024	0.053
70.0	59	5.0	0.64	-0.15	1.56	0.36	0.55	0.012	0.043

$^{(a)}$ Mass fraction of the element averaged in the whole stars at the end of the core hydrogen burning phase.

Table 3.1: Chemical yields and evolutionary properties of massive stars

5. The mass shaded by the individual binary systems into the ICM is summed, until a total mass typical of GCs is reached; in this case we stop when $10^5\ M_\odot$ are obtained. Depending on the choice of the minimum donor mass, this will also provide a maximum time for the whole evolution of these binaries; the time will be shorter, the larger is the minimum mass. The total mass of the first generation is eventually computed based on the assumed IMF.

6. To further enhance the possibility of producing a strongly contaminated gas, we even explore the possibility that at each time step only the masses that have already started the nuclear activity in the central regions are involved in binary interactions. This choice prevents the possibility that stars with homogeneous chemistry contribute to the total mass budget by releasing non processed gas.

Even if this scheme is highly simplified, it helps understanding the role of the different parameters in providing the final chemistry of the ICM, from which the second generation is assumed to form in the binary scenario.

3.4.1 The model parameters

All stars whose mass exceeds a threshold value $M \geq M_1^{min}$ and that belong to the first generation (FG) of the cluster, are assumed to be formed in a binary system, or to form a binary system via capture of a low mass companion, whose mass M_2 is assumed to be in the range :

$$M_2^{min} \leq M_2 \leq M_1$$

All stars form at time zero, and the evolution is divided into a finite number of timesteps (depending on the input parameters), at any of these steps we extract random the masses of the primary and of the companion, in agreement with the limitations given by the choice of the parameters M_1^{min} and M_2^{min}, from a mass distribution following a power-law mass function of the form $dN/dm \propto m^{-(1+x)}$. In the case (6) of the previous section, the minimum mass at each time step is taken as the mass that has just started H-burning in the core, and the internal chemical profile is no longer homogeneous. In this case M_1^{min} determines only the total duration of the process.
A mass transfer from M_1 and M_2 interests the first part of the evolution, for a total ΔM_{tr} assumed to vary from 0 to 40% of M_2. The mass ejected is thus:

$$\Delta M_1 = M_1 - M_2 - \Delta M_{tr} \tag{3.8}$$

or, in agreement with point (6) of the previous section,

$$\Delta M_1 = M_1 - M_c - \Delta M_{tr} \tag{3.9}$$

The chemistry of the gas expelled from the system will reflect the results of mixing of the material processed in the internal regions with the less processed or unprocessed matter in the more external layers and will depend on the inner nuclear processing reached at the considered timestep, function of M_1 and of time. Three main free parameters enter the determination of the composition of the gas ejected into the ICM:

- **x**: exponential index of the mass function;
- M_1^{min}: minimum mass for the primary star;
- M_2^{min}: minimum mass for the secondary star.

We will see that the role played by the parameter ΔM_{tr} is of limited importance. The range of values that we explore to allow a full, detailed coverage of the parameter space is: $0.0001 \leq x \leq 1.5$; $3 \leq M_1^{min}/M_\odot \leq 50$; $0.4 \leq M_2^{min}/M_\odot \leq 2.0$; $0 \leq \Delta M_{tr}\ 0.4 \times M_2$.
The timesteps and the total duration of the process are chosen according to the MS life time of the star with mass M_1^{min}; the number of extractions (hence, of non conservative evolution from the donor) is calculated in order to obtain a mass of the gas ejected $\Delta M = 10^5\ M_\odot$, to reproduce the SG of a GC of the size of NGC 2808. Our hypothesis implies that we are thinking of a cluster massive enough to allow this process of non-conservative binary evolution until we reach the desired amount of mass. Any other smaller value of the mass accumulated could have been chosen without changing the result.

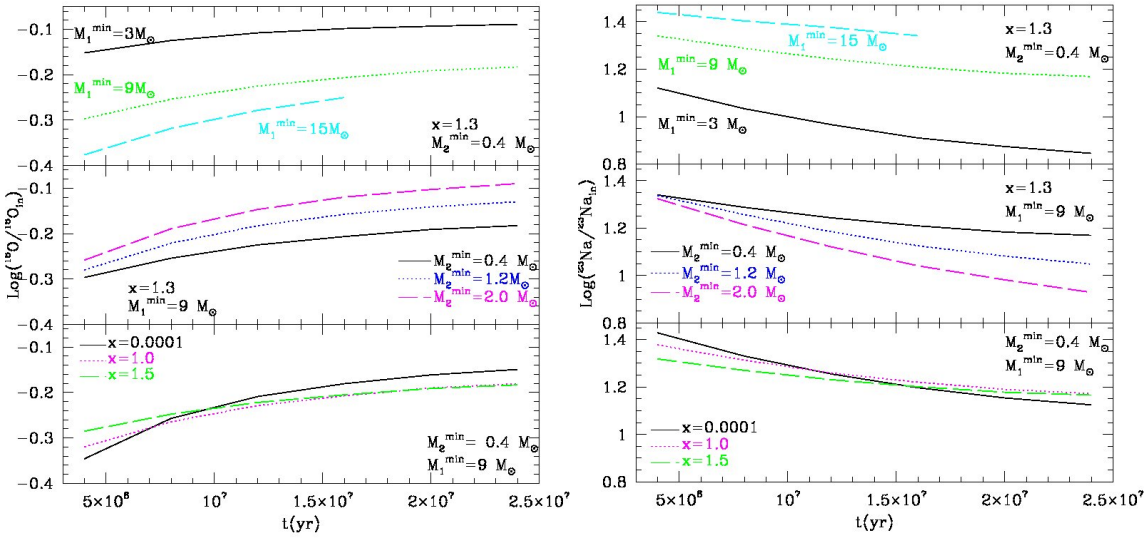

Figure 3.6: Evolution of the oxygen (left) and sodium (right) content of the gas ejected by the binary systems as a function of time, for various combinations of the parameters describing the slope of the IMF and the masses involved. The effects of a variation in the minimum mass of the primary (top), of the secondary (middle), and in the slope of the IMF (bottom) are shown.

Depending on the slope of the IMF, and on the limitation chosen for M_1, the total mass in FG necessary to obtain the above fixed mass budget is simply obtained by integrating the chosen IMF down to the minimum stellar mass, assumed to be 0.1 $M_\odot$. The total mass stars with $0.1 \leq \mathrm{M}/M_\odot \leq 0.8$, that is the range of stars presently evolving in the clusters, is always larger or much larger than $10^5\,M_\odot$. It goes without saying that also in this model, in order to achieve an approximate equality between the mass of FG and SG it is necessary to invoke a preferential loss of FG stars from the cluster, increasing with M_1^{min} and partially depending on the chosen IMF. The percentage of initial mass that must have been lost in order to achieve equality between FG and SG is listed in column 8 of Tab. 3.2 3.3. We see that the initial FG population must lose from the protocluster a percentage of mass similar to what required by the other models discussed in Chapter 1. Thus the binary scheme, even with the non stringent hypothesis made in our simple model, does not ease the problem of the initial mass budget of the globular clusters containing multiple stellar populations. Moreover, the column 9 of the Tab 3.2 lists the number of stars that are predicted to undergo SN II explosion. This number is generally very large, casting doubts on the survival of quiet star formation from the matter lost by the interacting binaries.

Our goal is to understand whether under some particular conditions binary stars with at least one massive component are able to eject into the ICM an amount of gas, quantita-

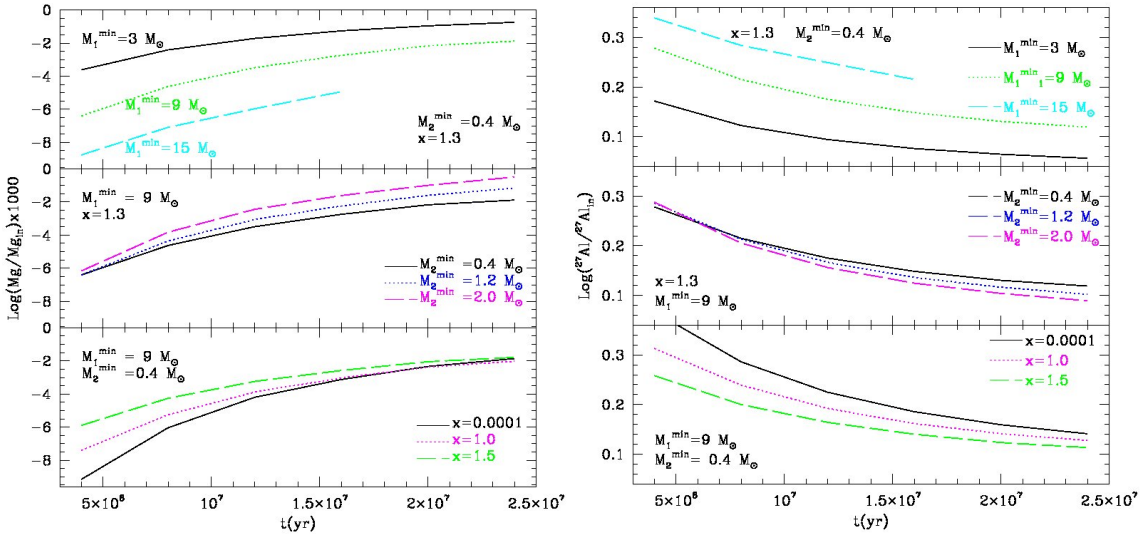

Figure 3.7: Same as Fig 3.6, but for magnesium and Aluminum.

tively equivalent to today's SG stars mass, whose chemistry may account for the chemical patterns observed: while we have seen that the hypothesis made on the binary number and relative masses distribution allow us to reach easily the necessary SG mass budget, we still have to investigate the resulting chemistry : in particular, it is necessary to reproduce also the most anomalous abundances of O, Na, Mg, Al. Observed this demands a full exploration of the effects of the three parameters entering this treatment. We provide a short description of the qualitative trends of the results obtained according to the choice of x, M_1^{min} and M_2^{min}. Their impact on the results can be seen in Fig 3.6 and 3.7, that reports the evolution of the oxygen-sodium and magnesium-aluminum contents of the gas ejected by the binary stripping.

A smaller x corresponds to a flatter IMF, thus to an enhanced probability that massive stars are randomly extracted. Since these objects burn at higher temperatures in their interiors, this choice increases the probability of producing gas that shows the imprinting of an advanced nucleosynthesis: the abundance of oxygen and magnesium in the early epochs is seen to decrease for smaller x's value, the opposite happens for sodium and aluminum. (bottom panel for the Fig 3.6 and 3.7).

The choice of M_1^{min} is crucial in determining the masses involved in this process. A small M_1^{min}, given that smaller masses are favored in any random extraction, diminishes the probability that the higher masses are involved, thus inhibiting a strong contamination by p-capture nucleosynthesis of the gas. In particular, if $M_1^{min} = 3\,M_\odot$, it is alleviated the constraint on the mass that must be lost from the GC. The gas ejected by these systems

will show up only modest traces of nuclear processing. In Fig 3.6 (left top panel) the oxygen depletion is limitated to 0.1 dex, to be compared to 0.8 dex , as indicated by the observations. If we consider $M_1^{min} = 15\,M_\odot$, the depletion is higher: in the early stages it can reach -0.4 dex. The same behavior can be seen for the other elements. Sodium (Fig. 3.6 right top panel) and aluminum (fig 3.7 right top panel) are produced in great quantities with a larger M_1^{min}: the abundances can reach, respectively, 1.4 dex and 0.3 dex. The magnesium depletion is so small that the difference is negligible.

M_2^{min} determines how much gas is stripped by the primary stars. A smaller M_2^{min} implies a greater mass ejection, up to more internal (and processed) layers, so that the gas ejected will be rich of processed material; conversely, if M_2^{min} is close to the mass of the primary, only the external and uncontaminated layers will be expelled from the primary, thus favoring only a poor (if any) contamination of the stellar surroundings. The impact of M_2^{min} becomes progressively important with time, when it is relevant in determining whether nuclearly processed layers from the primary are ejected into the ICM; at the earliest epochs the chemistry of the gas expelled is less sensitive to M_2^{min}, because the primary star is sufficiently massive (M_1^{min}=9 $M_\odot$), that material exposed to nuclear processing is stripped away, and released into the ICM (see Fig. 3.6 and 3.7 middle panel).

The most extreme contamination of the ICM (i.e the smallest abundance of oxygen and magnesium, and the highest sodium and aluminum) is thus obtained when small values of x and M_2^{min}, and high M_1^{min}, are chosen. It is expected to be more advanced in the early epochs, and to approach homogeneity later, when the material lost from binary systems is less processed, as only less massive stars are involved.

Despite the strong destruction of oxygen in the internal regions of massive models, the highest depletion found even with the most convenient choice of the parameters, barely exceeds a factor about 2.

The reason why producing ejecta enriched in the mass fraction of a given element i initially absent in the mixture is much easier than obtaining matter with a poor content of a species initially present in great quantities can be shown with the following arguments. As a first approximation the average abundance of an element X in stars is given by:

$$\bar{X} = \frac{M_c X_c + M_{env} X_{env}}{M_{tot}} \tag{3.10}$$

where M_c and M_{env} are, respectively, the core and the envelope mass, X_c and X_{env} are the fraction mass of the element in the core and in the envelope. If the element is destroyed, $X_c << X_{env}$, thus:

$$\bar{X} \sim \frac{M_{env} X_{env}}{M_c + M_{env}}$$

Because $M_{env} >> M_c$, $\frac{M_{env}}{M_{tot}} \sim 1$, thus $\bar{X} \sim X_{env}$: the effect of the internal destruction is negligible. When an element is produced in core, we have $X_c >> X_{env}$, thus:

$$\bar{X} \sim \frac{M_c X_c}{M_{tot}} \propto X_c$$

we can see the effect of the production.
The small oxygen content is obtained when mass processed in the core is mixed with unprocessed material from the exterior; thus, the degree of oxygen depletion is not particularly sensitive to the temperature at which the gas is processed, but rather to the mass fraction of the core that these stars develop during the MS evolution.
The variation with time of the sodium mass fraction of the ejected gas is shown in the right panel of Fig. 3.6.
We note that great sodium enhancements (a factor about 20) are found independently of the choice of the parameters: this is a mere consequence of the full activation of the Ne-Na cycle in the cores of models more massive than 2 $M_\odot$. Summarizing, we find the following results:

- Even if the internal temperatures are sufficiently high to burn oxygen, the final abundance of ^{16}O in the gas ejected hardly reaches twice the initial value;
- A great sodium enhancement ($\sim$ 1.5 dex) is possible when only massive stars (M > 9 $M_\odot$) are considered as primary stars.
- The overall magnesium content of the gas changes very little. Only in the early phases of the GC evolution, when the most massive objects are evolving, we note a modest depletion, not exceeding -0.01 dex, independently of the choice of the parameters;
- Even with the most favorable choice of the relevant parameters the possibility of producing aluminum is limited by the impossibility of burning ^{24}Mg. The maximum aluminum enhancement is found to be $\sim$ + 0.35 dex.

3.4.2 The overall yields by massive binaries

The results of our simulations are shown in Tab. 3.2, where we report the chemistry of the gas ejected (cols. 3 to 7 show the mass fraction of helium, oxygen, sodium, magnesium and aluminum) according to the choice for the minimum mass of the primary (col. 1) and the consequent duration of the process (col. 2). The last two columns indicate the percentage of mass that the cluster must have lost to reach a 1:1 ratio between FG and

Table 3.2: standard case

$M_1^{min}(M_\odot)$	t(Myr)	Y	[O/Fe]	[Na/Fe]	[Mg/Fe]	[Al/Fe]	% M cluster	N_{SNII}
initial chemistry		0.24	0.4	0.4	0			
40	4	0.58	-0.09	1.56	0.38	0.5	97%	300
30	7	0.52	-0.007	1.52	0.39	0.41	96%	2749
20	10	0.46	0.06	1.45	0.39	0.41	96%	3631
15	14	0.35	0.22	1.18	0.39	0.21	94%	6987
9	28	0.35	0.22	1.18	0.4	0.1	94 %	13343
6	30	0.32	0.25	1.05	0.4	0.08	89%	8631
3	200	0.33	0.26	1.11	0.4	0.01	76%	8440

SG stars, and the number of stars that are predicted to undergo SN II explosion under the hypothesis that only stars with M $\geq M_1^{min}$ provide the gas from which SG stars form. These results are based on a mass function with index x=1.3 (that is the most plausible), and a minimum mass for the secondary star M $\geq M_2^{min} = 0.4\ M_\odot$.

In agreement with the analysis of the previous sections, we find that the degree of contaminations of the gas (that can be seen, e.g., by the extent of the oxygen depletion) increases with M_1^{min}. For $M_1^{min} < 20\,M_\odot$, only a modest depletion of oxygen (smaller than a factor 2) can be achieved; the oxygen content of the gas decreases for larger M_1^{min}, and reaches a minimum value of $[^{16}O/Fe]$=-0.1 dex (corresponding to a reduction of a factor 3) for $M_1^{min} = 40\,M_\odot$. Note that in this latter case a severe problem exists for the mass that the system must have lost, that amounts to 97 % of the initial mass of the cluster, provided that the star formation efficiency of the SG is 100%.

The oxygen and the sodium content of the various models in Tab. 3.2 are shown in Fig. 3.8 as full squares; the open circles indicate the abundances measured in stars belonging to different GCs (Carretta et al., 2009a).

Compared to the observations, the gas ejected by binaries is extremely enriched in sodium, and fails to reproduce the strong oxygen depletion found in the stars with the most extreme chemistry, that lay in the left of the diagram. A possible dilution with pristine, uncontaminated gas would not help reconciling these results with the abundances determined spectroscopically. The 6_{th} and 7_{th} column of Tab 3.2 show that magnesium can be hardly destroyed in this context, which also limits the possibility or reproducing the strong Al-enhancements observed.

Tab. 3.3 show the evolution of the chemistry of the gas ejected under the hypothesis that

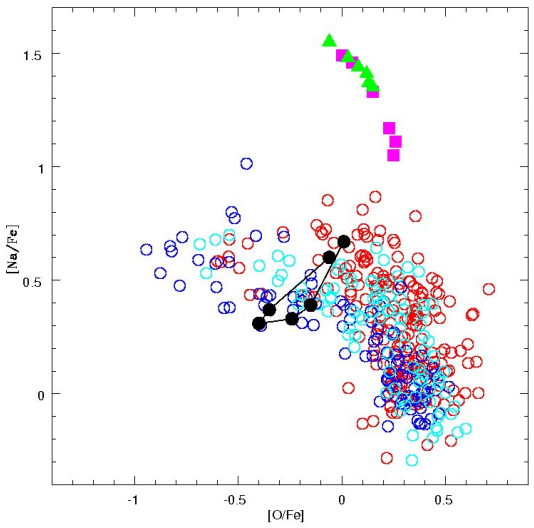

Figure 3.8: The open circle indicate the surface abundances of oxygen and sodium of GCs stars, taken fromCarretta et al. (2009a,b). The full squares and triangle points represet, respectively, the gas chemistry produced by pollution from binaries in the standard case and in the case where at any time only stars that have already started the central CNO nucleosynthesis contribute. The full dots indicate the yields from massive AGBs and SAGBs.

$\Delta M(M_\odot)$	t(Myr)	Y	[O/Fe]	[Na/Fe]	[Mg/Fe]	[Al/Fe]	lost % M cluster
30-80	4	0.52	-0.06	1.55	0.39	0.43	95%
16-80	8	0.48	0.03	1.48	0.39	0.35	92%
12-80	12	0.46	0.08	1.44	0.39	0.32	90%
10-80	15	0.44	0.12	1.41	0.39	0.28	89%
9-80	20	0.42	0.13	1.37	0.39	0.26	88%
8-80	22	0.41	0.15	1.35	0.39	0.24	87%
6-80	38	0.38	0.20	1.25	0.39	0.18	85%
5-80	50	0.36	0.22	1.19	0.39	0.15	83%
3-80	200	0.28	0.33	0.76	0.39	0.04	76%

Table 3.3: Non standard case

at a given time only stars that have already started at least their H-burning in the core contribute to the pollution of the ICM. This choice, though even more extreme that the already generous assumptions of the standard case, maximizes the degree of polluting that can be reached, because uncontaminated objects still on the ZAMS are ruled out from the process. In this case we do not include the number of SN II stars, because for each time step the number of stars is chosen according to the assumed IMF, and all the stars predicted to form the corresponding range of mass are extracted. In terms of the oxygen and sodium abundances, the results from this simulation are shown as full triangles in fig. 3.8, and are seen to share the same difficulties of the models previously discussed in reproducing the chemistry of the most contaminated objects. The impossibility to reproduce Al-enhancements in agreement with the observations is confirmed.

The overall framework of these findings is scarcely altered when the mass transfer is assumed to be partially conservative, so that part of the gas lost by the primary is allowed to be accreted by the secondary. Out simulations show that the gas reversed into the ICM will keep more race of contamination, but the differences in the mass fractions of the individual species hardly reach $\sim 5\%$. This result can be explained because the higher degree of contamination of the gas ejected by the primary into the ICM is partially counterbalanced by the smaller mass lost, due to the contemporary increase in the mass of the secondary.

The results presented so far have been based on rotating stellar models. Recent observations evidenced higher rotation velocities for stars in cluster compared to their field

counterparts (Hiang & Gies, 2006; Strom et al., 2005; Drufton et al., 2006). These findings provide a hint of a possible role of the higher stellar densities within GCs in favoring faster rotation rates. Rotational mixing, for high initial velocities, is a potentially efficient mechanism to alter the chemistry of the outermost layers of the stars during the MS, as nuclearly precessed matter in the core is mixed with uncontaminated external material. A considerable fraction of the stellar mass is lost to the ICM during the MS, with a velocity that should allow this gas to retained within the GCs (Decressin et al., 2007).
To quantify the way our results would change if part of the massive stars are fast rotators, we repeat our analysis by assuming that half of stars with mass exceeding 20 $M_{\odot}$ reach the break up velocity during the H-burning phase, and lose part of their mass before the mass transfer with the companion begins. The mass lost , and its average chemistry, is assumed to depend on the initial mass in the way found by Decressin et al. (2007) (see their table 5). To investigate the maximum modification expected, we choose M_1^{min} =20 $M_{\odot}$, to maximize the role of massive primaries. Our findings can be summarized as follows:

- The magnesium and aluminium content of the gas ejected into the ICM are unchanged. This stems by the intrinsic difficulty in achieving ^{24}Mg burning in the core, that prevents high Al enhancements (see col. 11 Tab 5 in Decressin et al. (2007)).

- The smaller oxygen contained in the most external layers of rotating stars decreases the overall content of ^{16}O reversed into the ICM. Assuming an exponential mass function with x =1.3, the total depletion of oxygen is increased by less than 0.1 dex, thus leading to $\Delta[^{16}O/Fe] \sim$ -0.4 dex. The quantity could be decreased by further 0.07 dex under the scarcely plausible assumption that all the massive stars reach the break-up velocity and belong to binary systems.

In Fig. 3.8 are shown also the abundances of oxygen and sodium produced by AGB and S-AGB stars (full circles); it is clear that they can reproduce the chemistry of most of the stars with the anomalous composition, and a possible dilution with pristine gas could easily trace the whole pattern observed. For the open points in the left side of Fig 3.8, that fall off the range of values covered by the models, D'Antona & Ventura (2007) suggested that their chemistry would be the outcome of deep extra-mixing during the red giant evolution, favoured by the reduced height of the entropy barrier separating the H-rich surface layers with the He-rich interior, determined by the higher helium content expected in SG stars.

CHAPTER 4

The self-enrichment scenario by AGB and SAGB stars

4.1 Introduction

Cottrel & Da Costa (1981) and Ventura et al. (2001) first suggested that new stars may form in GCs from the winds lost by intermediate mass stars during their AGB phase. While the research since then was focused on understanding whether the chemistry of the gas in these winds was in agreement with the patterns observed, the series of papers by D'Ercole et al. (2008, 2010), set the basis for a theoretical framework that follows the star formation process of a second stellar generation in a GC where the interstellar medium was polluted by the AGB ejecta. D'Ercole et al. (2008) followed the hydrodynamical formation of a cooling flow at the cluster center that follows the epoch of Supernovae type II (SN II) explosions and the associated loss of remnant gas from which the FG stars had formed. The cooling flow is due to the low-velocity stellar winds and planetary nebulae of massive AGB stars, and needs the physical conditions for a second epoch of star formation. This study outlines the role of S-AGB stars in the SG formation process.
S-AGB are found to produce He-rich ejecta (Y$\sim$ 0.34-0.40) (Pumo et al., 2008), in reasonable agreement with the helium invoked to explain the bluest main sequences of massive

clusters, such as NGC 2808 (Piotto et al., 2007) and Ω Cen (Bedin et al., 2004), and the anomalous HB morphology of NGC 2808 itself (D'Antona & Caloi, 2004).
D'Ercole et al. (2008) suggest that these stellar population, enriched in helium, might form directly from the winds of S-AGBs, before dilution of the winds with pristine gas would lead to the formation of a stellar component with 'intermediate' chemistry.
We have applied this model for the chemical evolution of two Globular Clusters, M 4 and NGC 2808, because they are the prototypes of extreme cases of GCs with multiple population: NGC 2808 is a massive GC with a Na-O anticorrelation very extended. M4 is a small one with a short anticorrelation

4.2 Model

AGB and S-AGB stars are considered an important ingredient for the formation of the SG population because the winds are slow enough to be retained in the potential well of the cluster; moreover their winds are processed through the hot CNO cycle by HBB at the bottom of the convective envelope (Cameron & Fowler, 1971; Sackmann & Anand, 1970; Blöcker & Schönberner, 1991; Ventura et al., 2001).
Since low-mass AGBs undergo several III dredge up episodes, their envelopes will be enriched in carbon and s-process elements (Straniero et al., 1997), which rules any possible role in the contamination of the gas from which SG stars formed.
D'Ercole model describes the current GC as composed by two stellar components: FG and SG stars. The nowdays total mass can be written as $M_{now} = M_{FG,n} + M_{SG,n}$, where $M_{FG,n}$ and $M_{SG,n}$ are, respectively, the amount of mass today in long-lived[1] FG and SG stars. If x indicates the relative abundance of the two populations, we have $M_{FG,n} = \mathrm{x}M_{now}$ and $M_{SG,n} = (1\text{-x})M_{now}$.
It is assumed that at the beginning of the process the GC was constituted only by FG stars, whose initial mass, M_{FG}, followed a continuous King (King, 1962) radial profile:

$$\rho_* = \rho_o \left[1 + \left(\frac{r}{r_c}\right)^2\right]^{-1.5} \tag{4.1}$$

up to the truncations radius r_t. ρ_o is the density at the center of the cluster, and r_c is the radius of the core.
The mass range of these stars is $0.1 < \mathrm{M}/M_\odot < 100$ distributed according to a Kroupa IMF $\Phi(m)$ (Kroupa et al., 1993).

[1] We define long-lived stars as those having initial masses in the range $0.1 < \mathrm{M}/M_\odot < 0.8$. The stars are still alive today in the GC.

The progenitors of the SG are assumed to be the stars of mass below the limit for the core-collapse SN explosion, i.e. M=8 $M_{\odot}$[2]. The theoretical model based on AGB ejecta can be divided in six temporal steps:

1. t=t_0 : the GC is formed by FG stars only;

2. t=5-10Myr: SNII explode, clearing the GC of all pristine gas and part of the FG stars. At this point , M_{FG} is reduced by the amount of $\Delta M_{FG} = \epsilon M_{FG}$;

3. t=38Myr[3]: S-AGB and AGB stars begin to evolve, and pollute the interstellar Cluster with their ejecta;

4. the gas loses energy by radiative cooling and falls down to the center of the Cluster;

5. When the density in the central regions is sufficiently large, the formation of SG begins, first with pure AGB ejecta. This period Δt_f must be long enough to allow the formation of a substantial SG population, but not so long as to include the evolution of stars of mass M $\leq$ 4-5 $M_{\odot}$, which do not provide yields compatible with the observation. For this reason the upper limit for the time considered is 100 Myr.
   The amount of gas returned by the FG in this period is $\Delta M_g = \beta M_{FG}$, where for a Kroupa IMF $\beta = 0.05$; if the efficiency of the star formation maximum(i.e $\nu = 1$), then $M_{SG,n} = \Delta M_g = \beta M_{FG}$.
   It follows that $M_{FG} = \mathrm{f} M_{now} = \frac{1-x}{\beta} M_{now}$; assuming x=0.5 , as is observed in several cases, and β =0.05, we obtain that $M_{FG} = 10 M_{now}$. From this consideration, we deduce that GCs are the relics of much more massive structures, whose mass was $\sim$ 10 times larger than today's.
   This huge extra amount of mass must be lost in the successive evolution of the cluster.

6. Stellar formation is halted by Sn Ia explotions: they put in positive energy breaking up the system, this contribute to the loss of mass in excess.

The investigations by D'Ercole et al. (2008, 2010) stressed that AGB and S-AGB winds alone cannot account for the patterns observed, and that a given degree of dilution, with

[2]This limit changes with the metallicity and overshooting, but theprecise choice does not make an important difference to the global pictures.

[3]In this model we adopt a 8 $M_{\odot}$as the maximum mass does not ignite as SN II which evolve in 38Myr

gas pristine, is required. The presence of this latter component can be due to initial asymmetries in the distribution of the gas, that allow to vent out the SN II ejecta along referential directions, creating an 'hourglass' cavity, and leaving part of the pristine gas in a substantially unperturbed torus at the outskirts of the cluster (e.g Recchi, Matteucci & D'Ercole (2001)). From there, this gas moves toward to the center, mixes with ejecta of AGB and forms SG stars.
Between the end of the SN II phase and the time in which the gas pristine has mixed with AGB ejecta, if the cluster is massive enough, the winds of the S-AGB stars are the only contributors to the cooling flow and the SG formation. Thus in this epoch SG stars with the most extreme helium abundance form.
The minimum mass leading to SN II explosion, and thus the duration of the SN II epoch, depends mostly on the assumptions made on the core overshooting during the core hydrogen burning. Our models employ a moderately large overshooting (Schaller et al., 1992; Ventura et al., 1998). If this is reduced, the minimum mass of possible SN II progenitors increases, and the lifetime of the SN II epoch decreases. This input defines not only the beginning of the phase during which the low-velocity winds accumulate for the SG formation, (after FG SN II stage), but also the duration of a possible subsequent SG SN II phase (from $\sim$ 30Myr to $\sim$ 40 Myr, see section 4.3) This early phase of very helium-rich SG star formation is followed by an epoch during which the pristine gas reaches the cluster inner regions and SG stars form from gas in which the helium of the AGB ejecta, collected in the inner regions by the cooling flow, is diluted with the primordial helium. If the cooling flow goes on after the pristine gas is exhausted, stars will again form with undiluted ejecta, but the evolving AGB mass and its Y will be smaller (e.g Pumo et al. (2008)).
The assumption of a large FG population is necessary for the formation of a significant SG population form the ejecta of the intermediate-mass stars.

4.2.1 Cluster mass loss

A more promising mechanism to reduce the mass of the cluster is the mass loss associated with the SN explosions in the FG population (Chernoff & Weinberg, 1990; Fukushige & Heggie, 1995). The fraction of mass loss depends on the cluster structure, IMF and initial degree of mass segregation.
For initially unsegregated , tidally limited clusters with a Salpeter IMF, it has been shown that the mass loss resulting from this mechanism is negligible if the cluster are suffi-

ciently centrally concentrated ($1 \leq c \leq 2$ McMillan & Potegies Zwart (2003)); Galactic GCs have typical value in this range (Vesperini & Heggie, 1997; Baumgardt & Makino, 2003; McMillan & Potegies Zwart, 2003). Instead, low concentration clusters can lose a significant fraction of their mass and quickly dissolve (Chernoff & Shapiro, 1987; Chernoff & Weinberg, 1990; Fukushige & Heggie, 1995).

Both the response of the cluster to this early mass loss and the critical concentration for its survival depend sensitively on the initial spatial distribution of massive stars. In an initially segregated cluster, the mass lost due to SN explosion is preferentially removed from the innermost regions of the cluster[4], and can lead to rapid and significant overall expansion, mass loss and possibly dissolution, even for an initially highly concentrated system. If it is ejected also the primordial gas, this increases the expansion rate of the cluster (see e.g Boily & Kroupa (2003); Baumgardt & Kroupa (2007)). Thus, after SN II explosions, the cluster expands beyond its tidal radius and the outer layers , which are predominantly populated by FG stars, are stripped. SG stars , which formed in the central regions, remain constant in number during this phase. Thus the number ratio of SG and FG stars increases rapidly.

The characteristic time-scale for this early evolution, expansion and stripping is the cluster dynamical time , $T_{dyn} \propto M^{-1/2}R^{3/2}$, that depends on the degree of initial mass segregation and the amount of impulsive mass loss (Vesperini et al., 2008), as the strength of the expansion.

In Fig 4.1 we show the result of a simulation by D'Ercole et al. (2008); most of FG stars are lost in $T_{dyn} \sim 1$ Gyr, that is rapid compared to the duration of whole evolution of the GC, but slow respect to the formation of the SG stars ($\sim$ 60Myr). The expansion velocity of the cluster is slow ($\sim$ 10 Km/s), thus the AGBs ejecta and gas pristine, through a cooling flow, have time to concentrate themeselves in the center of the cluster, and form SG stars.

Two important quantities are the radius of truncation r_t, and the tidal radius r_{tid} in the Galactic field: when the cluster is expanding and losing mass, r_{tid} increases, while r_t decreases: the expansion and the consequent mass loss stops when $\frac{r_t}{r_{tid}} < 1$.

The subsequent evolution is driven by two-body relaxation and proceeds on a time-scale $T_{relax} = M^{1/2}R^{3/2}$, significantly longer than the dynamical time-scale (for a 10^6 GC, T_{realx} $\sim$ 100 Gyr, see Fig 4.1). Two-body relaxation is responsible for mixing of SG and FG stars and for an additional mass loss, that now will involve both populations: in fact, FG

[4]This happens because many theoretical studies (e.g Klessen (2001), Bonnel et al. (2001), Bonnel & Bate (2006), Krumholz & Bonnel (2007)) show that massive star would preferentially form in the center of star-forming regions.

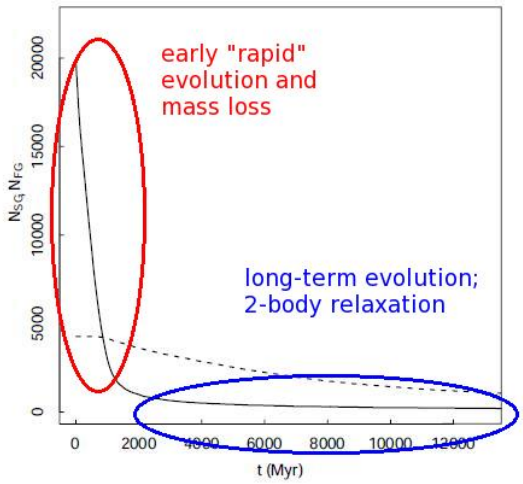

Figure 4.1: Time evolution of the number of SG (dashed line) and FG (solid line) (D'Ercole et al., 2008)

and SG are distributed about uniformly.

4.2.2 Code

The code that simulates the chemical evolution of the system is based on a hydrodynamic one-zone model (D'Ercole et al., 2008).
The evolution of gas density and the formation of SG stars are regulated by 4 equations, integrated by a fourth-order Runge-Kutta method:

$$\dot{\rho(t)} = \alpha\rho_{FG} + \dot{\rho_{pr}}(t) - \nu\frac{\rho(t)}{t_{sf}} \tag{4.2}$$

$$\dot{\rho^k_{ch}}(t) = \alpha^k\rho_{FG} + \beta^k\dot{\rho_{pr}}(t) - \nu\frac{\rho^k_{ch}(t)}{t_{sf}} \tag{4.3}$$

$$\dot{\rho_{pr}}(t) = \frac{\rho_{0,pr}}{\sqrt{\pi}\tau}exp{-[(t-t_{ac})/\tau]^2} - \nu\frac{\rho_{pr(t)}}{t_{sf}} \tag{4.4}$$

$$\dot{\rho_{SG}} = \nu\frac{\rho(t)}{t_{sf}} \tag{4.5}$$

The first equation describes the time evolution of the total gas density ρ. The first two terms on the right hand side represent, respectively, the gas ejected by AGBs (where $\alpha = \frac{\dot{\rho_{FG}}}{\rho_{FG}}$ is the rate of mass loss (Ciotti et al., 1991)) and the density of gas pristine (ρ_{pr}); the third term, negative, represents the amount of gas used to form SG stars, and is characterized by the star formation (SF) efficiency ν, and time-scale, t_{sf}.
In this model ν is a free parameter summarizing the uncertainties about star formation, its

t_{ac}	Time of maximum accretion of pristine gas
τ	Time-Scale of the pristine gas accretion
t_{in}	Initial time at which the simulation starts
t_{end}	Time marking the end of the SG formations phase
ρ_{FG}	Initial density of the FG stars (that we consider constant until the end of the process)
ρ_{pr}	Density regulating the amount of the available pristine gas
ν	SF efficiency
x	The ratio between the nowadays alive SG and the total stars.

Table 4.1: List of free parametes of the code.

value being in the range $0 < \nu < 1$; the time scale coincides with the free-fall time, and is thus proportional to $(\rho^{-1/2})^3$.
The second equation describes the time evolution of the density of every chemical element k. The nine species considered are: He, Li, C, N, O, Na, Mg, Al, Fe. We have thus a system of k_{max} =9 equations, each modelling the evolution of the density ρ^k_{ch} of the k_{th} element. $\alpha^k(t)$ and $\beta^k(t)$ represent the mass return rate of the k_{th} element in the FG, and the mass fraction of the k_{th} element in the pristine gas, respectively. The chemistry of the gas pristine is determined by the assumed initial chemical composition, while the chemistry of the ejecta for every element is obtained at each time by interpolation of the values given by our adopted ejecta abundances.
The third equation describes the time evolution of the gas pristine. The first and the second terms represent the pristine gas accretion and the gas used for the SG formation. Because an hydrodynamical model able to explain the dynamics and the presence of the pristine gas during the SG formation is not yet available, it is used a 'ad hoc' pristine gas . The Gaussian form adopted to model the pristine gas accretion is arbitrary, but allows us to easily explore different accretion scenarios. t_{ac} regulates the time at which the maximum accretion rate occurs, τ controls how the accretion evolves: a small τ corresponds to a sudden accretion, while a large value gives rise to more gradual growth. The constant ρ_{pr} controls the amount of available pristine gas.
The last equation describes the growth of the SG stellar population.

The free parameters of our model are summarizing in Tab.4.1. A more detailed description of the code can be found in D'Ercole et al. (2008); a exploration of this whole set of parameters has been presented in D'Ercole et al. (2010).

Table 4.2: Averaged abundance in the ejecta of Massive AGB and S-AGB stars. The values are obtained for the following set of initial abundances : H=0.75, He=0.24 Li =0.1× 10^{-10}, C=0.849 × 10^{-4}, N= 0.249 × 10^{-4}, O=0.58 × 10^{-3}, Na = 0.103 × 10^{-5}, Mg=0.497 × 10^{-4}, Al=0.178 × 10^{-5}, Fe=0.377 × 10^{-4}.

M/ $M_\odot$	$\tau/10^{6(a)}$	M_c/ $M_\odot^{(b)}$	Y	[O/Fe]	[Na/Fe]	[Mg/Fe]	[Al/Fe]	log$\epsilon(Li)^c$
3.0[1]	332	0.76	0.248	0.92	1.16	0.57	0.65	2.77
3.5	229	0.8	0.265	0.77	1.30	0.55	0.66	2.43
4.0	169.5	0.83	0.281	0.44	1.18	0.48	0.55	2.20
4.5	130.3	0.86	0.310	0.19	0.97	0.43	0.85	2.00
5.0	104	0.89	0.324	-0.06	0.60	0.35	1.02	1.98
5.5	85.1	0.94	0.334	-0.35	0.37	0.28	1.10	1.93
6.0	71.2	1.00	0.343	-0.40	0.31	0.29	1.04	2.02
6.3	65.2	1.03	0.348	-0.37	0.30	0.30	0.99	2.06
6.5[2]	61.5	1.08	0.352	-0.24	0.32	0.34	0.91	2.36
7.0	53.7	1.20	0.358	-0.15	0.39	0.36	0.86	2.12
7.5	46.8	1.27	0.359	0.01	0.67	0.415	0.65	2.75
8.0	38.8	1.36	0.344	0.20	1.00	0.440	0.50	4.39

[a] Total evolutionary time until the AGB phase.

[b] Core Mass at the beginning of the AGB phase.

[c] logϵ = log(N_{Li}/N_H) +12

[1] Yields for 3 ≤M/ $M_\odot$≤6.3 from Ventura & D'Antona (2009)

[2] Yields for 6.5 ≤ M/ $M_\odot$≤ 8.0 from Ventura & D'Antona (2011); Ventura, Carini & D'Antona (2011)

This code develops a chemical evolution model to test how the O-Na and Mg-Al anticorrelations could be built up in different clusters.
As D'Ercole et al. (2010), we adopt the Ventura & D'Antona (2009) yields for massive AGB ejecta and the new yields of S-AGB models from 6.5 to 8 $M_\odot$ computed by Ventura & D'Antona (2011) (see Tab. 4.2).

4.2.3 Extra-mixing

The recent investigation by Ventura & D'Antona (2009) showed that the degree of contamination of the ejecta of massive AGBs is not monotonic with mass; in particular, the gas ejected by SAGBs show a higher sodium and oxygen compared to models of low mass, at the edge between the AGB and the SAGBs regime: [O/Fe] never drops below -0.4 (see Tab. 4.2).
Unlikely, Carretta et al. (2009a) observed in giants of some clusters extremely small abundances of oxygen, [O/Fe] ∼ -1.

In agreement with D'Ercole et al. (2010), we assume that the extremely low oxygen abundances are due to deep extra-mixing from the base of the convective envelope during the RGB evolution: the surface convection penetrates inwards down to layers touched by advances p-capture nucleosynthesis, where oxygen destruction occurs.
This phenomenon is more likely to occur in SG stars, because they formed from He-enriched matter, such that the H-He discontinuity left behind by the first dredge-up is smaller. This would decrease the entropy barrier preventing the penetration of the envelope, thus rendering easier the extra-mixing process (D'Antona & Ventura, 2007).
We apply the following deep-mixing scheme to our models: a population of SG star is born from the pure ejecta of S-AGB stars and massive AGBs, in which, if the helium content is Y >0.34, we assume that the surface abundances in the atmospheres of the SG giants are modified by deep-mixing. We proceed in the following way:

1. We examine the helium abundance in star-forming gas at each time-step;

2. If the helium content exceeds 0.34 we adopt a 'deep-mixing' scheme to provide the oxygen content at the surface of giants. In absence of a no parametric models, the relation chosen to fix the oxygen content after the deep-mixing has some degree of arbitrariness. We assumed a linear dependence of the surface oxygen with the helium content. [O/Fe] is linearly interpolated between -0.4 and -0.9 dex, assumed, respectively, for Y=0.34 and Y=0.36. Consequentely, stars formed from the ejecta of the 7.5 $M_{\odot}$ model, will have the smallest content of oxygen [O/Fe]= -0.9 dex.

3. If the average helium abundance is smaller than the values for which deep-mixing occurs, the [O/Fe] of the SG stars is equal to the everage between the standard [O/Fe] $\sim$ 0.4 dex of the pristine gas and the mildly depleted [O/Fe] of Tab. 4.2.

4.3 Comparison with the real cluster

We applied the chemical evolution framework described above to build two specific models for NGC 2808 and M 4. This choice was motivated not only by the large data sample available, but also because they represent the examples of two opposite situations, where the O-Na anticorrelation extends to very small oxygen and high sodium abundances, or where the observed pattern is very narrow.
NGC 2808 is a very massive cluster ($1.6\times10^6\ M_{\odot}$). The study by Piotto et al. (2007), aimed at the interpretation of the three distinct MS observed, confirmed the earlier speculation by D'Antona & Caloi (2004): NGC 2808 harbors three distinct populations, dif-

	H	Y	Li	C	N	O	Na	Mg	Al	Fe
NGC 2808	0.75	0.24	1.047e-9	0.849E-4	0.249E-4	0.580E-3	0.103E-5	0.4e-4	0.25E-5	0.001*0.0377
M4	0.75	0.24	1.047e-9	0.849E-4	0.249E-4	0.580E-3	0.0.103E-5	0.6e-4	0.6e-5	0.001*0.0377

Table 4.3: Chemical abundances of the gas pristine.

fering in the helium content. According to the analysis made by Milone et al. (2012b) the fractions of standard (red MS), intermediate (middle MS) and high helium (blue MS) are, respectively, 62±2%, 24±2% and 14±3%.
M 4 is a much less massive ($6.7\times10^4\ M_\odot$) cluster, exhibiting a milder variation in elemental abundances, particularly in oxygen; apparently, the spread in sodium is larger. We use data of NGC 2808 by Carretta et al. (2006, 2009a,b), data for M4 from Marino et al. (2008b).
The chemistry of the gas pristine reflecting the composition of the FG stars can be deduced from the observations: FG stars populate the clump of star in the right-lower side of both O-Na and Mg-Al planes. In Tab. 4.3 we show the chemistry of the gas pristine used in our simulations.
In the present models for NGC 2808 we set x=0.4, because we assume that the fraction of FG stars, with standard helium (Y $\sim$ 0.24) is 60%, and set the other input parameters in order to obtain a reasonable result for the number ratio of the extreme and intermediate SG. Instead we set x=0.5 for M 4. The input parameters of the different model are shown in Tab. 4.4. To the list indicated in Tab. 4.1 we have added t_f and δt_t: the first is the time until which the AGB ejecta are accumulated before star formation begins, the second is the time interval during which there is no star formation, and is used in the models where we considered the explosions of SN II belonging to the SG. From Tab. 4.4 we note that t_{end} is not necessary linked to t_{acc} and τ_{pri}, as the phenomenon determining the end of the SG stars formation (e.g the phase of type I supernova explosions D'Ercole et al. (2010)) is not related.

4.3.1 NGC 2808

The Globular Cluster NGC 2808 (mass M = $1.6\times10^6\ M_\odot$) exhibits a well extended anticorrelation in the O-Na plane, with an overall spread of about 1.2 dex in oxygen, and 1.0 dex in sodium. The distribution is rather homogeneous, with no clear gaps separating FG and SG stars. Data show that the majority of the stars has aluminum and magnesium abundances expected for an α-enhanced population (with a small enhancement in the Al

Cluster	Model	SG formation	$t^a_{acc}(Myr)$	τ_{pri}(Myr)	$t_{end}(Myr)$	t_f or δ^b_t (Myr)	ρ_{FG} ($M_\odot$/pc^3)	$\rho_{0,pr}$	ν	x
NGC 2808	1	continuous	65	8	90		200	0.0095	1	0.4
NGC 2808	2	accum.	65	8	90	(50)	200	0.0095	1	0.4
NGC 2808	3	bursts	87	10	100	50-80	200	0.0045	1	0.4
NGC 2808	4	bursts	87	10	90	50-80	200	0.0045	1	0.4
NGC 2808	5	bursts	87	10	90	50-80	200	0.02	1	0.4
M4	1	continuous	43	1	100		40	0.085	0.1	0.5
M4	2	continuous	43	2	60		160	0.05	0.3	0.5
M4	3	accum	43	2	60	(45)	160	0.045	0.5	0.5
M4	4	accum	48	10	60	(48)	160	0.08	0.5	0.5

[b] t_f:time until which the AGB ejecta are accumulated before star formation begins. In model NGC 2808-3,4,5 we list δt, the time interval during which there is no star formation.

Table 4.4: Dynamical input parameters for the simulations

content) (Carretta et al., 2006). Three giants (indicated as open squares, taken from Carretta et al. (2009b, 2010) show an Al-enhancement by ∼1 dex and a magnesium reduction by a factor ∼ 2; this picture is completed by two TO stars by Bragaglia et al. (2010a), indicated with asterisks.

Fig. 4.2 shows the model NGC 2808-1 (see Tab.4.4 for the set of input parameters). After the phase of formation from super-AGB ejecta, the peak value of the re-accretion occurs at t_{acc} 65 Myr (cf. bottom-right panel). The epoch from 38.9 to $\gtrsim$ 50 Myr corresponds to the formation of the extreme population, with Y ∼ 0.35. This accounts for the presence of the blue MS. The following dilution phase leads to the formation of a less extreme SG (Y∼ 0.3) that populates the intermediate MS of this cluster.
The top-left panel of Fig 4.2 shows the Mg and Al predictions. Use of the new yields for Mg and Al listed in Tab 4.2 does not allow the fit of the three Mg-poor giants ($\delta[Mg/Fe]$ ∼ -0.6 dex) observed by Carretta et al. (2009b), neither the two blue MS observed by Bragaglia et al. (2010a).
Ventura, Carini & D'Antona (2011) investigated the details of the Mg-Al nucleosynthesis in massive AGBs, outlining the crucial role played by the $^{25}Mg(p,\gamma)^{26}Al$ cross section in the overall Mg-depletion, and showing that an increase by a factor 2 in the corresponding reaction rate leads to a better agreement betwee theoretical predictions and the aluminum values observed in blue MS stars (Bragaglia et al., 2010a)
The three red giants with low Mg constitute a problem for any pollution model, and can not be explained in the deep-extra mixing framework.
In the bottom-left panel of Fig 4.2 it is shown the O-Na anticorrelation. The new super-AGB sodium yields are able to reproduce the large sodium of the extreme populations, whereas the extremely small oxygen can be reproduced only by using the deep mixing

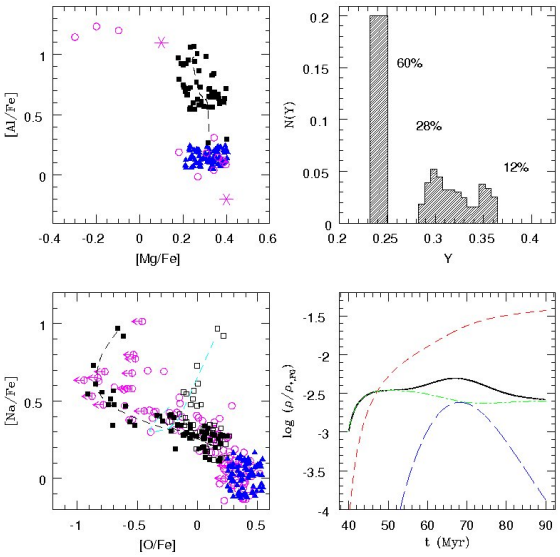

Figure 4.2: Results for the models NGC 2808-1 (left panel). The top-left panel and the bottom left panel show the [Mg/Fe]-[Al/Fe] and [O/Fe]-[Na/Fe] anticorrelations, respectively. Data for giants (open circles) are taken from Carretta et al. (2009a,b). The two turn-off stars examined by Bragaglia et al. (2010a) are shown in the Mg-Al panel with star symbols. The open squares in the O-Na panel represent the location of stars formed from ejecta with Y > 0.34 in the absence of the deep-mixing (e.g. for the blue MS turn.off stars). The black squares and blue triangles represent a sampling of the SG and FG stars by our model, respectively. The dashed lines represent the gas trajectory within the diagrams; the sampled stars in principle would be located on this line, but we introduced a random scatter in the range 0.1 dex in their coordinates in order to mimic the observational errors. The open squares represent the values of oxygen that should be found in MS stars with Y>0.34 when the deep-extramixing has not yet taken. The top-right panel illustrates the stellar He distribution. In the bottom-right panel is reported the evolution of the following quantities: total amount of gas (black solid line), AGBs ejecta (green dot-dashed line), pristine gas (blue long dashed line) and SG stars (red dashed line)

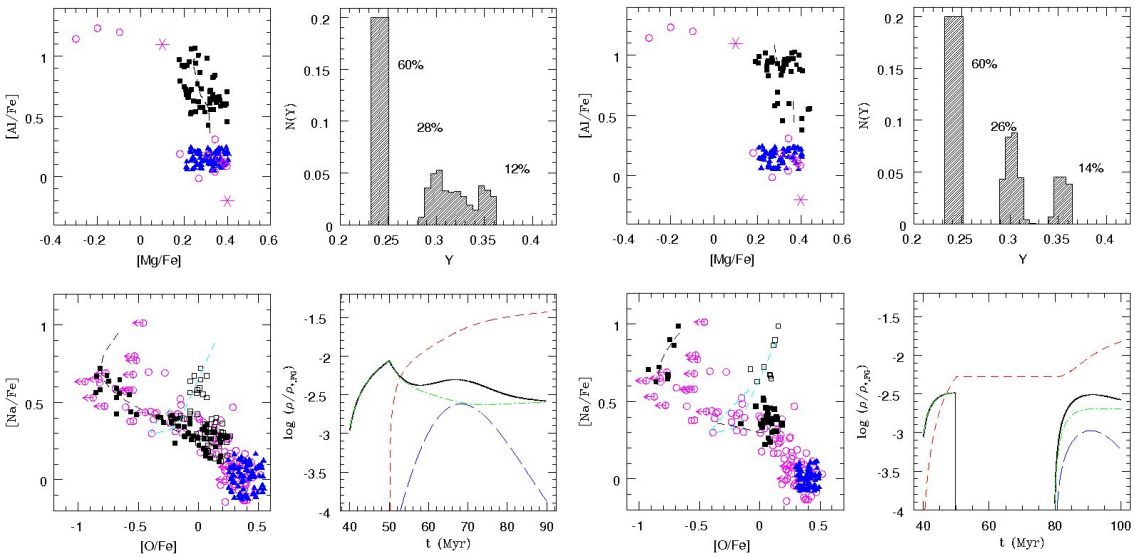

Figure 4.3: As in Fig 4.2 but for the model NGC 2808-2,3.

hypotheses (see section 4.2.3).

The open squares represent the values of oxygen that should be found in MS stars with Y > 0.34, based on the chemistry of the ejecta with no extra-mixing. These stars should be characterized by oxygen abundances larger than those of giant stars and fall along the Na-O curve determined by the new yields.

When dilution with pristine matter sets in, the model trajectories (dashed line) tend towards the FG abundances; however, during the last 10-15 Myr, star formation occurs again in only undiluted AGB ejecta, and the abundance revert back to lower O and larger Na values. This last phase of star formation is necessary to fill the gap in the O-Na plane values between the formation of the extreme population, and the intermediate populations with strong dilution. The bump in the helium distribution between the peaks at Y=0.3 and Y=0.35 forms during this stage as well. Stars with very large [Al/Fe] in the simulation also form in this last epoch of star formation. This can be understood by looking at the abundances listed in Tab 4.2, showing that the maximum Al enhancement and Mg depletion are reached with the evolution of the 5.5 $M_{\odot}$, evolving in ~85Myr.

The top-right panel of Fig. 4.2 shows the histogram of the helium abundances. The number ratio of the intermediate and extreme populations of the SG depends on the initial mass function, and on the timing and extent of the dilution with pristine gas; this is a powerful constraint for any model. In our model we can distinguish three peaks in the helium distribution, with percentage in agreement with the analysis by Milone et al. (2012b).

The left panel of Fig. 4.3 shows the results of the model NGC 2808-2, having the

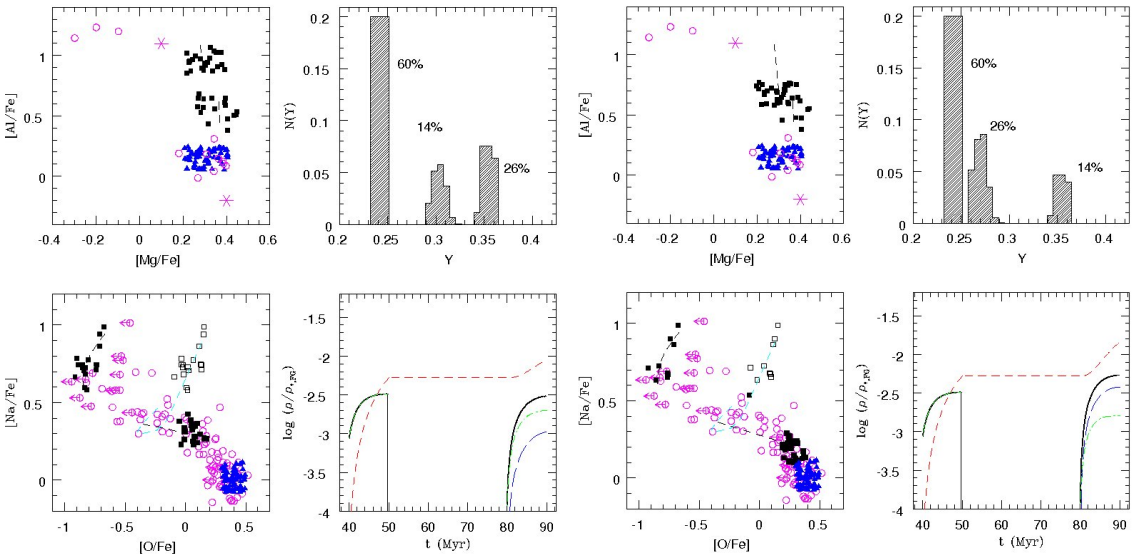

Figure 4.4: As in Fig 4.2 but for the model NGC2808-4,5.

same parameters of the previous model, with the difference that here the SG formation does not start immediately after the end of the SN II epoch, but burst occurs after the ejecta have been accumulated for 10Myr, from 40 to 50 Myr since the beginning.

The results are very similar, with the difference that the extreme populations does not reach the high sodium abundances obtained in the model NGC 2808-1; this is a mere consequence of the fact that, before the SG formation begins, the ejecta of stars with mass between 7.3 $M_{\odot}$ and 8 $M_{\odot}$ mix, so that the highest abundances are smaller. For the model 3 (Fig 4.3 right panel), 4 (Fig. 4.4 left panel) and 5 (Fig 4.4 right panel) we assume that $\sim$ 10 Myr after the extreme population began to be formed in the cluster, a new phase of the SN II phase occurs. We can have a second burst of star formation from the AGB ejecta starting at $\sim$ 80Myr.

We discussed in section 4.2 that the time between the two bursts may be reduced to $\sim$30 Myr for model employing a smaller core-overshooting. Thus we employ in the following $\sim$ 30 Myr as the total duration of the SG SN II epoch.

The main difficulty encountered in models including SN II explosions from the extreme SG is to reproduce at the same time the extension and distribution of stars along the O-Na anticorrelation and the helium distribution function. In the model NGC 2808-3 (Fig 4.3, right panel) we stop the formation from the pure ejecta at 50Myr, allow for a $\gtrsim$ 30Myr period without star formation and then resume star formation from the AGB ejecta mixed with pristine gas, with the choice t_{acc}= 87 Myr. The clumps in the distribution of stars in the O-Na plane are too separated to be consistent with the observations. Moreover, in

order to obtain a reasonable number ratio between the He-rich stars (Y > 0.34) and the intermediate population (Y ∼ 0.30), we are forced to extend the star formation of this latter population to ∼ 20Myr, much longer than allowed by the beginning of the new (third) SN II epoch.
The model NGC 2808-4 (Fig 4.4, left panel) is identical to the last, but the formation of the intermediate population is limited to 90 Myr. The fraction of stars in the intermediate population is only 14%, in clear disagreement with the data.
In the case NGC 2808-5 (Fig 4.4 right panel) we increase the relative number of intermediate population stars by increasing dilution. The second peak of helium content occurs at Y ∼ 0.28, and the number ratio of extreme to intermediate population becomes reasonable; however the O-Na values become much too close to the FG values, due to the strong dilution (this was discussed in D'ercole et al. (2011) in a different context). This last models can not reproduce the observations as well as NGC 2808-1 and NGC 2808-2. Nevertheless, the variety of observational results for different clusters may have their explanation in the variety of relevant paramenters. In fact, the model NGC 2808-4 could be relevant to explain the HB stellar distribution of the cluster NGC 2419 (di Criscienzo et al., 2011).

4.3.2 M4

Figs 4.5 and 4.6 show the comparison of the predictions for models 1-4 for M4 (see Tab. 4.4), and the results from the observations. The bottom-right panel shows the role of the ejecta (dash-dotted line) and of the pristine gas accretion (long dashed line) and their timing in the formation of the SG (dashed line). The bulk of the SG formation occurs when the pristine gas is re-accreted, at 43 Myr, and lasts for about 50 Myr. The dashed lines in the left-hand panels show the path of the O-Na and Mg-Al abundances along the simulation. When dilution with pristine matter sets in, the values tend towards the FG abundances. As discussed by D'Ercole et al. (2010), this choice of input parameters provides agreement with the data if we assume a yield of sodium 0.2 dex larger than the values in Tab 4.2. This would mean to assume that the neon abundance in the gas forming the FG stars of M4 is +0.2 dex larger than in other cluster-forming regions, in particular in NGC 2808, for which we used directly the value in Tab. 4.2.
The star formation efficiency in this model is smaller (ν =0.1) compared to NGC 2808; this means that no stars forms directly from super AGB ejecta (as wee also see from the distribution of the helium abundances). For all the models for M4 we assume x =0.5, because a fraction of 50% of FG stars is consistent with the fraction of red HB stars given

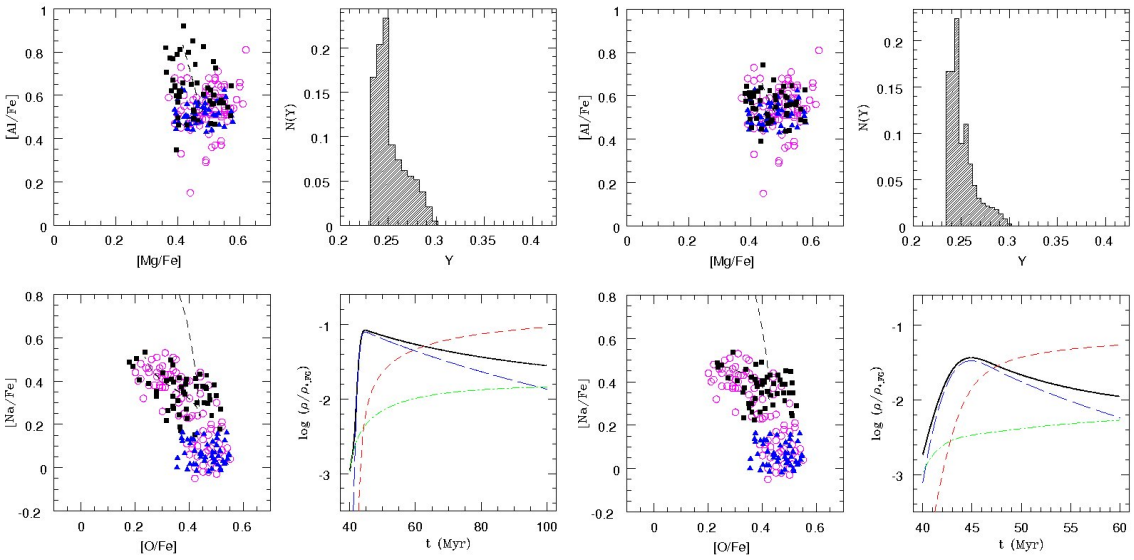

Figure 4.5: Simulations for the SG of M4, in the cases 1 (left) and 2 (right). For each one, the top-left and the bottom-left panels show the [Mg/Fe]-[Al/Fe] and [O/Fe]-[Na/Fe] diagrams. respectively. Data (open circles) are from Marino et al. (2008b). The squares and the triangles represent a sampling of the SG and the FG stars by our model, respectively. The dashed line represent the gas trajectory within the diagrams; the samples stars in principle would be located on this line, but we introduced a random scatter in the range of 0.1 dex in their coordinates in order to mimic the observational errors. The top-right panel illustrates the stellar He distribution. In the bottom-right panel the evolutions of the following quantities is reported : total amount of gas (solid line), stellar ejecta (dot-dashed line), pristine gas (long dashed line), SG (dashed line).

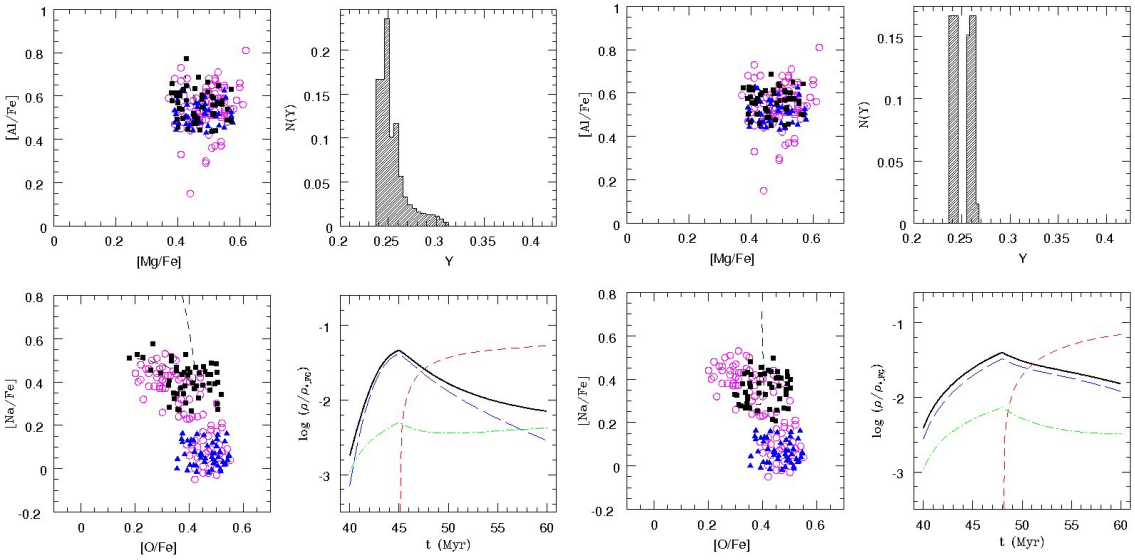

Figure 4.6: Left panel: Model M4-3. The pristine gas and the super AGB ejecta accumulate and a short-lasting burst of star formation occurs at 45 Myr (symbols as in Fig **??**.) Right panel: Model M4-4. The burst of star formation occurs after accumulation until an age of 48 Myr: FG and SG stars are born with a finite, although very small, difference in helium content (symbols as in Fig. 4.5).

in Marino et al. (2008b).

Model M4-1 requires the presence of pristine gas since the early phases of SG formation to efficiently dilute the S-AGB matter.

Thus the strong dilution of the high helium S-AGB ejecta leads to helium abundances not much larger than the pristine helium abundance in the gas forming SG. The oxygen content is not reduced by deep-mixing: the SG end up forming a group of stars with relatively large sodium (also thanks to the inclusion of δ[Na/Fe]=+0.2 in the yield table), but with oxygen depleted only by $\sim$ 0.1 dex. The small helium spread shown by this simulation is probably undetectable on the MS, but can lead to a distribution of the HB stars such that the Na-rich stars are bluer than the Na-normal stars, as found by Marino et al. (2011).

We have run model M4-2 to illustrate how acceptable solutions can be obtained even a significantly shorter evolutionary times. This shows that this kind of models are flexible enough to reproduce the observations in a variety of conditions; this also means, however, that these models can provide only limited constraints on the gas hydrodynamics and the related star formation history. In Fig 4.6 we show two different cases. We adopt ν =0.5 and let the S-AGB ejecta and pristine gas accumulate up to an age of 45 Myr, when a burst of formation occurs lasting until a total age t_{end} =60Myr.

The difference between the two models is that, in the second star formation begins at 48

Myr. The helium content of the SG is only slightly increased, but here it is well separated from the FG value. Possibly, a careful colour analysis of the MS width following the lines described, e.g in Milone et al. (2012a) could reveal this bimodality in helium, and discriminate between this model and the previous one. Models similar to this may be able to reproduce the abundances in other clusters showing a bimodal HB.
The helium abundance offer a strong possible way to choose among the models, by examining the morphology of the HB, and the abundance of sodium and oxygen at different location along the HB.
We have already outlined in Chapter 1 that D'Antona et al. (2002) proposed that the colour spread in the HB of most GCs is not an effect of a mass-loss spread, as generally thought, but as an effect of a helium increase from the cooler to the hotter side. At a given age, the mass of stars evolving off the MS is smaller for larger helium abundances. This implies that, for a similar mass loss, a star ends up with a smaller mass on the HB, thus in a bluer location. Depending on the metallicity, a very small helium increase (from Y=0.24 to Y=0.27) is necessary to produce the gap between the red clump and the blue HB in NGC 2808 (D'Antona & Caloi, 2004). In clusters like M4, having a more continuous distribution between red and blue, the helium variations may have been less abrupt. Marino et al. (2011) found that the blue HB stars of M4 have high Na, while the red HB stars have normal Na. Furthermore, Villanova et al. (2012) have recently observed six blue HB stars in M4, finding that they have high Na, low O and helium content Y $\sim$ 0.29. A similar location of Na-rich, O-poor stars at the blue side of HB has been recently discovered by Gratton et al. (2011b) in NGC 2808, confirming the scenario. We remark this same analysis shows a mild anticorrelation of the colour with Na/O ratio within the red clump stars, so that, contrary to the simple interpretation, even the red side of the HB may not only be fully populated by FG stars, but also by a few SG star having helium content barely larger than FG value. Quantitative simulations of the HB might help to determine which of models presented is the best.
The models presented here can potentially explain a variety of different HB morphologies and can be tested by spectroscopic observations similar to those by Marino et al. (2011) and Villanova et al. (2012). We summarize these results by concluding that:

- The mild O-Na anticorrelation and the small-if any- variation in helium shown by a class of GC can be due to pollution of super AGB stars into the re-accreted pristine gas forming the SG stars;

- The SG formation phase can have a short duration ($\sim$ 20Myr) and does not need to extend up to $\sim$ 100Myr as M4-1 and found by D'Ercole et al. (2010). The model

characterized by a shorter SG formation epoch, on the other hand, require a larger star formation efficiency, and can be compatible with a second phase of SN II explosions due to the evolution of SG massive stars, this relaxing any assumption of anomalous IMF.

- A shorter SG formation implies that the mass range of the AGB progenitors providing polluter ejecta for the SG formation is narrower and, therefore, that these models require a more massive FG cluster to be able to produce the observed amount of SG stars. Models with a short SG formation phase typically require an initial FG mas three to four times larger than that needed in models with a more extended SG phase.

4.4 Lithium

Lithium abundances offer a complementary approach to p-capture elements allowing to address several important issues.
Lithium is easily destroyed by proton capture in stellar interiors, so determining its abundance may be crucial to discriminate among the different models proposed to account for the origin of the gas from which the multiple populations form. In fact massive stars destroy lithium, while massive AGBs produce it at the beginning of the AGB phase (Ventura et al., 2002): thus the prediction of the two models differ. The polluting matter is Li-free also for the scenario of the massive binary stars (de Mink et al., 2009) or from runway collision between massive stars (Sills & Glebbeek, 2010).
Self-consistent models to study the chemical evolution of lithium in multiple population GCs are still lacking, while some sets of observational data are already available.
Decressin et al. (2007b) show that the Li-Na anticorrelation in the data of NGC 6752 (Pasquini et al., 2005) are fully compatible with a simple dilution model; on the other hand Shen et al. (2010) present new Li-O data, probably not compatible with dilution with Li-free matter. In other clusters, like NGC 6397 (Lind et al., 2009), M4 (D'Orazi & Marino, 2010; Monaco et al., 2012), 47 Tuc (D'Orazi et al., 2010) the two populations have very similar lithium content, and Li-depleted stars may be attributed to convective dilution. The similar abundances in these clusters seem in better agreement with the AGB scenario. In this section we show the lithium abundance pattern for NGC 2808 (for which there are not data available), and M4 (data by Monaco et al. (2012)).
Since there is still debated discrepancy between the predictions for primordial lithium from the standard Big Bang nucleosynthesis and the abundance observed in the atmo-

spheres of population II stars, we made models based on different initial lithium abundance in the diluting pristine gas.
The standard Big-Bang nucleosynthesis (BBN), with the cosmological parameter $\eta=\frac{N(baryons)}{N(photons)}$ constrained by the observations of the satellite WMAP, provides A(Li) =2.64±0.04 (Spergel et al., 2007), or even higher, A(Li)= 2.72±0.05, when updated rates for the $^3He(\alpha,\gamma)^7Li$ reaction are taken into account (Cyburt et al., 2008). The values computed from the analysis of spectra of population II dwarfs are A(Li)=2.37±0.06 (Meléndez & Ramírez, 2004), or A(Li) =2.23±0.07 in the non-LTE analysis by Asplund et al. (2006).
In our analysis we have taken into account these discrepancies; the possible choices are:

1. We assume as primordial abundance, the one observed in pop. II stars. Thus, we adopt A(Li)=2.2 or 2.3 as value for the pristine diluting gas and for the FG stars;

2. We accept the BBN, but assume that the lithium is depleted in the atmosphere of both FG and SG stars, as a consequence of phenomena such as diffusion, gravity waves, rotational mixing and so on. In this case A(Li)=2.6 or 2.7 for pristine gas, but the atmospheric effects reduces the abundances of $\delta A(li)$ =-0.3 -0.5 dex

3. the FG ejecta have no lithium at all; in this case the initial abundance of lithium in the pristine gas is not relevant;

4. Since there is an overestimate of the mass loss rate during S-AGB evolution, the Li-yield are uncertain, thus we decrease the yields of the 7.5 $M_\odot$ and 8 $M_\odot$ to A(Li)=2.0;

5. the AGB ejecta are diluted with gas having no lithium.

The last case can be reproduced considering the scenario by Gratton & Carretta (2010), which proposed that the source of the matter required for dilution comes from mass loss from FG stars. They can quantitatively provide the gas necessary to achieve this, if we consider the MS stars of all masses and reasonably large mass-loss rates. Consequently, this gas has no lithium, because lithium burns below the stellar surface as soon as the temperature increases above $\sim 2.5\times 10^6$ K, and the mass-loss rate required in this scenario implies that layers of matter that have reached this temperature must contribute to the dilution. Another possible case is when the diluting gas comes from the mass lost by non-conservative evolution of massive close binaries (Vanbeveren et al., 2012) or by close encounters of stars in the dense cores of the GCs (Carini et al., in preparation). It is clear that in the models for M4 in which there is a strong dilution with pristine matter (from M4-1 to M4-4), the abundance of lithium in the SG will be very small, at odds with the observations. Further observations of lithium in clusters may help to falsify this model.

Case	Processed ejecta	Dilution	Pristine gas Abundance
A	S-AGB and AGB	Prist	BBN A(Li)=2.6, 2.7
B	S-AGB and AGB	Prist	Pop II A(Li)=2.2, 2.3
C	matter with N(Li)=0	Prist	BBN A(Li) not relevant
D	A(Li) reduced in S-AGB	Prist	BBN A(Li)=2.6,2.7
E	A(Li) reduced in S-AGB	Prist	Pop A(Li)=2.2, 2.3

Table 4.5: Possible cases of the lithium dilution when forming the Second Generation stars.

An example of this case has been made for NGC 2808; the results are shown in Figs 4.9 and 4.10. The list of the cases treated here is in Tab 4.5.

The lithium abundance of the SG stars is very similar to that of the FG stars if we are dealing with case B [A(Li) = 2.2 or 2.3], because the lithium in the ejecta is very similar to what we assume to be the abundance in the pristine gas.
Conversely, if we deal with case A [A(Li) = 2.6 or 2.7], the abundances in the ejecta are on the average smaller than in the pristine gas, and the SG shows a slightly reduced lithium abundance, in full agreement with the data.
In order to explore the range of parameters, we assume an initial $A(Li)_{pristine}$=2.2 or $A(Li)_{pristine}$=2.7 for M4, and $A(Li)_{pristine}$=2.3, or $A(Li)_{pristine}$=2.6 for NGC 2808. This is motivated by the FG abundances listed by different authors for the FG stars in the two different clusters.
Since there are not observational data of Li-Na for NGC 2808, we analyze only the best model that reproduce the O-Na anticorrelation (NGC 2808-1) because the trends are very similar to each other. For M4 we compare our models with data of Monaco et al. (2012).

4.4.1 NGC 2808

In Figs 4.7 we examine the predictions of the Li-Na and Li-O patterns for the model NGC2808-1 considering A(Li)=2.3 (case B).
Stars with large lithium abundances could be formed from ejecta of S-AGB. We note the difference in the pattern obtained with a different lithium abundance for the gas pristine, A(Li)=2.6 (case B, see Fig. 4.8). In fact the maximum Li achieved is larger in case B, where the atmospheric abundance coincides with the initial gas abundance, as no reduction is ascribed to mechanism that deplete it. If the pristine gas has a larger, e.g. a standard Big Bang A(Li)=2.6, we implicitly assume that depletion mechanisms are acting at the surface to decrease this value by $\sim$ 0.3 dex. This same mechanism will apply also if the

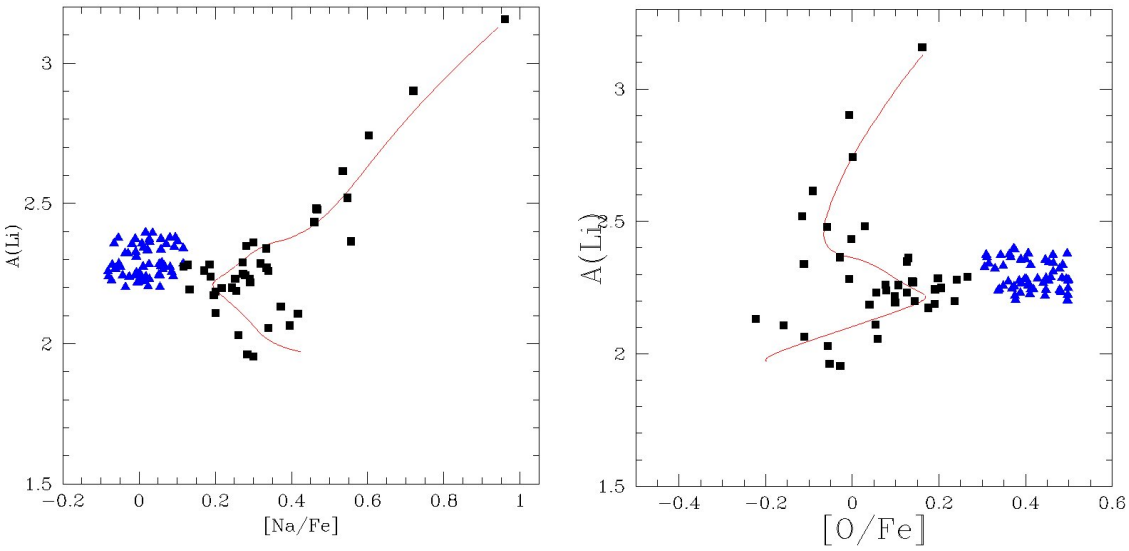

Figure 4.7: Li-Na(left panel) and Li-O(right pane) simulations for a cluster like NGC 2808, harboring an extreme, very helium rich populations, and an intermediate one. The parameter refer to the model NGC 2808-1 in Tab 4.4. The Lithium abundance is A(Li)=2.3. Blue triangle represent the first generation populations, black squares are the SG stars.

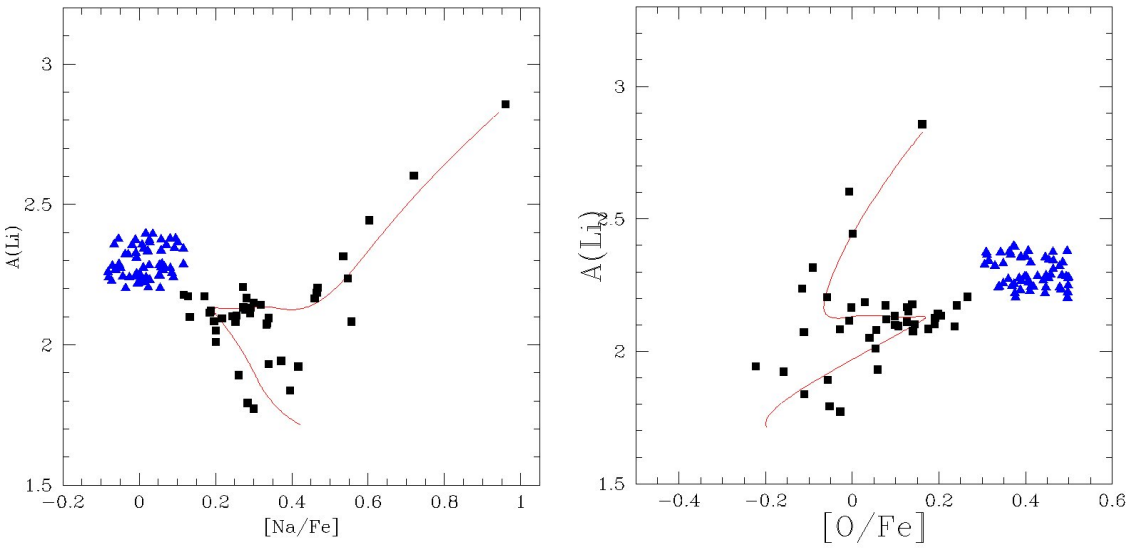

Figure 4.8: As in Fig 4.7, but the abundance of lithium is A(Li)=2.6

lithium abundance in the star is the result of the S-AGB ejecta high abundance.
Thus, contrary to simple intuition, lithium in SG stars (and in particular its maximum abundances, that are directly related to star formation from pure ejecta) will be ~ 0.3 dex smaller if the diluting gas has a larger abundance, in the stars that form from pure ejecta.
An observational confirmation of these predictions would provide strong support to the AGB scenario, as described by our models. However, we point out that if observations will not find a large lithium abundance in the blue MS, this would not falsify the AGB scenario but, rather, it would simply be an indication that the mass loss rates adopted for the models of 7.5 $M_{\odot}$ and 8 $M_{\odot}$ are too extreme. These observations are not yet available.
Another interesting property of the simulations for NGC 2808 are the abundances of lithium in the intermediate populations: these result from mixing of pristine gas (having a lithium content chosen according to cases A or B) with the lithium of the massive AGBs. As shown in Figs. 4.7 and 4.8, the lithium abundances in the intermediate population is lower than the pristine abundances, and the two cases provide interestingly different results. The choice of the pristine gas abundance affects the slope of the average relation Li-Na and Li-O, that are milder in the case B. In any case, the finite amount of lithium in the ejecta of massive AGBs produces slopes milder than predicted in the case of pure dilution of pristine gas with lithium free, sodium rich and oxygen poor matter (see Figs 4.9 and 4.10).

4.4.2 M4

In Fig 4.11 we show the recent data provided by Monaco et al. (2012) for a sample of main sequence and subgiant branches in the Globular Cluster M4, compared with the data of giants in the same cluster given by D'Orazi & Marino (2010). The giants data are shifted to take into account the dilution with respect to the abundance in dwarfs, that we are assuming to be uniform. The difference between the two samples is the trend of the Na-Li anticorrelation: in fact, data by D'Orazi & Marino (2010) show a larger spread between FG (low sodium) and SG (higher sodium) stars. We have compared the Na-Li anticorrelations from our models with data by Monaco et al. (2012). We have considered the cases listed in Tab 4.5.
The slight trend of the Na-Li anticorrelation is a fundamental ingredient to compare the results with observational data.

Fig. 4.12 shows the results of the model M4-1, in which the bulk of accretion of pristine matter and star formation of the SG stars occur during the evolution of the masses from ~ 7.5 $M_{\odot}$ down to 7 $M_{\odot}$. As in the previous figures, we show as blue triangles and

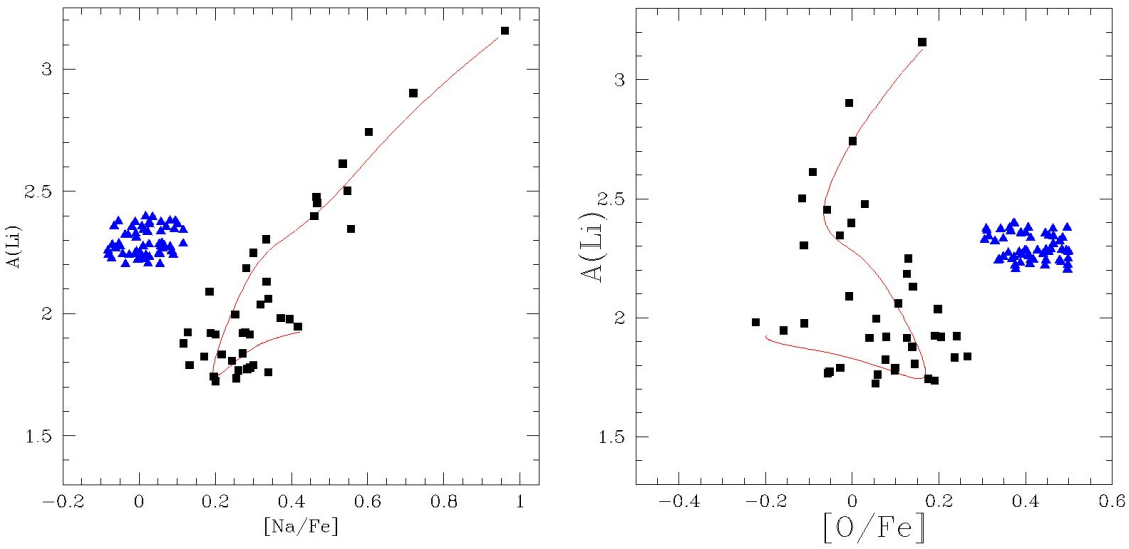

Figure 4.9: Li-Na(left panel) and Li-O(right pane) simulations for a Custer like NGC 2808-1. In this case we assume the absence of lithium in the diluting gas. Notice that the extreme population is similar to that shown in Fig. 4.7, because the SG formation occurs in the undiluted matter, has much loser lithium abundances

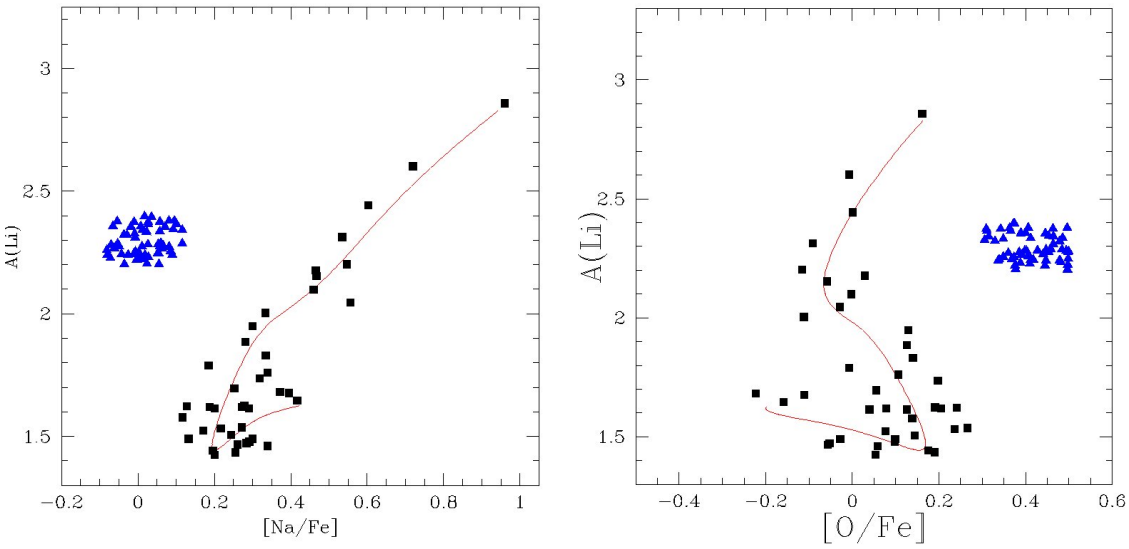

Figure 4.10: As in Fig 4.8, with the assumption of a lithium free pristine gas.

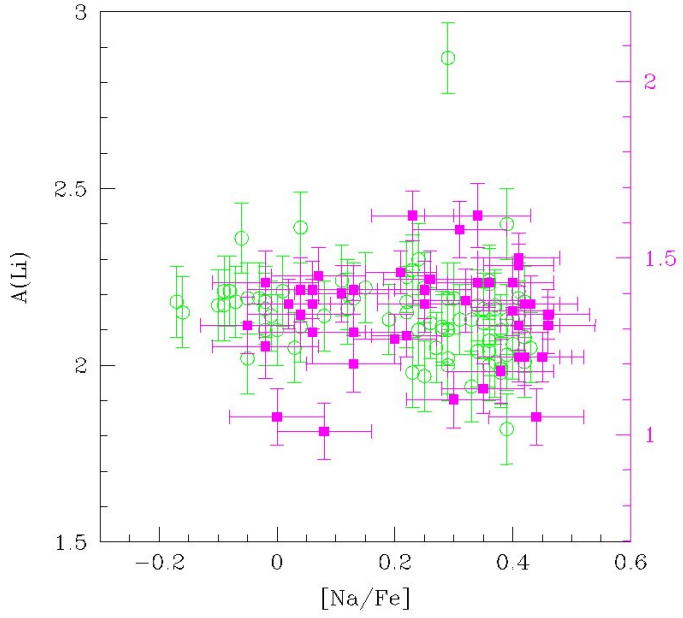

Figure 4.11: The lithium versu sodium data in sample in Monaco et al. (2012) for turnoff-subgiant Branch stars in M4 (green open circle with error bars scale) are compared with dated by D'Orazi & Marino (2010) (scale on Right) for giants stars. The abundance in the giants is depleted by convective dilution with respect to the abundance in dwarfs, we assume that this dilution is uniform, and compare the data by simple shift of the scale of the A(Li) logarithmic abundances

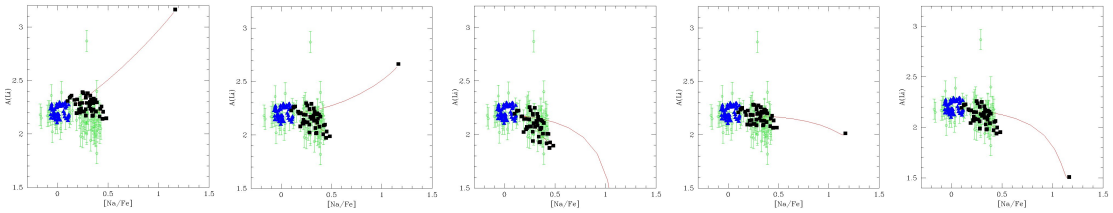

Figure 4.12: Comparison of the result of M4-1 model with data of Monaco et al. (2012) (Opens green pentagons with error bars. The FG and SG generation stars are represented by blue triangle and black squares, respectively. The first panel show the B case, in which the A(Li)=2.2 dex in the pristine diluting gas, the second is the case A, in the third we assume the abundance in the AGB ejecta is negligible, in this case the different between A(Li)=2.2 or 2.7 in the gas pristine is irrelevant; in the following cases we assume that the polluting S-AGB matter (7.5 $M_{\odot}$ and 8 $M_{\odot}$) are reduced to 2.0 dex.)

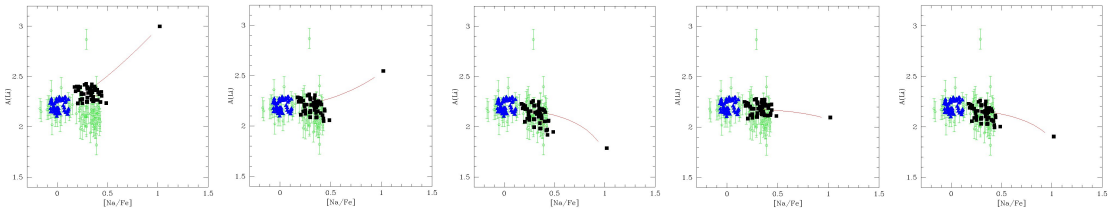

Figure 4.13: Comaprison of the result of M4-2 model with data of Monaco et al. (2012) (Opens green pentagons with error bars. The FG and SG generation stars are represented by blue triangle and black squares, respectively.)

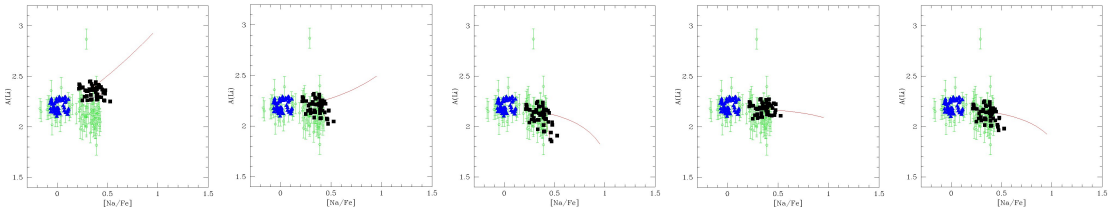

Figure 4.14: Comaprison of the results of M4-3 model with data of Monaco et al. (2012) (Opens green pentagons with error bars. The FG and SG generation stars are represented by blue triangle and black squares, respectively.)

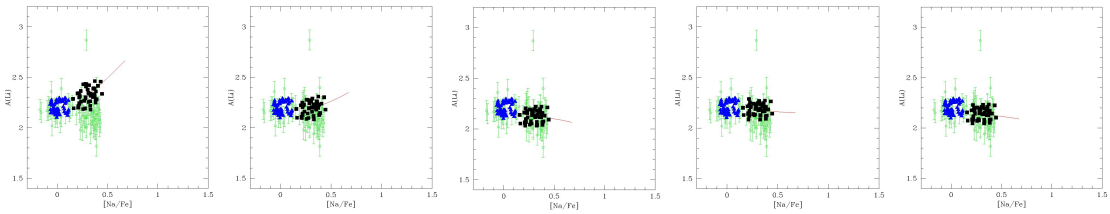

Figure 4.15: Comaparis on of the results of M4-4 model with data of Monaco et al. (2012) (Opens green pentagons with error bars. The FG and SG generation stars are represented by blue triangle and black squares, respectively.)

black squares the FG and SG stars, respectively. A stochastic error in the range 0-0.1 dex is introduced, comparable to the observational errors. The red line represents the path of the gas composition during the SG formation, starting from top right and ending at the bottom left.
In Figs 4.13, 4.14 and 4.15, we show the results of the other simulations (M4-2, M4-3. M4-4) in which the super-AGB stars have a dominant role for the formation of the SG. It is clear that the huge lithium abundances in the 7.5 $M_{\odot}$ and 8 $M_{\odot}$ ejecta favored an increase in the average SG star lithium abundance.
In case B, the average lithium in the SG is $\sim$ 0.15- 0.2 dex larger than the FG abundance, while the observations show that it is $\sim$0.1 dex lower: this factor of 2 difference rules out case B.
The second column from left shows case A: here the situation is more ambiguous, and these models cannot be ruled out.
In the third and fourth columns, we show, respectively, cases E and D ,where we reduce the yields from the 7.5 $M_{\odot}$ and 8 $M_{\odot}$ models to A(Li) = 2.0: both cases are acceptable.
Finally, the rightmost column shows the results obtained assuming that the ejecta are lithium-free, but maintaining the sodium abundances of AGB and super-AGB ejecta in the polluting matter (case C). It is obvious that, in this case, assuming different big bang initial lithium is not relevant. The results show a very good agreement with the observations in all cases. We see that M4 data do not allow us to discriminate between the AGB scenario and other scenarios in which the polluting matter is very sodium rich, but Li free like in the FRMS model. Some models of the AGB scenario reproduce well the M4 Li-Na patterns, but the Li in the super-AGB ejecta is not a necessary ingredient. Figs 4.12 and 4.13 also show that the models predict the presence of a few stars with very large lithium abundance. In M4, Monaco et al. (2012) find that the star 37934 has A(Li) $\sim$ 2.9 and relatively high sodium ([Na/Fe] = 0.37). Unfortunately the abundance of sodium predicted by the simulations is too large ([Na/Fe] $\sim$ 1)

4.4.3 The Bing Bang Lithium Abundance

The study of the chemical evolution model for the multiple populations of GCs, has revealed an interesting implication for the BBN. In fact, despite the scarcity of lithium abundance determinations in GCs, these data may result to be a powerful and independent way to constrain the lithium abundance emerging from the big bang. The abundance of lithium in the gas forming the SG stars contains information on the abundance of lithium in the gas in which the hot-CNO processed ejecta are diluted. If we can assume (and this is very

reasonable) that, at first order, the possible phenomena that deplete lithium at the surface of Population II stars are independent of them being FG or SG stars, the difference in lithium between FG and SG stars will keep track of the pristine gas abundance.
In the case of M4, we have seen that the case B [A(Li) = 2.2 in the pristine gas] shown in Fig. 4.12 can be excluded. This could be a very interesting result, but it is subject to a confirmation of the large lithium yields shown in Tab. 4.2 for super-AGB stars. As far as we have seen from the other observations, there is no present confirmation of those yields. Further, they are theoretically very uncertain, being linked to the choice (unconstrained by observations) of the mass-loss rate adopted in these computations. A confirmation could come from observation of large lithium abundances in the blue MS stars of NGC 2808 or ω Cen. If, in the future, the yields of super- AGB stars are constrained to be much smaller than those used here, case B will still be possible, and we will have to resort to different comparisons.
Thus, more and better data, and stronger constraints on the dilution model and on the AGB yields are necessary.

CHAPTER 5

An alternative source for gas pristine: Close Encounters

5.1 Introduction

Until today, there is no hydrodynamical model able to explain the dynamics and the presence of pristine gas during the SG formation; AGB and FRMS scenarios use an 'ad hoc' pristine gas.
Our aims was to explore a more consistent case, in which the gas with the primordial chemistry had internal origin. We consider the possibility that the 'pristine' matter is lost by first generation stars during gravitational interactions within the cluster compact core, mostly populated by the SG stars formed by the accumulating cooling flow of AGB winds.
We study the abundances resulting in the matter forming the second generation stars thanks to this process, and the requirements on the frequency and extent of the mass loss events that can make this process compatible with the observed O-Na anticorrelation.
We assume that the polluted gas comes from the super-AGB and massive AGB winds, as in D'Ercole et al. (2010), but the diluting gas is not re-accreting on the cluster, rather comes from FG stars. We propose that this gas is due to the strong gravitational inter-

action of FG stars passing through the core of the cluster, where the SG star formation in a cooling flow has developed a high density stellar region, increasing the number of destructive encounters between stars. We compare our data with the observed chemical patterns of M4 and NGC 2808, that represent the prototypes of Globular Clusters with a mild and an extended O-Na anticorrelation, as discussed in the previous Chapters.

5.2 Gas 'pristine'

We assume that FG stars, crossing the dense core of the cluster, interact with the newly formed SG stars, and lose mass by tidal effects. If we consider a simple model, where FG stars are shots and SG stars targets, the density of the gas emitted during the encounters in unit of time will be:

$$\dot{N} = n^2 v S \tag{5.1}$$

where n is the number density of stars for unit volume, v is the central velocity dispersion of the cluster, and S is the gravitationally focused cross-section of stars of mass M and radius R (e.g. Dale & Davies (2006)):

$$S = \pi R^2 \left(1 + \frac{2GM}{Rv^2}\right) \tag{5.2}$$

We distinguish between the cross-section of MS stars, and stars in advanced phases of evolution, including the whole core He-burning phase. For MS stars, we use the classical radius-mass relation, R'=$M'^{0.8}$, where solar units were used for both mass and radius.
For any reasonable value of the parameters, the second term inside the brackets of eq. 5.2 dominates; thus we can write:

$$S_{MS} = \frac{2\pi G}{v^2} M_\odot R_\odot M'^{1.8} \tag{5.3}$$

$$S_{AD} = \frac{2\pi G}{v^2} M_\odot R_\odot M' R' \tag{5.4}$$

Because the cross sections depend on mass, it turns useful to consider two mean values of the stellar mass defined as:

$$\overline{M'_{MS}} = \left(\frac{\int_{0.1}^{8} M'^{-2.35} M'^{1.8} dM'}{\int_{0.1}^{8} M'^{-2.35} dM'} \right)^{1/1.8} \approx 0.5$$

$$\overline{M'_{AD}} = \frac{\int_{5}^{8} M'^{-2.35} M' dM'}{\int_{5}^{8} M'^{-2.35} dM'} \approx 6$$

where we have assumed a Salpeter IMF for the FG population. In the following, we make use of the mass values in eqs. 5.3 to evaluate the S_{MS}/S_{AD} ratio, that can be expressed as:

$$R \equiv \frac{S_{MS}}{S_{AD}} = \frac{\bar{M'_{MS}}^{1.8}}{R'\bar{M'_{AD}}} \simeq 3.2 \times 10^{-3} \tag{5.5}$$

In the previous expression we assumed R'=15 $R_{\odot}$ for all the stars of mass 5-8 $M_{\odot}$in post-MS phase .

We understand that the probability that the star involved in an encounter is in a post-MS phase is much higher.

The total stellar density is n=n_{FG}+n_{SG}, where n_{FG} and n_{SG} are the density of the first and the second population, respectively; the rate of collisions is thus $\dot{N} \propto (n_{FG} + n_{SG})^2$. Initially $n_{SG} << n_{FG}$, thus we obtain:

$$\dot{N} = (S n_{FG}^2 + 2S n_{FG} n_{SG})v \tag{5.6}$$

Using n_{FG}=n_{MS}+n_{AD}, we can write:

$$S n_{FG}^2 = (S_{MS} n_{MS}^2 + 2S_{AD} n_{MS} n_{AD} + S_{AD} n_{AD}^2)$$

Defining $f_t = \frac{n_{AD}}{n_{MS}}$, because $f_t << 1$, we obtain:

$$S n_{FG}^2 \simeq (R + 2f_t) n_{MS} S_{AD} \tag{5.7}$$

$$2S n_{FG} n_{AD} S_{AD} \tag{5.8}$$

Considering n_{FG}=n_{MS}, substituting the stellar density with the density $\rho = n\overline{M*}$, where $\overline{M*}$ ~0.5 $M_{\odot}$ is the stellar mean mass and considering that the velocity for a King distribution can be expressed in terms of the central velocity dispersion σ:

$$v \simeq \sigma = r_c \sqrt{\frac{4\pi G \rho_{FG}}{9}}$$

where G is the gravitational constant, r_c is the core radius of the cluster, we obtain:

$$\dot{\rho} = \sqrt{9\pi G}\beta \frac{\bar{M_{AD}}^2}{M*^2} \frac{R_{AD}}{r_c} \rho * 3/2 \times \left[(R\frac{\bar{M_{MS}}}{\bar{M_{AD}}} + 2f_t) + 2(R\frac{\bar{M_{MS}}}{\bar{M_{AD}}} + f_t)\frac{\rho_{SG}}{\rho_{FG}} \right] \tag{5.9}$$

β is the fraction of mass lost during each encounter. The first terms within the round brackets in the above equation are only a few hundredths of the second ones, indicating that the contribution of the interactions among MS stars is negligible compared to that of the collisions involving RG stars; therefore, they will be neglected in the following. We can finally write the expression for the mass return:

$$\dot{\rho} = C\rho_{FG}^{3/2}(f_r + \frac{\rho_{SG}}{\rho_{FG}}) \tag{5.10}$$

where

$$C = 2\sqrt{9\pi G}\beta\frac{\bar{M}_{AD}^2}{\bar{M}_{*}^2}\frac{R_{AD}}{r_c}f_t f_r \tag{5.11}$$

We added a further coefficient, f_R, to take into account the fact that SG stars are mostly located within a small central volume (D'Ercole et al., 2008), thus only the fraction f_r of the advanced stars situated in the same volume actually interacts with the SG population. The parameters characterizing the model are:

- t_{end}: time at which the formation of SG stars end;
- ρ_{FG}: density of the FG stars
- c: constant regulating the quantity of the available pristine gas
- ν: star formation efficiency
- x : fraction of SG stars with respect to the total nowadays alive stars.

We assume as initial density of the Globular Cluster NGC 2808 ρ_{FG}= 200 $M_{\odot}/pc^3$, whereas for M4 it is 160 $M_{\odot}/pc^3$; the process of formation of SG stars begins after 40 Myr. To study the chemistry of the gas ejected by encounters, we split the FG time evolution into a finite number of time steps. For each of them we extract randomly the mass of the FG stars involved in the encounter, following a Kroupa power-law mass function. When MS stars are extracted, we assume that they lose a random percentage of their mass; on the other hand, RG or HB stars are stripped of the whole envelope, so the mass loss β is the initial mass of the stars M deprived of core mass: β = M - M_c .

5.3 Results

Yields from encounters involving low or massive stars in the MS phase or stars in more advanced phases will be different, as discussed in Chapter 4. To obtain processed gas, MS stars must be stripped until internal regions, where nucleosynthesis is active.
Gas stripped by RG stars is likely to show the signature of nuclear processing, because it is sufficient that surface layers exposed to nucleosynthesis during previous phases are ejected.
In the last section we have seen that the the probability of encounters for a RG is higher than for a MS star. To understand the chemistry of the gas that we should expect, we show in Fig 5.1 the sodium and aluminum yields of gas from encounters (black solid line), and from AGB (red dotted line) (Ventura & D'Antona, 2009, 2011).

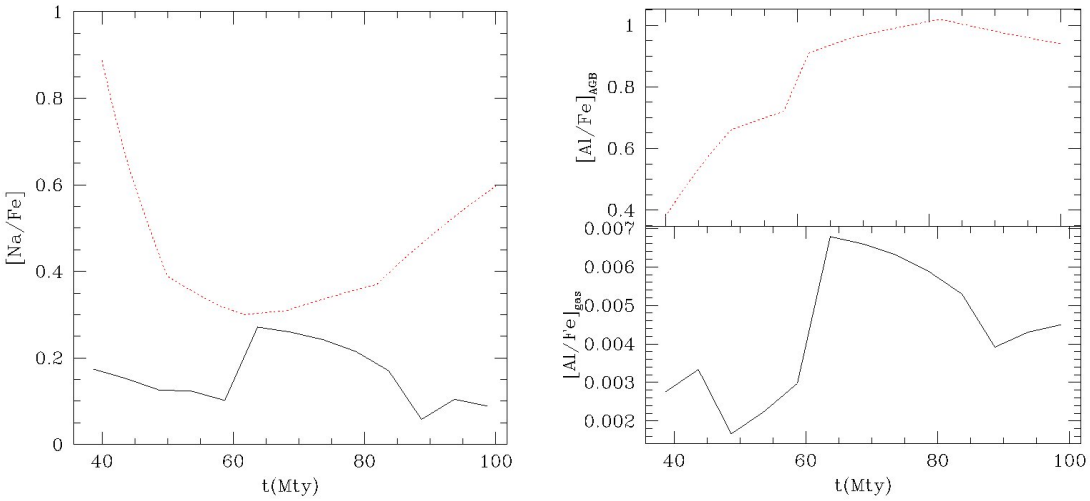

Figure 5.1: Variation with time of the sodium (left panel), aluminum (right panel) content in the gas expelled by AGBs (red, dotted line), and in the matter from encounters (black, solid line)

We consider the formation of a second generation of stars from gas coming from AGB winds and encounters, in such a way that FG and SG stars are numerically equivalent. We follow the chemistry of SG stars in terms of the abundances of sodium, oxygen, magnesium and aluminum. In Fig. 5.2 we show the two cases where the SG formation process lasts until 100 Myr (i.e. the beginning of the SNIa epoch, lower panel), or is limited to 20 Myr (top panel). FG stars (with the original chemistry) are indicated with open blue circles, whereas SG stars are shown with different symbols, according to the assumed degree of dilution of AGB winds with gas pristine: magenta triangles, green pentagons and cyan squares indicate a dilution where the ratio between gas pristine and the total gas ejected is about 10%, 50%, and 80% respectively.

The simulation used to determine the position of the individual stars in the O-Na plane accounts for the extramixing expected in giant stars when they are more helium-rich (see section 4.2.3).
The dashed lines in the four panels of Fig. 5.2 indicate the theoretical pattern determined by dilution without extra-mixing. When dilution is negligible, SG stars form directly from the winds of AGBs and SAGBs, with little contribution from pristine matter. When the duration of the process is limited to 20Myr, the SG stars formed show the same chemistry as the ejecta of SAGB stars evolving rapidly in the cluster: these are expected to be enriched in sodium by a factor ~ 5, Al-enhanced by almost 1 dex (see Fig. 5.1), with a modest depletion of magnesium. This is indeed the position of the open triangles in the

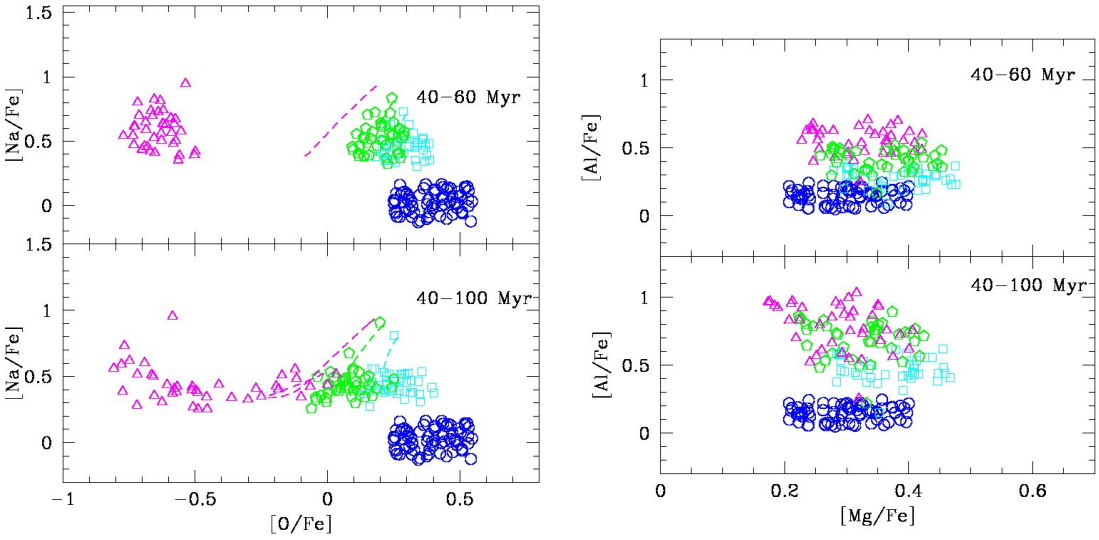

Figure 5.2: O-Na (left panel) and Mg-Al (right panel) pattern of SG stars formed by gas ejected by AGB and encounters of stars. To simulate extreme population we have considered extra-mixing. In the top panel the process goes on until 60 Myr, in the bottom until 100 Myr. Open circles indicate FG stars. The extent of dilution is represented by the constant c: Top panel: open triangles c= 5×10^{-17}; open pentagons c=4×10^{-16} and open squares c=1×10^{-15}. Bottom panel: open triangles c=3×10^{-17}; open pentagons c=1.5×10^{-16} and open squares c=5×10^{-15}.

two upper panels of Fig. 5.2. The extremely small oxygen abundances are a consequence of the assumed extra-mixing during the giant phase, that favors a further depletion of the surface oxygen. Both in the O-Na and Mg-Al planes FG and SG stars are well separated in this hypothesis. In case that the process lasts longer, SG stars are expected to occupy a position similar to the previous case in the Mg-Al plane (compare the upper and lower panels in the right part of Fig. 5.2), with a small shift towards higher Al abundances, caused by the larger fraction of Al in the ejecta of stars with mass in the range 5 $M_{\odot}$< M <6.5 $M_{\odot}$, evolving in the period 60-100Myr. In the O-Na plane, SG stars are much less clumped when the gas from encounters is only 10% in comparison with the previous case, thus we can reproduce extreme and intermediate families of stars.

The cases with intermediate and strong dilution are less sensitive to the duration of the process: points corresponding to SG stars (open pentagons and squares respectively) tend to the position occupied by FG stars as the contribution from pristine gas becomes more important. The magnesium burning region is extremely deep inside giants, so that the gas ejected shows only a modest signature of the Mg-Al nucleosynthesis (see the right-lower panel of Fig. 5.1). The total gas of the SG stars will be very similar to FG stars.

Turning to the O-Na plane, we note that SG stars are not sufficiently enriched in helium to

t(Myr)	45	50	55	60	65	70	75	80	85	90	95	100
NGC2808-1	13	12	12	15	13	13	13	13	16	30	22	16
NGC2808-2	3	3	3	4	3	3	3	3	4	7	5	3
M4-1	0.22	0.17	0.12	0.12	.	.	.	.	.	.	.	.
M4-2	0.8	0.8	0.8	1	0.9	0.8	0.7	0.7	0.7	1	0.8	0.6

Table 5.1: Ratio between available and required number of RG stars in the models of NGC 2808 and M4

experience extra-mixing (if we suppose the threshold limit Y=0.34). For an intermediate dilution it is possible to have extra-mixing, the threshold limit above which we assume that deep extra-mixing occurs is decreased to Y=0.32. The ejecta from encounters are sodium-rich (see Fig 5.1); for this reason SG stars exhibit a higher content of sodium compared to their FG counterparts.

5.3.1 NGC 2808

Here we present the best models to fit data from Carretta et al. (2006, 2009a,b), corroborated by the two turnoff stars in the Mg-Al plane by Bragaglia et al. (2010a). In the attempt of reproducing the star distribution in the O-Na plane, we follow two clear indications from the data:

1. the distribution of the stars is homogeneous, with no distinguishable gap separating FG and SG stars;

2. the O-Na distribution extends to extremely small oxygen abundances.

Point 1 rules out the possibility that the dilution of AGB winds with pristine matter from encounters was negligible, because this would produce a gap between FG and SG stars, independently of the duration of the process (see Fig 5.2). On the other hand, a dilution process dominated by the gas pristine would lead to an overlap between the two populations which is not observed. The second point can be discriminant for the duration the process. The extremely small oxygen abundances observed suggest that extra-mixing occurred; we have seen this to be highly likely if matter from which the SG stars formed is helium-rich, i.e. if the contribution of FG winds is limited to SAGBs and very massive AGBs.
In Fig. 5.3 we present the best models for NGC 2808. In both cases we used an intermediate quantity of ejecta (c=5×10^{-17} (left panel) and 2×10^{-16} (right panel) that corresponds

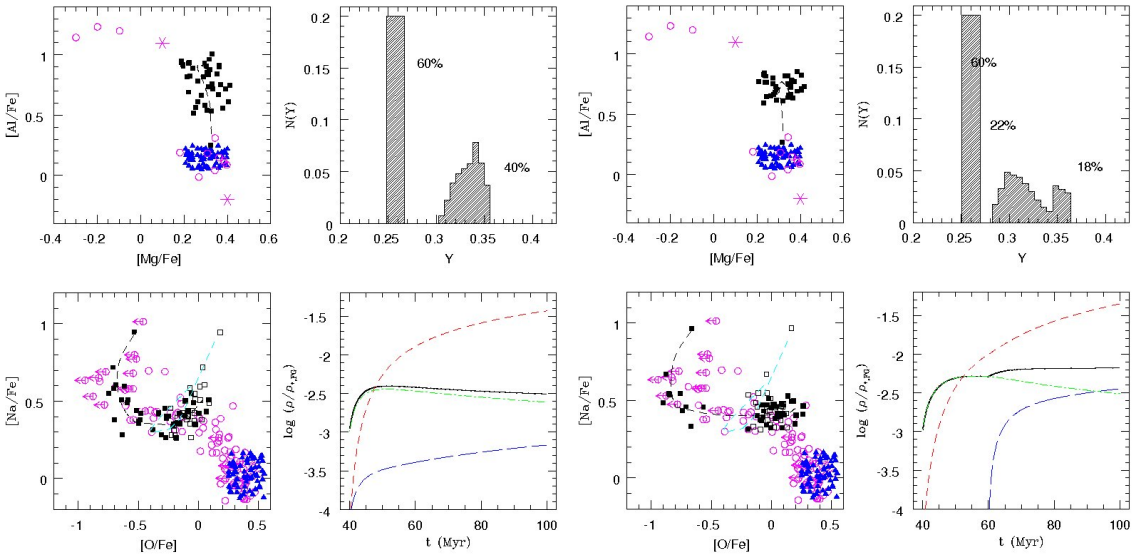

Figure 5.3: Numerical simulations for stars in NGC 2808, where formation of the SG occurs from mixing of pristine gas with matter ejected by AGBs. The formation of SG stars is allowed to carry on for 60Myr, and to star either after the epoch of SN II explosions (left panels), or with a delay of 20Myr (right). In the first case a large star formation efficiency (ν=1) and a mild dilution with gas pristine was adopted ($\sim$ 10%), whereas in the second case we used ν=0.5 and a contribution of pristine gas about 30%. The upper and lower panels with data in the O-Na and Mg-Al planes, where the meaning of symbols is as follows; open circles: giats from Carretta et al. (2009a) and Carretta et al. (2009b), asterisks : MS stars from Bragaglia et al. (2010a); blue triangles: FG stars; black squares: SG stars. The top right panels show the overall helium distribution of FG and SG stars, whereas the bottom right panels indicate the variation with time of the density of AGB gas (dotted-dashed), gas from encounter (long-dashed line), SG stars (dashed line) and the total amount of gas (solid line).

to 10% and 30% respect the total gas) from encounters; the efficiency of the SF process is ν =1 for the first model and 0.5 for the second one. Full triangles and squares represent, respectively, FG and SG stars, to be compared with the data, indicated with open circles. The whole Na-O anticorrelation cannot be reproduced. In the model shown in the left panel, whose total duration is 60Myr, we obtain a fair fit of the extreme and intermediate chemistry populations, but stars with chemistry close to the FG component are not reproduced. Increasing the fraction of gas from encounters would be of little help, because this latter is expected to be sodium rich. Moreover, the distribution of helium of this model is in disagreement with the results of Milone et al. (2012b)(see top-right panel).
In the model shown in the right panel, the duration of the SG formation process is again 60Myr, but the contribution from gas pristine begins after 20Myr; this leaves the possibility of forming a pure population from the SAGB ejecta, enriched in sodium and helium and exposed to deep extra-mixing, that decreases the surface oxygen. The following dilution allows the formation of stars with intermediate chemistry (see bottom left panel). The O-Na anticorrelation is reproduced with a process that lasts 20 Myr (see the bottom-left panel of Fig. 5.3). This can be understood from the right-lower panel of the figure, showing the relative densities of the various components of gas and of SG stars formed: pristine gas from encounters (long-dashed), AGB contribution (dot-dashed), total gas available (solid), and SG stars (dashed). AGB winds dominate the gas composition in the earliest times, whereas matter from encounters takes over $\sim$ 20Myr after the beginning of the process. We therefore expect that the most contaminated, sodium-rich objects are formed in the initial period, when the composition of the gas reflects the chemistry of the SAGB ejecta (see the AGB line in the left panel of Fig. 5.1), with a later formation of SG stars with an intermediate chemistry, once AGB winds are mixed with gas from the encounters. These two groups of SG stars correspond, respectively, to the extremely helium-rich stars (see the peak at Y $\sim$ 0.35 in the upper-right panel of Fig. 5.3), and to those clustering at Y $\sim$ 0.30. In this case, our results are in agreement with the study by Milone et al. (2012b). To obtain this we had to increase the quantity of gas from encounters. Turning to the Mg-Al pattern, we clearly see in the top-left panels of Fig. 5.3 that reproducing the abundances of the three giants discussed above is not possible in the present context: although we predict that Al-enhanced SG stars are formed, yet the measured surface magnesium is too small in comparison with our predictions. These three stars represent a problem also for any other model.

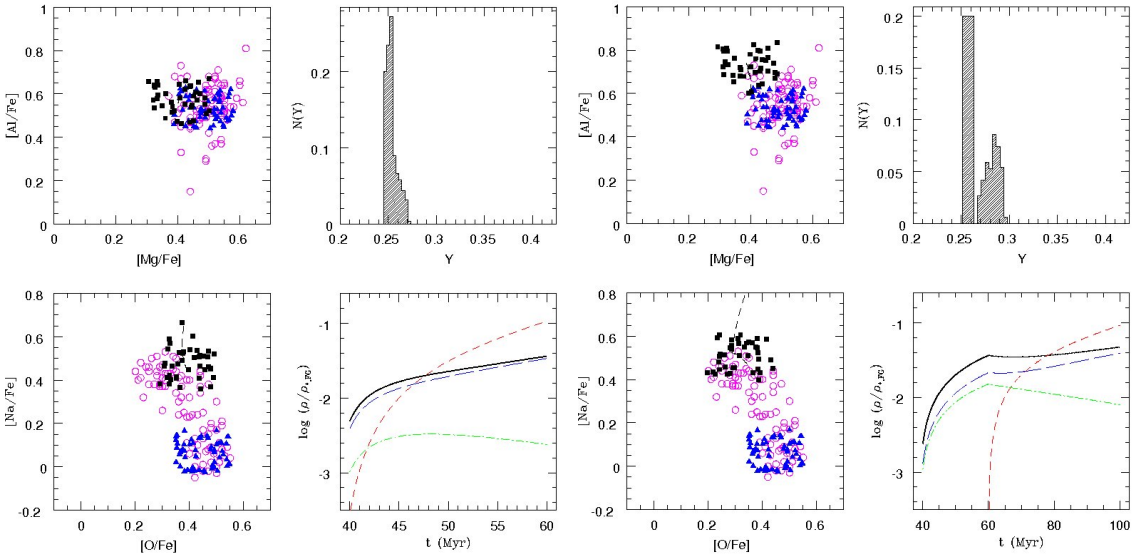

Figure 5.4: Models of M4. Panels in the left refer to a process of duration 20Myr, whereas in the right we show the simulation for a total duration of 60Myr. The star formation efficiencies used are, respectively, ν =0.5 and ν=0.1. Open circles indicate data from Marino et al. (2011). The meaning of the other symbols is the same as in the Fig 5.3.

5.3.2 M4

The Globular Cluster M4 (mass M=6.3×10^4 $M_\odot$) hosts two different stellar populations. The observed patterns suggest a strong dilution between AGB winds and gas pristine, to prevent the formation of Al-enhanced SG stars, and the presence of an extended tail towards extremely small oxygen abundances in the O-Na plane. The clear separation in the sodium abundances between FG and SG stars points in favor of a relevant contribution from giants We obtain a fair agreement with data when we assume a strong dilution (corresponding to c= 2.5×10^{-15} and c=8×10^{-16}) and a duration of the process of 20 Myr and 60 Myr. In the first model we use an efficiency of ν=0.5, in the second ν=0.1 and gas from encounters begins to contribute after 20Myr.

The consistency of this scenario is however hampered by a major problem associated with the mass budget available, because the number of RGB stars required is too high for any realistic IMF used to describe the mass distribution. Tab. 5.1 shows the ratio between available and required number of RG stars in the models that reproduce the data. We note a not negligible fraction of SG star with extreme chemistry, due to pure AGB ejecta emitted in the early phases of the process. Even if we can find the right contribution of dilution, we can not eliminate these stars, also using a low efficiency.

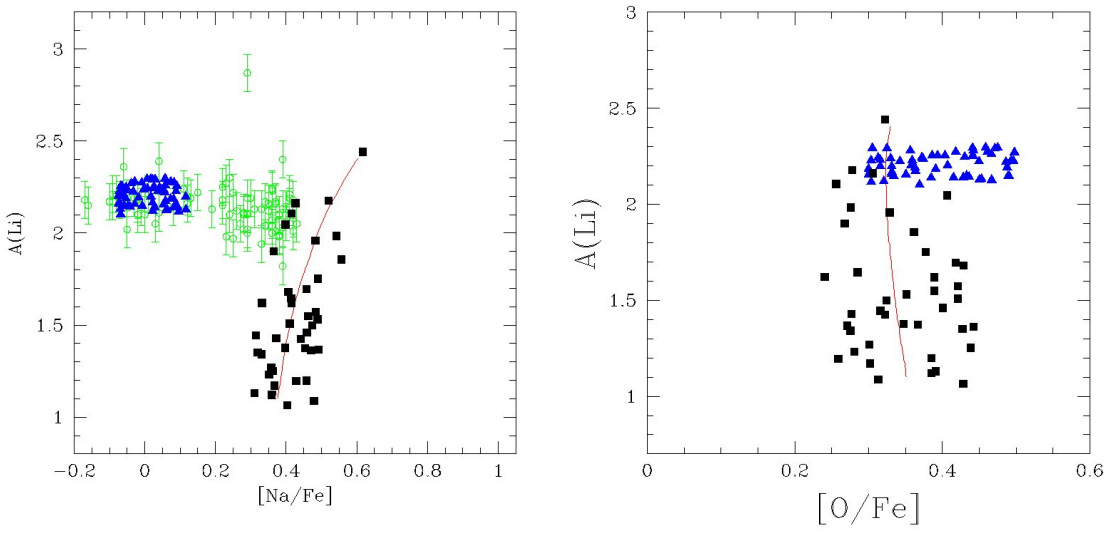

Figure 5.5: Comparison between data of M4 Monaco et al. (2011) and the simulations of the first model of M4. Left panel: Li-Na anticorrelation, the right panel: Li-O correlation.

5.4 Lithium

We focused on the abundances of lithium in our scenario. We assume that the initial lithium abundance was A(Li) = 2.2 for M4 and A(Li)= 2.3 for NGC 2808. We compared our data of M4 with the observations of Monaco et al (2012), who found a well defined Li-Na anti-correlation. Fig 5.5 shows the results of our simulations for M4 .
The lithium in the AGB ejecta is very similar to what we assume to be the abundance of the primordial gas. The average abundance of Lithium in the gas ejected by encounters is about 1.1, whereas in the gas of stellar wind it is about 2.2; hence the final ejecta could form part of SG stars with abundances of lithium and sodium in agreement with the data. On the other hand, the 7.5 $M_{\odot}$ and 8 $M_{\odot}$ models produce ejecta greatly enriched in lithium, which is the reason for the presence in Fig. 5.5 of a considerable number of stars with an excess of lithium, not observed; this holds even if a low-efficiency star formation is considered. However, these findings are dependent on the lithium yields by the SAGB models, that are extremely uncertain, due to the scarce knowledge of the mass loss mechanism. A smaller mass loss rate would diminish the lithium yields, because the star would lose a smaller amount of mass during the Li-rich phase, achieved at the beginning of the thermal pulses phase. In Fig. 5.6 we show the simulations for NGC 2808. Large lithium abundances are found in stars formed from pure super-AGB ejecta. When the quantity of gas from AGB and encounter are similar, we can build the intermediate

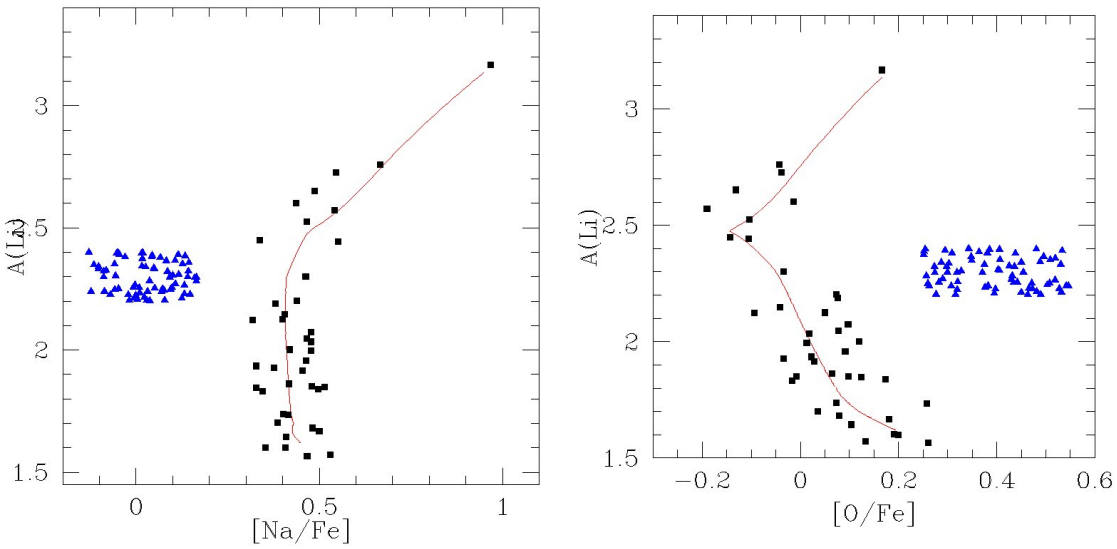

Figure 5.6: Li-Na (left panel) and Li-O (right panel) trends for NGC 2808. The parameters refer to the second model of NGC 2808

population, that has a lithium abundance equal or greater than FG stars. At the end of the process the abundance is lower, because both contribution of the AGB star and encounters are lower than FG stars. If we confront this model with the results of the precedent chapter, we note that our results are lower in lithium, because with encounters it is possible lost gas from internal parts of the stars, where it has destroyed the Li (average lithium ejected A(Li)= 1.09)

CHAPTER 6

Conclusions

In this work we focus on one of the mostly investigated and debated topics within the astrophysical community: the formation of multiple populations in Globular Clusters. This study finds its motivation in the collection of spectroscopic and photometric data accumulated in the last decades, that indicate that the majority of Globular Clusters harbor more stellar populations, differing in the abundances of elements lighter than silicon. The main scope of the present investigation is to shed new light on the formation process of the second stellar generation, and to analyze critically some of the mechanisms present in the literature.
We first explore the hypothesis that the second stellar generation forms by gas ejected by massive binaries evolving during the first phases of the cluster life. We maximize the gas that can be lost by these systems, assuming that the initial cluster dynamical evolution allows the formation of a large number of compact interactive binaries, in which mass transfer and loss from the massive components occurs mainly during the MS lifetime. In spite of the most favorable choices made to maximize the mass and chemical processing of the matter ejected by these binaries, we find that the model does not agree with the observations for the following reasons:

- The gas ejected by these systems shows a great enhancement of sodium, and only a modest depletion of oxygen, at odds with the pattern observed;

- The Mg-Al anticorrelation is not reproduced, as massive stars are not able to deplete

^{24}Mg, and thus cannot increase substantially the abundance of aluminum. The Al-synthesis is limited to the proton capture by the two heavier magnesium isotopes, that are present in limited quantities;

- In order to achieve a 1:1 ratio of FG and SG stars, as indicated by the observations, an initial FG mass much larger than today's cluster mass must be invoked, a problem shared with the other models for self-enrichment: the initial FG mass that must have been lost from the proto-cluster is in the range 80%-90%;

- The most extreme chemistry, still not in agreement with the measured quantities, is obtained by considering only high mass stars in the binary formation process. However in this case the total mass budget would be an even major issue, since a severe loss of FG stars from the cluster (of the order of 95%) is necessary to reproduce the observed ratio between FG and SG stars. As suggested by de Mink et al. (2009), the further contribution of stars down to $4\,M_{\odot}$would alleviate this problem, though in this case the gas would be only poorly contaminated.

We explored the possible role of super-AGB stars in the formation of the observed abundance patterns in multiple populations of Globular Clusters. The results of our investigation show that the new super-AGB yields by Ventura & D'Antona (2011) broaden the range of possible formation histories leading to the observed abundance patterns. We focused on two clusters that can be assumed as representative of structures exhibiting extended, or short patterns: NGC 2808 and M4

- For M4, we show that the observed patterns can be reproduced by models with a short SG formation phase ($\sim$ 10-20 Myr), involving only super-AGB ejecta and pristine gas. We confirm that models presented in the previous work by D'Ercole et al. (2010), characterized by a more extended SG formation epoch involving super-AGB and AGB ejecta (along with pristine gas), can also reproduce the observed abundance patterns. While models with a shorter SG formation epoch can include the effect of SG SN II, the narrower range of AGB progenitors providing gas for SG formation implies that they require a larger FG initial mass (increased by a factor 3-4 compared to models with a more extended SG formation phase).

- The oxygen-poor sodium-rich stars of NGC 2808 can be explained by assuming deep-mixing in SG giants forming in a gas enriched in helium: this significantly reduces the surface oxygen content, while preserving sodium. Use of the super-AGB yields does not change the main requirements on SG formation history of

models for the more complex clusters, like NGC 2808. In these structures, an extreme population, with a very large helium content, form directly from the ejecta of super-AGB stars, followed by formation of an intermediate population by dilution of massive AGB ejecta with pristine gas. We also attempted to model the three populations of NGC 2808 allowing for a long hiatus between the formation of the Extreme and Intermediate population (possibly due to SN II explosions of the Extreme populations), but our attempts to model each star formation epoch in a period as short as ∼10 Myr were not satisfactory. Nevertheless, further study is probably needed to settle this issue.

We stress here that one-zone models, such as those presented here (and in D'Ercole et al. (2010)), while are very useful to understand rather easily and very quickly the role of different ingredients in shaping the GC chemical evolution (AGB ejecta, amount of pristine gas, duration of the system evolution, etc.), cannot of course capture the complexity and variety of effects connected with the gas hydrodynamics. As a simple example, we mention that, during the cooling flow evolution of the GC gas (D'Ercole et al., 2008), most of it accumulates in the center of the cluster which therefore at each time hosts not only the AGB ejecta delivered "in situ", but also that delivered at earlier times by FG stars located at the GC outskirts. It is thus expected that SG stars with different chemical properties can form in different places at the same time, and not only at different times, as in one-zone models. For this reason we plan to work out hydrodynamic models similar to those of D'Ercole et al. (2008), but taking into account the detailed chemistry as in the present models.
In this work, we present the first predictions for the abundance of lithium in FG and SG stars of GCs, based on quantitative models, that can successfully reproduce the O-Na anticorrelation and the helium abundance distribution in the clusters M4 and NGC 2808. Our main findings are:

- An important ingredient of this study is the abundance of lithium in the pristine gas diluting the ejecta, and thus whether we interpret the surface abundance of lithium in Population II stars as the primordial abundance, or as due to in situ depletion mechanisms. A better understanding of the SG formation could perhaps help us to constrain better the big bang abundance, although this is at present only wishful thinking.

- Not all models for M4 are consistent with the observed slight decline in lithium (∼ 0.1 dex) between FG and SG. A good fit of the data is also achieved assuming zero lithium in the super-AGB matter.

- In complex clusters, in which a very He-rich extreme population is present, we should expect that this population is born from pure super-AGB ejecta, and thus is very Li-rich. Observations of lithium in the blue MS of ω Cen and NGC 2808 may verify or disregard this prediction.

We investigated in details the possibility that the chemistry of gas from which SG stars form is given by mixing of AGB and SAGB winds with matter ejected by stellar encounters, taking placed between FG and SG stars in the central regions. The probability of encounters involving giant stars is much higher, thus the gas produced show traces of sodium enhancement and oxygen depletion; only a modest variation in the magnesium and aluminum content is expected, because the temperature are not high enough to active Mg-Al cycle.
This model was also tested against data for NGC 2808 and M4. For what concerns NGC 2808, the results obtained are not fully satisfactory. The O-Na anticorrelation could be reproduced only partially, given the high sodium in the gas coming from encounters. Also, a gap separating FG and SG stars seems inevitable, and this is at odds with the observational evidence. The Mg-Al anticorrelation is also hard to reproduce, though this difficulty is shared by all the other mechanisms.
A continuous star formation process is also scarcely compatible with the three, separated, helium abundances, characterizing the three populations of this cluster (Milone et al., 2012b); a possible escape from this shortcoming would be that gas pristine begins to contribute 20Myr after the SAGB evolve.
To reproduce the chemical patterns of M4 we need a strong dilution. In this case, even if it is possible reproduce the Na-O anticorrelation, the number of RG stars required is too high for any realistic IMF used to describe the mass distribution.
We have analyzed also the abundances of lithium. With our simulations we can not reproduce the data of Monaco et al. (2012) for the cluster M4. For NGC 2808 we obtain a very extended pattern in A(Li), from 3.2 dex, due to the pure S-AGB ejecta, to 1.6 dex, due to the contribution of encounters. Unfortunately, there are not experimental data, where with we can compare our results. We could conclude that binaries system and interaction play a marginal role into the formation of the second generations of stars in Globular Clusters. The AGB scenario remains the most plausible and can reproduce a greater number of observational features.

Conclusioni

In questo lavoro ci siamo focalizzati su uno dei più investigati e dibattutti temi della comunità astrofisica: il fenomeno delle popolazioni multiple negli Ammassi Globulari. Questo studio è motivato dalla collezione di dati spettroscopici e fotometrici accumulati nelle ultime decadi, le quali indicano che la maggior parte degli Ammassi Globualri ospitano più popolazioni stellari, differendo nelle abbondanze degli elementi più leggeri del silicio.
Il principale scopo della presente investigazione è chiarire il processo di formazione della seconda generazione stellare, e analizzare criticamente alcuni dei meccanismi presenti in letteratura.
Per prima cosa abbiamo esplorato l'ipotesi in cui la seconda generazione stellare si forma dal gas emesso dalle binarie massive che evolvono durante le prime fasi di vita dell'ammasso. Abbiamo massimizzato la quantità di gas che può essere persa da questi sistemi, assumendo che l'evoluzione dinamica dell'ammasso iniziale permette la formazione di un gran numero di binarie compatte interagenti, nelle quali la massa trasferita e persa dalle componenti massive avviene soprattutto durante la fase di MS. Nonostante abbiamo fatto tutte le scelte possibili per favorire non solo che sia espulsa la maggiore quantità di massa, ma che questa abbia il massimo grado di contaminazione, troviamo che il modello non è in accordo con le osservazioni per le ragioni seguenti:

- il gas emesso mostra un grande arricchimento di sodio, e solo un modesto deplemento di ossigeno, in contrasto con gli andamenti chimici osservati;

- L'anticorrelazione Mg-Al non è riprodotta, le stelle massive non sono capaci di depletare il ^{24}Mg e quindi non possono aumentare in modo sostanziale l'abbondanza

di alluminio. Perciò la sintesi di questo elemento è limitata alla cattura protonica dagli isotopi del magnesio più pesanti, che sono presenti in minore quantità;

- Per raggiungere il rapporto tra le stelle SG e FG, come indicato dalle osservazioni, la massa iniziale dell'ammasso deve essere molto più grande di quella attuale, un problema condiviso con gli altri modelli di auto-arricchimento: deve essere stata persa dal proto-amasso l'80%-90% della massa iniziale delle FG;

- La chimica più estrema, ancora non in accordo con le quantità misurate, è ottenuta considerando nel processo di formazione delle binarie solo le stelle molto massive. In questo caso il budget di massa totale dovrebbe essere un problema ancora maggiore, poichè è necessaria una forte perdita di stelle FG dall'ammasso (circa il 95%) per riprodurre il rapporto tra SG e FG osservato. Come suggerito da de Mink et al. (2009), il cotributo di stelle sotto le 4 $M_{\odot}$ dovrebbe alleviare il problema, anche se in questo caso il gas sarebbe poco contaminato.

Abbiamo esplorato il possibile ruolo delle stelle super-AGB nella formazione degli andamenti chimici osservati nell popolazioni multiple negli Ammassi Globulari. I risultati della nostra investigazione mostrano che i nuovi yield delle SAGB calcolati da Ventura & D'Antona (2011) allargano la gamma di possibile storie di formazione. Ci focalizziamo su due ammassi che possono essere considerati come strutture rappresentative degli ammassi con andamenti estesi e corti: NGC 2808 e M4.

- Per M4, mostriamo che gli andamenti osservativi possono essere riprodotti dai modelli con una fase di formazione breve (~10-20 Myr) coinvolgendo solo materia emessa dalle SAGB e il gas 'pristine'. Confermiamo che i modelli presentati nel precedente lavoro di D'Ercole et al. (2010), caratterizzati da un'epoca di formazione di SG più estesa, che quindi considerano anche il gas della AGB massive, possono riprodurre i dati osservativi. Anche se i modelli con una formazione dei stelle di seconda generazione più breve possono includere gli effetti delle SN II di seconda generazione, l'intervallo più stretto di AGB che forniscono gas implica che sia necessaria una massa iniziale di FG più grande, di un fattore 3-4 maggiore rispetto i modelli con fase di formazione estesa.

- Le stelle povere di ossigeno e ricche di sodio di NGC 2808 possono essere spiegate assumendo un 'extra-mixing' nelle giganti SG che si formano da un gas ricco in elio: questo fenomeno riduce significativamente la superficie contenente ossigeno, mentre preserva il sodio. L'uso degli yield delle SAGB non cambia i principali

requisiti per la storia di formazione dei modelli per gli ammassi più complessi, come NGC 2808. In queste strutture, una popolazione estrema con un contenuto di elio molto alto, si forma direttamente dal gas puro delle stelle SAGB, seguita poi dalla formazione della popolazione intermedia formata dal gas delle AGB massive diluito con quello 'pristine'. Abbiamo anche tentato di modellare le tre popolazionei di NGC 2808 considerando un'interruzione tra la formazione della popolazione estrema ed intermedia (possibilmente dovuta alle esplosioni di SN II della popolazione estrema), ma i nostri risultati non sono stati soddisfacenti. Nonostante tutto ulteriori studi sono probabilmente necessari.

Sottolineamo qui che i modelli one-zone, come quello presentato qui (e in D'Ercole et al. (2010)), sebbene siano molto utili per capire piuttosto facilmente e molto velocemente il ruolo dei differenti ingredienti nell'evoluzione chimica degli GC (gas delle AGB e pristine, durata di evoluzione del sistema, ecc.), non possono catturare la complessità e la varietà degli effetti connessi con l'idrodinamica del gas.
In questo lavoro presentiamo anche le prime predizioni per le abbondanze di litio nelle stelle di FG e SG degli GCs, basate su modelli quantitativi, che possono riprodurre l'anticorrelazione O-Na e la distribuzione dell'abbondanza di elio negli ammassi M4 e NGC 2808. Le nostre principali scoperte sono:

- Un ingrediente importante di questo studio è l'abbondanza di litio nel gas 'pristine' che viene diluito con il gas delle AGB, e quindi se interpretiamo l'abbondanza di litio superficiale osservato nelle stelle di Pop II come abbondanza primordile, oppure dovuto a meccanismi di deplezione avvenuti in situ. Una comprensione migliore della formazione di SG possono forse aiutarci a vincolare meglio l'abbondanza del Big Bang, sebbene questo sia al momento solo un pio desiderio.

- Non tutti i modelli per M4 sono consistenti con la leggera diminuzione in litio (circa 0.1 dex) tra le stelle FG e SG. Un buon fit dei dati è raggiunto assumendo che nel gas emesso dalle SAGB non ci sia litio, ipotesi accettabile se consideriamo una perdita di massa inferiore a quella usata solitamente.

- Negli ammassi complessi, nei quali è presente una popolazione estrema molto ricca in elio, ci dovremmo aspettare che questa sia nata da il gas puro delle AGB, quindi ricche in Li. Osservazioni di litio nella blu MS di ωCen e NGC 2808 potrebbero verificare o meno questa predizione.

Inoltre abbiamo investigato in dettaglio la possibilità che la chimica del gas dal quale si formano le stelle SG è dato dal mix tra i venti delle SAGB e AGB massive e la materia

emessa dagli incontri stellari, che avvengono tra stelle FG e SG nelle regioni centrali. La probabilità che gli incontri coinvolgano stelle giaganti pittosto che stelle di MS è molto più alta, quindi il gas prodotto mostra tracce di arricchimento di sodio e deplemento di ossigeno; si riscontra solo una modesta variazione nel contenuto di magnesio e alluminio, perché la temperatura interna non è sufficientemente alta per attivare il ciclo Mg-Al.
Questo modello è stato testato di nuovo comparando i dati di NGC 2808 ed M4. Per quello che concerne NGC 2808, i risultati ottenuti non sono pienamente soddisfacenti. L'anticorrelazione O-Na potrebbe essere riprodotta solo parzialmente: il gas proveniente dagli incontri è ricco in sodio, quindi sembra inevitabile una lacuna tra le stelle FG ed SG, in contrasto con le osservazioni. L'anticorrelazione Mg-Al è difficile da riprodurre, sebbene tale difficoltà sia condivisa dagli altri meccanismi.
Un processo di formazione continuo è scarsamente compatibile con le tre abbondanze di elio separate, che caratterizzano le tre popolazioni dell'ammasso (Milone et al., 2012b); una possibile via d'uscita da questa mancanza potrebbe essere che il gas 'pristine' incomincia a contribuire 20 Myr dopo che le SAGB sono evolute.
Per riprodurre gli andamenti chimici di M4 abbiamo bisogno di una forte diluizione. In questo caso, anche se è possibile riprodurre l'anticorrelazione O-Na, il numero di stelle giganti richiesto è troppo alto per ogni IMF realistica usata per descrivere la distribuzione di massa.
Abbiamo analizzato anche le abbondanze di litio. Con le nostre simulazioni non possiamo riprodurre i dati di Monaco et al. (2012) per l'ammasso M4. Per NGC 2808 otteniamo un andamento molto esteso in A(Li), da 3.2 dex, dovuto al gas delle SAGB, fino a 1.6 dex, dovuto al contributo degli incontri. Sfortunatamente non ci sono dati sperimentali con i quali possiamo comaparare i nostri risultati. Possiamo concludere che il sistema di binarie gioca un ruolo marginale nella formazione della seconda generazione di stelle negli Ammassi Globulari.
Lo scenario delle AGB rimane il più plausibile a può riprodrre un maggior numero di caratteristiche osservative.

Appendices

APPENDIX A

Thermal Pulse

The first law of thermodynamics:

$$dQ = dU + PdV \tag{A.1}$$

The equation of state is:

$$\rho = P^{\alpha} T^{-\delta} \tag{A.2}$$

where

$$\alpha = \left(\frac{\partial lg\rho}{\partial lgP}\right)_T = -\frac{P}{V}\left(\frac{\partial V}{\partial P}\right)_T \tag{A.3}$$

and

$$\delta = -\left(\frac{\partial lg\rho}{\partial lgT}\right)_P = \frac{T}{V}\left(\frac{\partial V}{\partial T}\right)_P \tag{A.4}$$

We want to find the energy released when is triggered ^4He, this we want to find dQ as function of dT , thus we write again the first law of thermodynamics, replacing the internal energy with its differential form:

$$dQ = \frac{\partial U}{\partial T}|_v dT + \left[\frac{\partial U}{\partial V}|_T + P\right] dV \tag{A.5}$$

The first term on the right is the heat capacity at volume constant; we can the second term from the entropy, $ds = \frac{dq}{T}$, considering that it is a state function: $\frac{\partial^2 S}{\partial T \partial V} = \frac{\partial^2 S}{\partial V \partial T}$.
Knowing that:

$$\frac{\partial S}{\partial T} = \frac{1}{T}\frac{\partial U}{\partial T}|_v$$

and

$$\frac{\partial S}{\partial V} = \frac{1}{T}\left[P + \frac{\partial U}{\partial V}|_T\right]$$

it is simple to obtain:

$$\frac{\partial U}{\partial V}|_T = T\frac{\partial P}{\partial T}|_v - P \tag{A.6}$$

Now we can repalce it to the eq. A.5 and get:

$$dQ = c_v dT + T\frac{\partial P}{\partial T}|_v Dv \tag{A.7}$$

Now we consider the isobar dV=0:

$$\frac{\partial V}{\partial T}|_p dT + \frac{\partial V}{\partial P}|_T dP = 0 \Rightarrow \frac{dP}{dT}|_v = -\frac{\frac{\partial V}{\partial P}|_T}{\frac{\partial V}{\partial T}|_p}$$

Eventually, considering eq. A.3 and A.4, we obtain: $\frac{\partial P}{\partial T}|_V = \frac{P\delta}{T\alpha}$; replacing to eq. A.5 we have:

$$dQ = c_v dT + \frac{P\delta}{\alpha}dV = c_v dT - \frac{P\delta}{\alpha\rho^2}\partial\rho = c_p dT - \frac{\delta}{\rho}dP \tag{A.8}$$

Introducing the adiabatic gradient : $\Delta - ad = \frac{dlgT}{dlgP} = \frac{P\delta}{Tc_p\rho}$ we can write again

$$dQ = c_p T\left(\frac{dT}{T} - \Delta_{ad}\frac{dP}{P}\right) \tag{A.9}$$

Now we consider that, during the expansion, the shells have the same velocity,thus we can use the homology relations : $\frac{\dot{r}}{r} = \text{cost.}$

For this reason:

$$\frac{\partial}{\partial m}\left(\frac{\partial lgr}{\partial t}\right) = \frac{\partial}{\partial t}\left(\frac{1}{r}\frac{\partial r}{\partial m}\right) = 0$$

$$\frac{\partial m}{\partial r} = 4\pi r^2\rho \Rightarrow \frac{1}{r}\frac{\partial r}{\partial m} = \frac{1}{4\pi r^3\rho}$$

Thus

$$\frac{\partial}{\partial t}\left(\frac{1}{r}\frac{\partial r}{\partial m}\right) = \frac{1}{4\pi r^3\rho}\left(-3\frac{\dot{r}}{r} - frac\dot{\rho}\rho\right) \Rightarrow \frac{\dot{\rho}}{\rho} = -3\frac{\dot{r}}{r} = -3x \tag{A.10}$$

where x is a constant. Now we consider the hydrostatic equilibrium:

$$\frac{dP}{dm} = -g\rho\frac{dm}{dr} \tag{A.11}$$

thus if we integrate

$$P = \int_m^M \frac{Gm}{4\pi r^4}dm \Rightarrow \dot{P} = \int_m^M \frac{Gm}{4\pi}\frac{\partial}{\partial t}\left(\frac{1}{r^4}\right)dm = -4Px \tag{A.12}$$

Thuw we have $\frac{dP}{P}$ = -4xdt and $\frac{d\rho}{\rho}$ =-3xdt, and we can write:

$$dQ = cp\left(1 - \Delta_{ad}\frac{4\delta}{4\alpha - 3}\right)dT = c * dT \tag{A.13}$$

If we consider the very little dimension shell of helium, D, we find that

$$\frac{d\rho}{\rho} = -\frac{r}{D}\frac{dr}{r} = -\frac{r}{D}x \Rightarrow 3 \sim \frac{r}{D}$$

and we can replace it in the eq.A.13, getting:

$$dQ = c_p[1 - \frac{4\Delta_{abs}\delta}{4\alpha} - \frac{r}{D}] = c * dT \tag{A.14}$$

For an expansion we have an instability for c*>0. In this case, for every value of δ and α, thus indipendelntly from degeneration (differently from Flash helium case in which there is instability for a degenerate gas where δ = 0), we have instability for D<<r, and this is true in the shell of helium, for this reason thermal instability is only dued to little dimension of the shell. The energy released is too much for the reduces size of the shell, for this reason the system expands and the CNO shell turns off, until also the He shell decrease its efficienty, the system contracts and the CNO shell turns on again. The thermal pulses are periodic.

Bibliography

Angulo C., Arnould M., Rayet M., et al., 1999, Nucl Phys. A., 656, 3

Asplund M., Lambert D. L., Nissen P. E., Primas F., Smith V. V., ApJ, 644, 229

Baumgardt H., Kroupa P., 2007, MNRAS, 380, 1589

Baumgardt H., Makino J., 2003, MNRAS, 340,1589

Bedin L. R., Piotto G., Anderson J., Cassisi S., King I. R., Momany Y., Carraro G., 2004, ApJ, 605, L125

Bedin L. R., Piotto G., Zoccoli M., Stetson P. B., Saviane I., Cassisi S., Bono G., 2000, A&A, 363, 9

Bekki K., Campbell S. W., Lattanzio J. C., Norris J. E., 2007, MNRAS, 377, 335

Blöcker T., 1995, ApJ, 605, L125

Blöcker T., Schönberner D., 1991, A&A 244, L43

Boily C., Kroupa P., 2003, MNRAS, 338, 673

Bonnel I. A. & Bate M. R., 2006, MNRAS, 338, 665

Bonnel I. A., Clarke C.J., Bate M. R., Pringle J. E., 2001, MNRAS, 324, 573

Bowen G. H., 1988, ApJ, 329, 299

Bragaglia A., Carretta E., Gratton R., D'Orazi V., Cassisi S., Lucatello S., 2010, A&A, 519, A60

Caloi V., D'Antona F., 2008, A&A, 463, 949

Cameron A. G. W., Fowler W. A., 1971, ApJ 164, 111C

Canuto V.M.C, Goldman, I., Mazzitelli, I., 1996, ApJ,473,570

Canuto V.M.C, & Mazzitelli I., 1991,ApJ, 370, 295

Caughlan & Fowler e leggi bene la ref, 1988.

Carretta E., Bragaglia A., Gratton R. G., Recio-Blanco A., Lucatello S., D'Orazi V., Cassisi S., 2010, A&A, 516, A55

Carretta. E., Bragaglia A., Grattona R.G., Lucatello S., Catanzaro G., et al., 2009 A&A 505, 117

Carretta E., Bragaglia A., Gratton R., Lucatello S., 2009, A&A, 505, 139

Carretta E. et al., 2007, A&A, 464, 957

Carretta E., Bragaglia A:, Gratton R., Leone R. G., Recio-Blanco F., Lucatello S., 2006, A&A 450, 523

Carretta E., 2003, MSAIS, 3, 90

Chernoff D. F., Weinberg M. D., 1990, ApJ, 351, 121

Chernoff D. F., Shapiro S. L., ApJ, 322, 113

Ciotti L., Pellegrini S., Renzini ., D'Ercole A., 1991, ApJ, 376, 380

Cloutman L.D. & Eoll J.G., 1976, A.J., 206, 548

Cohen J. G., Briley M. M., Stetson P. B., 2005, AJ, 130, 1377

Cottrel P.L., Da Costa G. S., 1981, ApJ, 245, L79

Cyburt R. H., Fields B. D., Olive K. A., 2008, J. Cosmol. Astro-Part. Phys., 11, 12

Dale J. E., Davies M. B, 2006, MNRAS, 366,1424D

D'Antona F., Ventura P., Caloi V., D'Ercole A., Vesperini E., Carini R., Di Criscienzo M., 2010, ApJ, 715L, 63

D'Antona F., Caloi V., 2008, IAUS, 246, 156D

D'Antona F., Ventura P., 2007, MNRAS, 379, 1431.

D'Antona F., Bellazzini M., Caloi V., Pecci F. Galleti S., Rood R.T., 2005, ApJ, 631, 868

D'Antona F., Caloi V., 2004, ApJ, 611,871D

D'Antona F., Caloi V., Montalban C., Ventura P., Gratton R., 2002, A&A, 295, 69

D'Antona, F., Gratton, R., Chieffi, A., 1983, Mem.S.A.It., 54, 173

Decressin T., Meynet G., Charbonnel C., Prantzos N., Ekström S., 2007, A&A 464, 1029

Decressin T., Charbonnel C., Meynet G., 2007, A&A, 475, 859

de Mink S.E., Ols O.R., Langer N., Izzard R.G., 2010, IAUS, 266, 169D

de Mink S. E., pols O. R., Langer N., Izzard R. G.,, 2009, IAU 5:169-174 Cambridge University Press

Denissenkov P.A., Weiss A., 1996, A&A, 308, 773

D'Ercole A., D'Antona F., Carini R., Vesperini E., Ventura P., 2012, MNRAS, 423, 1521

D'Ercole A., D'Antona F., Vesperini E., 2011, MNRAS, 415, 1304

D'Ercole A., D'Antona F., Ventura P., Vesperini E., McMillan S.L.W., 2010, MNRAS 407, 854

D'Ercole A. Vesperini E., D'Antona F., McMillan S.L.W., Recchi S., 2008, MNRAS 391, 825

di Criscienzo M., D'Antona F., Milone A. P., Ventira P., Caloi V., Carini R., D'Ercole A., Vesperini E., Piotto G., 2011, MNRAS, 414,3381

di Criscienzo M., Ventura P., D'Antona F., Milone A., Piotto G., 2010, MNRAS, 408, 999

Doherty C. L., Siess L., Lattanzio J. C., Gil-Pons P., 2010, MNRAS, 401, 1453

D'orazi V., Marino A. F., 2010, ApJ, 716, L166

D'orazi V., Lucatello S., Gratton R., Bragaglia A., Carretta E., Shen Z., Zaggia S., 2010, ApJ, 713, L1

Drufton P. L., Ryans R. S. I., Simn-Daz S., Trundle C., Lennon D. J., 2006, A&A, 451, 693

Dupree A. K., Strader J., Smith G. H., 2011, ApJ, 728, 155

Ferraro F.R., Dalessandro E., Mucciarelli A., Beccari G., Rich R.M., Origlia L., Lanzoni B. et al., 2009, arXiv:0912.0192

Formicola A., Imbriani G., Costantini H., et al., 2004, Phys. Lett. B, 591, 61

Frost C. A., Lattanzio J. C., 1995, Liege International Astrophysical Colloquia, 32, 307

Fukushige T., Heggie D. C., Murray S., Mateo M., Richtler T., 1998, AJ, 331, 592

Fynbo H., O. U., Diget C. A., Bergmann U. C., et al., 2005, nature 433, 136

Gratton R. G., Carretta E., Bragaglia A., 2012, arXiv: 1201.6526v1

Gratton R., G., Lucatello S., Carretta E., Bragaglia A., D'Orazi V., Momany Y. Al, 2011, AUS, 276, 343G

Gratton R. G., Carretta E., 2010, A&A, 521, A54

Gratton R., Sneden C., Carretta E., 2004, ARA&A, 42, 385

Gratton R. g., Bonifacio P., Bragaglia A., Carretta E., et al., 2001, A&A, 369, 87G

Gratton R., Sneden C., Carretta E., Bragaglia A., 2000, A&A, 354,169

Grevesse N., Sauval A. J., 1998, SSrv, 85, 161

Grundstrom E.D., Gies D.R., Hillwig T.C., et al., 2007, ApJ, 667,505

Hale S. E., Champagne A. E., Iliadis C., et al., 2002, Phys. Rev. C., 65, 5801

Hale S. E., Champagne A. E., Iliadis C., et al., 2004, Phys. Rev. C., 70, 5802

Hanes D.A., 1977, MNRAS, 179,331

Hanes D.A., 1977, MNRAS, 180,309

Harris W. E., 1974, ApJ, 192 L161

Heggie D., Hut P., 2003, The Gravitational Millio-Body Problem, Cambridge Univ. Press, Cambridge

Hesser J. E., Bell R. A., 1980, ApJ, 238, L149

Huang W., Gies D. R., 2006, ApJ 648, 580

Itoh N., Mutoh H., Hikita A., Kohyama Y., 1992, ApJ 395, 622

Ivans I. I., Sneden C., Kraft R.P., Suntzeff N. B., Verne V. S., Langer G. E., Fulbright J. P., 1999, AJ, 118, 1273

King I., 1962, AJ, 67, 471

Kippenhahn R., Weigert A., 1991, A&A library, Stellar Structure and Evolution.

Klessen R., 2001, ApJ, 556, 837

Kraft R. P., 1994, PASP, 106, 553

Kroupa P., Tout C. A., Gilmore G., 1993, MNRAS, 262, 545

Krumholz M. R., Bonnel I., 2007, arXiv, 0712.0828

Kunz R., Fey M., Jaeger M., Mayer A:, Hammer J.W., Staudt G., Harossopulos S., Paradellis T., 2002, ApJ, 567, 643

Langer N., 1998, A&A, 329, 551

Lee J.-W., Lee J., Kang Y.-W., Lee Y.-W., Han S.-I., Joo S.-J., Rey S.-C., Yong D., 2009, ApJ, 695, L78

Lind K., Charbonnel C., Decressin T., Primas F., Grundahl F., Asplund M., 2011, A&A, 527, A148

Lind K., Primas F., Charbonnel C., Grundhal F., Asplund M., 2009, A&A, 503, 545

Mackey A. D. & Brody Nielsen P., 2007, MNRAS, 379, 151

Maeda K., & Nomoto K., 2003, A&A, 347, 551

Maeder A:, Meynet G., 2002, A&A, 390, 561

Maeder A:, Meynet G., 2006, A&A, 448, L37

Marino A. F., Villanova S., Milone A. P., Piotto G., Lind K., Geisler D., Stetson P. B., 2011, ApJ 730, L16

Marino A. F., Villanova S., Piotto G., Milone A.p., Momany Y., Bedin L.R., Medling A. M., 2008b, A&A, 490, 625

cLaughling D. E., van der Marel R. P., 2005, ApJS, 161, 304

McMillan S., Portegies Zwart S., 2003, ApJ, 596, 314

Meléndez J., Ramírez I., 2004, ApJ, 615, L33

Milone A. P., Marino A.F., Piotto G., Bedin L.R., Anderson J., Aparicio A., Cassisi S., Rich R. M., 2012, ApJ, 745, 27

Milone A. P. et al., ApJ, 744,58

Milone A. P., Piotto G., Bedin L. R., Cassisi S., Anderson J., Marino A. F., Pietrinferni A., Aparicio A., 2012b, A&A, 537, A77

Milone A. P., Piotto G., King I. R., Bedin L. R., Anderson J., Marino A.F., Momamy Y., Malavolta L., Villanova S., 2010, ApJ, 709, 1183

Milone A. P., Bedin L. R., Piotto G., Anderson J., et al 2008, ApJ, 673, 341

Monaco L., Vilanova S., Bonifacio P., et al., 2012, A&A, 539, A157

Monaco L., Villanova S., Moni Bidin C., Carraro G., Geisler D. et al., 2011, A&A, 529A, 90M

Moretti A., Piotto G., Arcidiacono C., Milone A.P., et al.,2009, A&A 493,539

Mowlavi N., 1999, A&A, 344,617

Norris J. E., Cottrell P. L., Freeman K. C., Da Costa G. S., 1981, ApJ, 244, 205

Osborn W., 1971, Obs, 91, 2230

Pacino E., Rejkuba M., Zoccoli M., Carrera R., 2010, A&A, 524, A44

Paczynski B., 1970, AcA, 20, 47

Pasquini L., Mauas P., K*ä*ufl H. U., Cacciari C., 2011, A&A, 531, A35

Pasquini L., Bonifacio P., Molaro P., Francois P., Spite F., Gratton R. G., Carretta E., Wolff B., 2005, A&A, 441, 549

Piau L., Beers T. C., Balsara D. S., Sivarani T., Truran J. W., Ferguson J. W., 2006, ApJ, 653, 300

Piotto G., Milone A.P., Anderson J., Bedin L.R., Bellini A., Cassisi S., Marino A. F., Aparicio A., Nascimbeni V., 2012, ApJ, 760, 39

Piotto G., 2008, IAUS, 258, 233P

Piotto G., Bedin L. R., Anderson J., King I. R., Cassisi S., Milone A. P., Villanova S., Pietrinferni A., Renzini A., 2007, ApJ, 661, L53

Piotto G. et al., 2007, ApJ, 661, L53

Piotto G., Villanova S., Pietrinferni A., Renzini A., 2005, ApJ, 621, 777

Prantzos N., Charbonnel C., 2006, A&A, 458,135

Pumo M.L., D'Antona F., Ventura P., 2008, ApJ, 672, L25

Ramírez Solange V., Cohen Judith G., 2002, AJ, 125, 224

Ramírez Solange V., Cohen Judith G., 2002, AJ, 123, 3277

Recchi S., Matteucci F., D'Ercole A., 2001, MNRAS, 322, 800R

Renzini A., Voli M., 1981, A&A, 94,175

Rich R.M., Sosin C., Djorgovski S.G., Piotto G., King I.R., Renzini A., Phinney E. S., Dorman B., Liebert J., Meylan G., 1997, ApJ, 484, L25

Rosenberg A., Recio-Blanco A., García-Marn M., 2004, ApJ, 603, 135

Sackmann I.-J. & Anand S. P. S., 1970, ApJ, 162, 105.

Schaller G., Schaerer D., Meynet G., Maeder A., 1992, A&A 96, 269

Shen Z.-X., Bonifacio P., Pasquini L., Zaggia S., 2010, A&A, 524, L2

Siess L., 2008, IAUS, 252, 297S

Siess L., 2007a, A&A, 476, 893

Siess L., 2005, A&A 448, 717

Sills A., Glebbeek E., 2010, MNRAS, 407, 277

Smith N., Gehrz R. D., Stahl O., Balick B., &Kaufer A., 2002, ApJ, 578, 464

Sollima A:, Ferrero F. R., Bellazzini M., Origlia L., Straniero O., Pacino E., 2007, ApJ, 654, 915

Sollima A:, Pancino E., Ferrero F. R., Bellazzini M., Straniero O., Pasquini L., 2005, ApJ, 634,332

Spergel D. N., Bean R., Dore' O., Nolta M. R., et al., 2007, ApJS, 170, 377

Straniero O., Chieffi A., Limongi M., Busso M., Gallino R., Arlandini C., 1997, ApJ, 478, 332

Strom S. E., Wolff S. C., Dror D. H. A., 2005,, ApJ, 129, 809 CONTROLLAAAA

Tonry J.L. & Schneider D.P., 1988, AJ, 96, 807

Valiante R., Schneider R., Bianchi S., Andersen A. C., 2009, MNRAS 397,1661

Vanbeveren D., Mennekens N., De Greve J. P., 2012, A&A, 534, A4

Ventura., P, Carini R., 2012, Astrophysics and Space Science Proceedings, Star Clusters in the Era of Large Surveys, Part 2, Pages 191-1983

Ventura P., Carini R., D'Antona R., 2011, MNRAS, 410, 2760

Ventura, P, D'Antona F., 2011, MNRAS, 410,2760

Ventura P., 2010, IAUS, 268,147V

Ventura, P., Carini, R., proceeding non so per quale congresso.

Ventura P., D'Antona F., 2009, A&A, 499, 835

Ventura P., D'Antona F., 2005, A&A 431,279-288

Ventura, P., D'Antona, F., Mazzitelli, I., 2002, A&A, 393, 215

Ventura, P., D'Antona, F., Mazzitelli, I., Gratton, R., 2001, ApJ, 550, L65

Ventura P., D'Antona F., Mazzitelli I., 2000, A&A, 363, 605

Ventura P., Zeppieri A., Mazzitelli I., D'Antona F., 1998, A&A, 334, 953

Vesperini E., McMillan S. L. W., Potegies Zwart S. F., 2008, in Vesperini E., Gierz M, Sills A., eds Proc. IAU Symp. 246, Dynamical Evolution of Dense Stellar System Cambridge Univ. Press, Cambridge, p. 181

Vesperini E., Heggie D. C., 1997, MNRAS, 289, 898

Villanova S., Geisler D., Piotto G., Gratton R., 2012, ApJ, 748, 62

Villanova S. et al., 2007, ApJ, 663, 296

Vitense E., 1953,Zs.Ap.,32,135

Walker A. R., 1992, PASP, 104, 1063

Zwart S. F. P., McMillan S. L. W., Gieles M., 2010, A. R. A. A. 48,431